Phosphoinositide 3-Kinase Gamma Inhibition Protects from Anthracycline Cardiotoxicity and Reduces Tumor Growth

Phosphoinositide 3-kinase gamma inhibition protects from anthracycline cardiotoxicity and reduces tumor growth

Li et al.

Running title: PI3Kγ inhibition in Cardio-Oncology

Correspondences:

Alessandra Ghigo, PhD

Department of Molecular Biotechnology and Health Sciences

Molecular Biotechnology Center, University of Torino

Via Nizza 52, 10126, Torino, ITALY

Phone: +39 011 670 6335

Fax: +39 011 670 6432

Email: alessandra.ghigo@unito.it

and

Emilio Hirsch, PhD

Department of Molecular Biotechnology and Health Sciences

Molecular Biotechnology Center, University of Torino

Via Nizza 52, 10126, Torino, ITALY

Phone: +39 011 670 6425

Fax: +39 011 670 6432

Email: emilio.hirsch@unito.it

Total word count: 9762

Abstract

Background: Anthracyclines, such as doxorubicin (DOX), are potent anti-cancer agents for the treatment of solid tumors and hematological malignancies. However, their clinical use is hampered by cardiotoxicity. This study sought to investigate the role of PI3Kγ in DOX-induced cardiotoxicity and the potential cardio-protective and anti-cancer effects of PI3Kγ inhibition.

Methods: Mice expressing a kinase-inactive PI3Kγ or receiving PI3Kγ selective inhibitors were subjected to chronic DOX treatment. Cardiac function was analyzed by echocardiography and DOX-mediated signaling was assessed in whole hearts or in isolated cardiomyocytes. The dual cardio-protective and anti-tumor action of PI3Kγ inhibition was assessed in mouse mammary tumor models.

Results: PI3Kγ KD mice showed preserved cardiac function after chronic low-dose DOX treatment, and were protected against DOX-induced cardiotoxicity. The beneficial effects of PI3Kγ inhibition were causally linked to enhanced autophagic disposal of DOX-damaged mitochondria. Consistently, either pharmacological or genetic blockade of autophagy *in vivo* abrogated the resistance of PI3Kγ KD mice to DOX cardiotoxicity. Mechanistically, PI3Kγ was triggered in DOX-treated hearts, downstream of TLR9, by the mitochondrial DNA released by injured organelles, and contained in autolysosomes. This autolysosomal PI3Kγ/Akt/mTOR/Ulk1 signaling provided maladaptive feedback inhibition of autophagy. Finally, PI3Kγ blockade in models of mammary gland tumors prevented DOX-induced cardiac dysfunction, and concomitantly synergized with the anti-tumor action of DOX, by unleashing anticancer immunity.

Conclusions: Blockade of PI3Kγ may provide a dual therapeutic advantage in cancer therapy, by simultaneously preventing anthracyclines cardiotoxicity and reducing tumor growth.

Key Words: PI3Kγ, Anthracyclines, Cardiotoxicity, Autophagy, Immunosuppression

Clinical Perspective

What is new?

- The present study uncovers PI3Kγ as a major player of anthracyclines cardiotoxicity.
- The present study proposes PI3Kγ inhibition as an effective means of preventing the cardiac side effects of DOX, while boosting its anti-cancer action.

What are the clinical implications?

- By virtue of its dual cardio-protective and anti-cancer action, PI3Kγ inhibition may ideally fit within chemotherapeutic regimens both of solid and hematological tumors, including the highly prevalent form of breast cancer.
- PI3Kγ inhibitors are currently in clinical trials and future translational studies might help to validate our findings.

Introduction

Anthracyclines, such as doxorubicin, are amongst the most potent and widely prescribed chemotherapeutics since the late 1960s, and still remain cornerstones in cancer treatment in combination with new-generation targeted drugs. Their clinical use, however, is limited by cardiotoxicity, often requiring modification or even discontinuation of potentially successful anticancer regimens[1]. Cardiotoxicity occurs commonly within the first year after therapy completion, thus increasing morbidity and mortality also among cancer survivors[2].

Although clinical evaluation allows early detection of cardiotoxicity, effective prevention represents a still unmet clinical need. Small clinical trials have showed only modest effects of standard heart failure pharmacotherapy[2]. Dexrazoxane is the only cardio-protectant approved by the Food and Drug Administration (FDA), but its use has been hindered by increased risk of developing secondary malignancies[3,4]. Ideally, optimal cardioprotective treatments should not only interfere with the primary mechanisms of cardiotoxicity, but at least preserve or even enhance the antitumor efficacy of chemotherapy.

Phosphoinositide 3-kinase γ (PI3Kγ) has emerged as a crucial regulator of both cardiac function and tumorigenesis. Among class I PI3Ks, including also PI3Kα, PI3Kβ and PI3Kδ isoenzymes[5], PI3Kγ is the unique to play a key maladaptive role both in heart disease and in tumor growth[10,11]. In the heart, the catalytic subunit of the PI3Kγ holoenzyme (p110γ, the product of the *PIK3CG* gene), is upregulated under stress conditions, and triggers adverse cardiac remodeling and, ultimately, heart failure[6,7]. PI3Kγ is also enriched in the tumor microenvironment and indirectly favors cancer growth, by promoting macrophage trafficking and immunosuppressive polarization which, together, prevent T cell-mediated tumor killing[8,9]. Accordingly, PI3Kγ inhibition protects against pressure overload-induced heart failure[6,7], and delays the progression of highly

immunosuppressive tumors, such as lung and pancreatic cancers[8,10]. Nonetheless, the role of PI3Kγ and the therapeutic potential of PI3Kγ inhibitors in anthracycline-mediated cardiomyopathy are so far unknown. Furthermore, how PI3Kγ-directed immunity interacts with anthracycline-based chemotherapy in the tumor remains unexplored.

Herein, we identify PI3Kγ as a key determinant of anthracycline cardiotoxicity and we provide proof-of-concept that pharmacological inhibition of PI3Kγ is a unique means of preventing doxorubicin cardiotoxicity, while boosting its anticancer efficacy. In cardiomyocytes, doxorubicin engages PI3Kγ signaling downstream of Toll-like receptor 9 (TLR9), converging on autophagy inhibition and maladaptive metabolic rewiring which, ultimately, cause cardiomyocyte death and systolic dysfunction. Genetic or pharmacological blockade of PI3Kγ prevents anthracycline-induced heart disease and concomitantly synergizes with chemotherapy, delaying tumor growth and improving survival in xenograft and spontaneous mammary tumor models.

Methods

The authors declare that all supporting data, analytic methods, and study materials are available within the article and its online supplementary files.

Expanded methods can be found in the Methods section of the Online Supplementary Materials. Key resources tables, including primary antibodies and quantitative RT-PCR primers, can be found in Supplementary Table 1 and Supplementary Table 2 of the Online Supplementary Materials.

Mice

Knock-in mice expressing an inactive PI3Kγ holoenzyme (kinase dead, KD) were generated by inserting a point mutation in the *Pik3cg* gene encoding the p110γ catalytic subunit, as previously described[11]. For studies on spontaneous tumors, BALB/c mice overexpressing the activated form of the Neu oncogene (BALB/c rHER-2/NeuT) in the mammary gland were used[12]. Authorities approved all animal experiments.

In vivo treatments

To mimic human therapeutic regimens, a cumulative dose of 12 mg/kg of doxorubicin (DOX) was administered via 3 weekly i.p. injections (4 mg/kg on days 0, 7 and 14)[13]. Survival was monitored daily. To investigate Akt/mTOR/Ulk1 signaling, WT and KD mice received a single i.p. injection of 4 mg/kg DOX alone or in combination with 100 μg of ODN2088 (TLR9 antagonist) for 3 days.

To study the autophagic flux *in vivo*, mice were treated i.p. with 10 mg/kg Bafilomycin A1 (BafA1) or Vehicle 1 hour before a single injection of 4 mg/kg DOX. Mice were sacrificed 6 hours after DOX.

To inhibit autophagy *in vivo*, PI3Kγ KD mice were treated with DOX or saline, followed by daily i.p. injection of 60 mg/kg of hydroxychloroquine (HCQ) or 0.3 mg/kg of BafA1 or saline, for 4 weeks. Cardiomyocyte-restricted, genetic inhibition of autophagy was performed by i.v. injection of either AAV9-GFP-U6-ATG7-shRNA or AAV9-GFP-U6-scrmb-shRNA.

Echocardiography

Cardiac function was evaluated in mice anesthetized with 1% isoflurane using a Vevo2100 High Resolution Imaging System (Visual Sonics Inc, Toronto, Canada). Echocardiographic parameters were measured under the long-axis M-mode when heart rate was about 450 bpm.

Tumor studies

Mice were subcutaneously injected with 1×10^5 4T1 or TUBO cells. One week after cell injection, mice were treated with DOX or saline. Tumor size was measured twice/week for up to 4 weeks. PI3Kγ was inhibited pharmacologically by using IPI145[14] and AS605240[15].

Isolation of Neonatal Mouse Ventricular Myocytes (NMVMs)

Neonatal mouse cardiomyocytes (NMVMs) were isolated as previously described[16]. Briefly, hearts from 1 to 3-day-old pups were minced and pre-digested with 0.5 mg/ml trypsin overnight, followed by 3-4 digestions with 330 U/ml collagenase type II. Isolated cells were centrifuged at 800 rpm to separate non-myocardial cells, re-suspended in DMEM/M199 (3:1) containing 10%

horse serum, 5% fetal bovine serum and 5 mM penicillin/streptomycin and pre-plated twice to further reduce fibroblast contamination. 0.3-1$\times 10^6$ cardiomyocytes/well were finally plated in gelatin (0.2%)/fibronectin (10 μg/ml) coated plates. Expanded methods can be found in the Supplemental Materials.

***In vitro* treatments**

24 hours before stimulation, NMVMs were cultured in serum-free DMEM/M199 (3:1) and H9c2 cells in DMEM supplemented with 0,5% Fetal Bovine Serum (FBS). Cells were then treated with 1 μM DOX for the indicated times, alone or in combination with AS605240 (0.5 μM, 1-hour pretreatment) or with the TLR9 antagonist ODN2088 (0.2 μM, 5-hour pretreatment), as described previously[17]. Alternatively, NMVMs and H9c2 cells were stimulated with the TLR9 agonist ODN1826 (0.2 μM, 1 hour), with or without AS605240 pretreatment. At the end of the treatment, cells were processed as described previously[6].

Flow cytometry staining and analysis

Single-cell suspensions from mouse tumor samples (1x10^6 cells) were incubated with the blocking reagent anti-CD16/CD32, followed by incubation with fluorophore-labelled antibodies. For staining of surface markers, the following primary antibodies were used: Gr1 Ly6G/Ly6C, F4/80, CD11b, and MHC class II. For CD206 staining, formalin-fixed cells were incubated with a fluorophore-labelled antibody. Cells were acquired with the AccuriC6 and analyzed with FlowJo x7.5.

Histological and immunohistochemical analysis

mtDNA, TLR9, PI3Kγ and LAMP2 co-localization was assessed in NMVMs stimulated with either ODN1826 or DOX for 1 hour. Standard protocols were used for immunofluorescence (IF) staining. For *ex-vivo* analyses, hearts from WT and KD mice treated with DOX or saline were processed for histological and IF analysis[18].

Human heart samples were collected from a 21-year-old woman diagnosed with Ewing sarcoma and subjected to triple therapy with Adriamycin, Cyclophosphamide and Vincristine. The patient manifested heart failure symptoms 5 years after chemotherapy and underwent heart transplantation 10 years after the diagnosis of chemotherapy-induced cardiomyopathy (Ejection fraction: 40%). Samples were archived at the institute of Pathological Anatomy of the University of Padova. Samples were anonymous to the investigators and used in accordance with the directives of Authorities. Formalin-fixed, paraffin-embedded human heart samples were processed for IF study[19].

Statistical analysis

Prism software (GraphPad software Inc., La Jolla, CA, USA) was used for statistical analysis. *P* values were calculated with one-way ANOVA, two-way ANOVA, two-way repeated-measures ANOVA followed by Bonferroni post-hoc test or Student's t-test as appropriate. Log-rank test was used for survival analysis. Data are presented as Mean ± SEM; $P<0.05$ was considered as statistically significant.

Results

Genetic inhibition of PI3Kγ protects against DOX cardiotoxicity

To explore the role of PI3Kγ in anthracycline-induced cardiotoxicity, knock-in mice expressing a kinase-inactive PI3Kγ (PI3Kγ kinase-dead, KD) and wild-type controls (WT) were subjected to a low-dose doxorubicin (DOX) treatment[13] (Supplementary Fig. 1A). The treatment was well tolerated by both WT and KD mice, as evidenced by preserved food intake and locomotor activity (Supplementary Fig. 1B and 1C). In line with clinical evidence of weight loss in DOX-treated patients[20,21], DOX induced a 10% decrease in body weight in both genotypes, without significantly affecting survival (Supplementary Fig. 1D and 1E). Echocardiographic assessment at 6 weeks after the first DOX administration revealed a significant reduction of cardiac contractility in WT mice (Fig. 1A and Supplementary Table 3), which was accompanied by upregulation of markers of cardiac injury, such as plasma concentrations of troponin T (TnT) (Fig. 1B) and myocardial *Anf* and *Bnp* mRNA levels (Fig. 1C). The absence of lung and liver congestion in these mice (Supplementary Table 4) excluded the development of overt heart failure and indicated the establishment of a subclinical myocardial dysfunction, reminiscent of that observed clinically in chronic DOX cardiomyopathy. Conversely, left ventricular systolic function, plasma TnT, *Anf* and *Bnp* mRNA levels were all unchanged in DOX-treated KD mice (Fig. 1A-C and Supplementary Table 3), highlighting the protective effects of PI3Kγ inhibition against DOX-induced cardiac injury.

Cardiac wasting, apoptosis, and fibrosis are key hallmarks of anthracycline-related cardiotoxicity[22]. In keeping with preserved cardiac contractility, KD mice showed normal cardiac mass and cardiomyocyte size after DOX (Supplementary Table 4 and Fig. 1D). Furthermore, TUNEL and cleaved caspase-9 assays revealed that, after DOX treatment,

apoptosis was significantly lower in KD than in WT hearts (Fig. 1E and 1F). Finally, myocardial collagen deposition was significantly less abundant in DOX-treated KD than in WT hearts, as evidenced by reduced PicroSirius Red staining (Fig. 1G) and by weaker expression of pro-fibrotic genes, such as *Tgfb*, *Ctgf*, *Col1a1* and *Col3a1* (Fig. 1H).

Altogether, these findings demonstrate that PI3Kγ inhibition protects against DOX-induced myocardial damage and dysfunction.

PI3Kγ inhibition promotes mitochondrial autophagy

Although PI3Kγ can contribute to maladaptive cardiac remodeling by driving inflammation[7], analysis of inflammatory responses after DOX showed no significant leukocyte recruitment to the myocardium of either WT or KD mice (Supplementary Fig. 2). This excluded the involvement of leukocyte PI3Kγ in DOX-induced cardiac remodeling.

Conversely, the PI3K pathway is a master regulator of autophagy[23] and dysregulation of autophagy in the myocardium is implicated in cardiovascular diseases including DOX cardiotoxicity[24–27]. The possible link between myocardial PI3Kγ signaling and autophagy was thus investigated in DOX-treated animals. The levels of LC3-II, a hallmark of autophagosome formation, were slightly but significantly increased in WT hearts at 3 days after the first injection of DOX (Fig. 2A). In contrast, LC3-II accumulation was significantly higher in KD than in WT hearts, starting from this time point (Fig. 2A) and up to the end of the treatment (Fig. 2B), thus indicating that PI3Kγ acts as a negative regulator of autophagy. This result was further demonstrated in primary neonatal mouse ventricular myocytes (NMVMs) expressing YFP-LC3, where LC3-puncta (autophagosomes) elicited by DOX were significantly more abundant in KD than in WT cells (Supplementary Fig. 3A).

To assess whether LC3-II accumulation in KD hearts resulted from enhanced autophagosome formation or impaired autophagosome-lysosome fusion, autophagic flux was studied after blocking autophagosome-lysosome fusion with Bafilomycin A1 (BafA1). BafA1 further increased LC3-II levels (Fig. 2C) and LC3 puncta density (Fig. 2D) in DOX-treated KD hearts, thus revealing that loss of PI3Kγ catalytic function enhances activation of the autophagic flux. These findings were confirmed in primary NMVMs expressing the mRFP-GFP-LC3 probe, which allows the concomitant detection of autophagosomes (yellow dots) and autolysosomes (free red dots) in living cells[28]. Both yellow and red puncta were significantly more abundant in KD than in WT NMVMs (Fig. 2E and Supplementary Fig. 3B), confirming an accelerated autophagic flux in KD cardiomyocytes exposed to DOX. Pre-treatment with BafA1 prevented the formation of autolysosomes in both groups and further proved enhanced formation of autophagosomes in KD cells, as compared to WT controls (Supplementary Fig. 3C). Thus, PI3Kγ acts as a negative regulator of autophagy in DOX-treated hearts.

Alteration of the autophagic flux in cardiomyocytes can reduce their ability to eliminate DOX-damaged organelles, such as mitochondria[29]. Electron microscopy studies revealed the presence of autophagic vacuoles containing damaged mitochondria in DOX-treated WT hearts (Fig. 3A), indicating the activation of mitochondrial autophagy. In keeping with an enhanced autophagic flux (Fig. 2C-E), these structures were more abundant in KD hearts than in WT controls (Fig. 3A). Immunofluorescence studies, showing the co-localization of mitochondrial DNA (mtDNA) with the autophagosome marker LC3 (Fig. 3B), and LC3-II immunoblot in mitochondria-enriched fractions (Supplementary Fig. 4A), both confirmed that mitochondrial autophagy was significantly more active in KD than in WT hearts after DOX.

Enhanced elimination of injured organelles led to preserved mitochondrial respiration in NMVMs exposed to DOX concomitantly to the PI3Kγ inhibitor AS605240 (Supplementary Fig. 4B). Instead, in cells treated with DOX alone, the bioenergetic efficiency of mitochondria (P/O ratio) was significantly reduced and triggered a compensatory metabolic switch from fatty acid oxidation to glycolysis, as indicated by increased activity of major glycolytic enzymes, higher lactate dehydrogenase activity and lactate production (Supplementary Fig. 4B). Of note, PI3Kγ was not expressed in mitochondria (Supplementary Fig. 4C), thus excluding the involvement of PI3Kγ in intrinsic mitochondrial regulation and suggesting that PI3Kγ inhibition preserves mitochondrial metabolism indirectly, by favoring autophagic disposal of damaged organelles.

DOX activates an autolysosomal TLR9/PI3Kγ pathway promoting feedback inhibition of autophagy

Given that damaged mitochondria within autolysosomes can trigger Toll-like receptor 9 (TLR9)[17], and TLRs can signal through PI3Kγ activation[30], the ability of mtDNA from DOX-injured mitochondria to engage TLR9 and, in turn, PI3Kγ signaling was investigated. Immunofluorescence assays revealed that mtDNA co-localized with both TLR9 and PI3Kγ in NMVMs exposed to DOX (Fig. 4A), in line with the localization of PI3Kγ in endosomes[31] as well as with the enrichment of these three moieties in similar endocytic compartments. In resting cells, TLR9 mainly resides in the endoplasmic reticulum, but translocates to lysosomes upon induction of autophagy[32]. Consistently, immunofluorescence (Fig. 4B) and co-immunoprecipitation studies (Fig. 4C) showed that co-localization of TLR9 with PI3Kγ can be detected only in cells challenged with the TLR9 activator ODN1826, a CpG-rich oligonucleotide similar to mtDNA, but not in untreated controls. Remarkably, in NMVMs treated with ODN1826,

both TLR9 and PI3Kγ were found in LAMP2-positive compartments (autolysosomes) (Fig. 4D), thus indicating that the TLR9/PI3Kγ signaling complex assembles on these organelles.

Next, PI3Kγ pathway activation by the DOX/mitochondrial damage/mitochondrial autophagy/mtDNA/TLR9 cascade was investigated in H9c2 cardiac-like cells, in primary NMVMs, and in whole hearts. In H9c2, DOX increased the phosphorylation of the PI3K downstream target Akt, as early as 30 minutes and up to 2 hours after treatment, and the PI3Kγ selective inhibitor AS605240 completely prevented DOX-dependent Akt activation (Supplementary Fig. 5A). Similarly, Akt phosphorylation was upregulated by 2-fold in WT, but not in KD primary NMVMs exposed to DOX (Supplementary Fig. 5B). Notably, DOX-dependent PI3Kγ/Akt activation occurred downstream of TLR9, as the TLR9 antagonist ODN2088 prevented Akt phosphorylation in both NMVMs (Fig. 5A) and H9c2 (Supplementary Fig. 6A), mimicking the effects of PI3Kγ inhibition (WT NMVMs treated with AS605240 and KD NMVMs in Fig. 5A; AS605240-treated H9c2 cells in Supplementary Fig. 6A). In further support of the activation of a TLR9/PI3Kγ/Akt signaling on induction of mitochondrial autophagy, the mtDNA-like oligonucleotide and TLR9 agonist, ODN1826, significantly elevated Akt phosphorylation in NMVMs (Fig. 5A) and H9c2 cells (Supplementary Fig. 6B). Remarkably, this effect was completely abolished by PI3Kγ inactivation in KD NMVMs (Fig. 5A) and in AS605240-treated H9c2 cells (Supplementary Fig. 6B).

Under stress conditions, engagement of the PI3K/Akt pathway may result in mTOR-mediated suppression of autophagy[33]. Therefore, activation of the autolysosomal TLR9/PI3Kγ/Akt signaling may provide a negative feedback regulation of autophagy. In H9c2 cells, DOX-mediated activation of Akt correlated with increased phosphorylation of mTOR targets, including S6 kinase, but also the autophagy inducer Ulk1 that, when phosphorylated on Ser-

757[34], is inactive (Supplementary Fig. 6A and 6C). In agreement, blockade of either TLR9 or PI3Kγ abrogated the inhibitory phosphorylation of Ulk1 (Supplementary Fig. 6A). Conversely, direct activation of TRL9 with ODN1826 resulted in a PI3Kγ-dependent increase of Ulk1 phosphorylation (Supplementary Fig. 6B). To confirm these observations in the heart of DOX-treated mice, activation of the PI3Kγ/mTOR pathway was studied by immunohistochemistry three days after treatment. While WT hearts stained positive for phospho-Akt, phospho-mTOR and phospho-Ulk1, no staining was detected in KD tissues (Fig. 5B). This response was accompanied by the canonical TLR9-dependent transcriptional upregulation of inflammatory cytokines in WT but not KD hearts (Supplementary Fig. 6D), thus indicating a TLR9 involvement *in vivo*. In further agreement, inhibition of TLR9-mediated sensing of mtDNA by intravenous administration of the TLR9 antagonist ODN2088 blocked DOX-induced Akt/mTOR/Ulk1 signaling in WT hearts (Fig. 5B).

Altogether, these data indicate that DOX triggers an autolysosomal TLR9/PI3Kγ signaling converging on Ulk1 inactivation and, in turn, on feedback inhibition of autophagy.

Inhibition of autophagy in KD mice abrogates the protection from DOX cardiotoxicity

Resistance of KD mice to DOX-induced cardiotoxicity appeared linked to the loss of a negative feedback inhibiting autophagy. To test this hypothesis, autophagy was blocked genetically by an adeno-associated viral vector (AAV9) encoding a small hairpin RNA (shRNA) targeting the key autophagy initiating gene *Atg7* as well as a GFP probe labeling infected cells (AAV9-ATG7sh). Six weeks after infection, AAV9-ATG7sh led to a 45% reduction of cardiac *Atg7* mRNA levels (Supplementary Fig. 7A) and, as expected, KD animals either transduced with a control vector (AAV9-CTRLsh) or infected with AAV9-ATG7sh showed normal cardiac contractility (Fig. 6A).

Conversely, infection with the AAV9-ATG7sh significantly blunted the protection of KD mice against DOX-induced deterioration of fractional shortening (Fig. 6A). In these hearts, the area of infected green cardiomyocyte was significantly lower than in non-infected controls (Fig. 6B and 6C). Thus, genetic inhibition of cardiac autophagy abrogated the protection of PI3Kγ KD mice against DOX cardiotoxicity. Similar results were observed when autophagy was inhibited pharmacologically, with either BafA1, or compounds in clinical use, like hydroxychloroquine (HCQ). Similar to AAV9-ATG7sh, BafA1 and HCQ impaired cardiac contractility in DOX-treated KD mice (Supplementary Fig. 7B and Fig. 6D) and restored their susceptibility to DOX-induced cardiomyocyte atrophy, apoptosis and myocardial fibrosis (Fig. 6E-G).

To test if enhanced autophagy triggered by PI3Kγ inhibition protects against other known DOX-induced toxic effects[35], disruption of mitochondrial membrane potential, calcium (Ca^{2+}) mishandling, reactive oxygen species (ROS) production and DNA damage were studied. In DOX-treated WT cardiomyocytes, the PI3Kγ inhibitor AS605240, but not the combination of this drug with the autophagy blocker BafA1, prevented both the impairment of mitochondrial membrane potential and the induction of spontaneous Ca^{2+} waves (Supplementary Fig. 8A-B). Furthermore, KD hearts and AS605240-treated NMVMs showed a significant protection against DOX-induced ROS production and DNA damage, which was abrogated by blocking autophagy with either BafA1 or an adenovirus harboring an ATG7 shRNA (Supplementary Fig. 8C-E).

Altogether, these results corroborate the view that PI3Kγ inhibition protects against DOX cardiotoxicity by unleashing autophagy.

PI3Kγ inhibition potentiates the anti-cancer activity of anthracyclines by restoring anti-tumor immune responses

To evaluate the potential use of PI3Kγ inhibitors as cardio-protectants in the context of anthracycline therapy, the combined effect of DOX and PI3Kγ inhibition on tumor growth was explored. DOX-sensitive 4T1 breast cancer cells, which do not express PI3Kγ[36], were initially studied. Accordingly, *in vitro* administration to 4T1 cells of the PI3Kγ inhibitor AS605240 did not affect growth (Supplementary Fig. 9A), but treatment of the same cells with DOX resulted in a concentration-dependent lethality (Supplementary Fig. 9B). Nonetheless, 4T1 cells grew *in vivo* significantly less in KD than in WT mice (Fig. 7A) and DOX further delayed tumor growth, leading to significantly smaller tumors in KD than in WT mice (Fig. 7A).

Because PI3Kγ regulates cancer immune suppression[8,9], to understand how PI3Kγ inhibition synergizes with DOX, tumor-associated leukocytes were analyzed. CD11b immunostaining revealed reduced myeloid infiltration in 4T1 tumors implanted in KD recipients (Fig. 7B). FACS analysis on $CD11b^{+}$ cells from the same tumors confirmed a lower number of $Gr1^{int}F4/80^{low}$ pro-tumor macrophages in KD than in WT, while $Gr1^{low}F4/80^{hi}$ anti-tumor macrophages were unchanged (Fig. 7C). To better characterize this population, the expression of CD206, in combination with that of MHC class II molecule, was analyzed[37]. The percentage of $CD206^{+}$ cells (Fig. 7D) characterized by low MHC-II expression (Fig. 7E), showing a phenotype typically associated to pro-tumor macrophages, was significantly lower in tumors grown in KD than in WT recipients. In line with reduced recruitment of pro-tumor macrophages, KD tumors expressed significantly smaller amounts of pro-tumor cytokines (*Tgfb, Il-13, Il-10, Ccl17 and Ccl22*) than WT, while anti-tumor signals were not different between the two groups (Fig. 7F).

In accordance with the immune suppressive action of pro-tumor macrophages[38], tumor killing $CD8^+$ T cells were more abundant in tumors from KD than from WT mice (Fig. 7G).

Overall, these data indicate that inhibition of PI3Kγ synergizes with the anti-tumor action of DOX by interfering with the recruitment of pro-tumor macrophages and eventually unleashing anti-tumor T-cell responses.

PI3Kγ inhibition simultaneously prevents cardiotoxicity and tumor growth under anthracycline treatment

The clinical translatability of PI3Kγ inhibition was next evaluated. PI3Kγ protein expression was analyzed in human heart sections from a patient who developed a severe DOX-induced cardiomyopathy requiring heart transplantation. Immunofluorescence assays revealed higher and more punctate expression of the catalytic p110γ subunit in DOX-damaged hearts than in healthy controls (Fig. 8A, Supplementary Fig. 10A-B), highlighting a correlation between PI3Kγ upregulation and DOX-induced cardiotoxicity. PI3Kγ upregulation might also occur in other more easily accessible tissues, and potentially represent a biomarker of DOX-induced cardiotoxicity. *In silico* analysis of *PIK3CG* (encoding p110γ) mRNA levels in blood samples from patients subjected to anthracycline chemotherapy showed that *PIK3CG* mRNA was 50% more abundant in patients who developed heart disease after anthracycline treatment (Group 3) than in healthy controls (Group 1). More importantly, no *PIK3CG* upregulation was detected in subjects showing normal heart function after chemotherapy (Group 2) [Relative *PIK3CG* mRNA level: Group 1 = 1.00±0.02, Group 2 = 1.09±0.09, Group 3 = 1.52±0.16; Group 3 vs Group 2 **P*<0.05 by one-way ANOVA with Bonferroni's post-hoc test]. Remarkably, this modulation appeared isoform-specific, as the mRNA levels of *PIK3CA* (the gene encoding the p110α

catalytic subunit of PI3Kα, the most abundant cardiac PI3K isoform) were not affected by DOX [Relative *PIK3CA* mRNA level: Group 1 = 1.00±0.06, Group 2 = 1.12±0.07, Group 3 = 1.02±0.05; no significance among groups by one-way ANOVA with Bonferroni's post-hoc test]. Overall, these data provide preliminary evidence that aberrant expression and activation of PI3Kγ may correlate with DOX cardiotoxicity in human patients.

Finally, the ability of PI3Kγ inhibition to delay tumor growth and, at the same time, protect the heart during DOX treatment was assessed in preclinical models of breast cancers. Consistent with the findings in tumor-free animals, KD mice bearing a tumor derived by the injection of either 4T1 or TUBO mammary gland cancer cells were protected against DOX-induced remodeling and contractile dysfunction (Supplementary Fig. 11A-B, Supplementary Table 5, Supplementary Fig. 12A-C). With both cell lines, the tumor led to 50% of mortality in WT mice but significantly higher survival was observed in KD mice (Supplementary Fig. 11C-D). Thus, PI3Kγ inactivation improves survival by limiting tumor growth, and concomitantly prevents DOX cardiotoxicity.

Next, the ability of pharmacological inhibition of PI3Kγ to recapitulate the protection observed in the genetic model was explored. AS605240 significantly prevented DOX-induced contractile dysfunction, cardiomyocyte atrophy and apoptosis as well as myocardial fibrosis in tumor-free mice (Supplementary Fig. 13A-C and Supplementary Table 6). Similarly, the more clinically advanced PI3Kγ (and PI3Kδ) inhibitor IPI-145[14] delayed tumor growth *per se*, and potentiated the anti-tumor effect of DOX (Fig. 8B), while preventing DOX-induced contractile dysfunction (Fig. 8C) in 4T1 tumor-bearing animals. Finally, the dual therapeutic potential of PI3Kγ inhibitors was validated in a model of spontaneous mammary tumor growth. Her2/NeuT tumors grew significantly less in mice treated with AS605240 compared to vehicle, and the PI3Kγ

inhibitor synergized with DOX when administered in combination (Fig. 8D). The antitumor effects of AS605240 were accompanied by cardioprotection of DOX-treated mice (Fig. 8E, Supplementary Fig. 12D-F), and ultimately resulted in significantly lower mortality than in vehicle-treated animals (Fig. 8F).

Altogether, these data uncover PI3Kγ inhibition as a unique means of synergizing with the antitumor activity of standard chemotherapy, while defending the heart from the iatrogenic cardiotoxicity.

Discussion

The present study uncovers PI3Kγ as a major player of anthracyclines cardiotoxicity and proposes PI3Kγ inhibition as an effective means of preventing the cardiac side effects of DOX, while boosting its anti-cancer action.

Despite major efforts in understanding the mechanism of anthracyclines-induced cardiotoxicity, molecular and cellular details are not yet fully understood. Potential mechanisms include generation of reactive oxygen species (ROS) and targeting of topoisomerase II-β (TOP2B), together leading to DNA damage, mitochondrial dysfunction and Ca^{2+} mishandling[13,39,40]. Yet, the ROS-scavenging iron chelator and TOP2B modulator dexrazoxane, failed to provide significant benefit, suggesting the existence of additional factors. Whether PI3Kγ, a well-known inducer of maladaptive responses in various cardiac conditions[11,41,42], was involved in DOX-elicited cardiotoxicity has remained so far unknown. Our findings now fill this gap and support PI3Kγ-mediated block of autophagy as a major driver of DOX-evoked cardiotoxicity.

Although the role of cardiac autophagy in anthracyclines cardiotoxicity has been subject of debate[43,44], our results support the notion that DOX impairs - but does not abolish - the autophagic flux in cardiomyocytes[26] and that this reduction is detrimental to the heart[42,45]. Our study also indicates that DOX-related cardiomyopathy can be prevented by stimulation of autophagy, likely driving efficient disposal of damaged mitochondria, the major sites of DOX-induced ROS production[26,29,46]. Consistent with this view, our findings showed that the prompt clearance of injured and potentially harmful organelles ensured a general protection against ROS-related toxic effects, including DNA damage, Ca^{2+} mishandling and disruption of mitochondrial metabolism.

Nonetheless, activation of PI3Kγ was found to trigger a negative feedback loop eventually inhibiting autophagy. Mitochondrial damage elicited by DOX led to an initial mitochondrial autophagy, which stimulated PI3Kγ through the activation of endosomal TLR9, a receptor sensing CpG-rich mitochondrial DNA (mtDNA) released in autolysosomes[17]. This finding was unexpected, especially in view of the classical role played by PI3Kγ signaling downstream of G protein-coupled receptors[47]. Conversely, this result appeared in agreement with studies showing PI3Kγ being non-canonically activated downstream of TLRs[30] and being localized in endosomes[31]. Our findings showed that in the absence of PI3Kγ, TLR9 signaling is severely impaired and that the TLR9-dependent cytokine production is decreased. However, while in pressure overloaded hearts TLR9 engagement by mitochondrial damage initiates inflammation, leucocyte infiltration, and, ultimately, maladaptive cardiac remodeling[17], leukocyte recruitment to the myocardium is almost negligible in DOX-induced cardiomyopathy[48]. Instead, TLR9-mediated activation of PI3Kγ converged on the feedback inhibition of autophagy (Figure 8G), and the concomitant metabolic reprogramming of cardiomyocytes. This likely represents an attempt of PI3Kγ to cope with the cardiac damage elicited by chemotherapy through a two-pronged action. On one hand, the block of autophagy may avoid the accumulation of potentially harmful undegraded autolysosomes[26,45]. This situation is likely to occur in DOX-treated hearts, where lysosomes are dysfunctional and cannot properly deal with an exaggerated autophagosome formation[26,45]. On the other hand, PI3Kγ activation may be poised to interrupt the vicious cycle of ROS formation by injured organelles, by promoting a switch towards a more ROS-sparing, non-mitochondrial metabolism. Although these PI3Kγ-directed events may be initially compensatory, anaerobic glycolysis may eventually fail to sustain cardiac energy demand and, together with impaired autophagic disposal of injured mitochondria, may lead to

metabolic derangement and cardiotoxicity. Intriguingly, this metabolic switch and its long-term consequences can account for the emergence of cardiac damage long after completion of anthracyclines treatment.

Pharmacological interference with PI3Kγ-dependent signaling in cardiomyocytes may indirectly improve cancer prognosis by increasing tolerability of cardiotoxic anti-cancer treatments. PI3Kγ inhibitors also display major antineoplastic properties and are thus particularly attractive dual-action therapeutic agents for cancer patients. Of note, PI3Kγ does not impact on tumor growth directly, but promotes both the trafficking and the differentiation of a subset of immunosuppressive pro-tumor macrophages, which ultimately block T cell-mediated tumor killing[8,10]. Accordingly, PI3Kγ inactivation unleashes adaptive immunity and delays tumor growth *per se*, but also allows overcoming resistance to immune checkpoint blocking antibodies[8,10]. How PI3Kγ-directed immunity interacts with anthracyclines is unknown. The present study demonstrates that PI3Kγ inhibitors not only synergize with antitumor effects of DOX, but also concomitantly defend the heart from iatrogenic cardiotoxicity.

This cardioprotective approach is potentially applicable to most patients undergoing anthracyclines-based regimens, including pediatric leukemia patients, for whom long-term cardiotoxicity is a devastating complication during adulthood[49]. Similarly, this applies to breast cancer patients exposed to the highly effective, but extremely cardiotoxic combination of anthracyclines and anti-ErbB2 monoclonal antibodies[50]. Intriguingly, cardioprotective strategies may potentially allow cancer chemotherapies in frail, elderly individuals, even in the presence of pre-existing cardiac diseases. Our finding that patients with DOX-induced cardiac toxicity showed over-expression of PI3Kγ further indicates that targeting this kinase might not only be effective in mouse models, but also in patients. Inhibition of PI3Kγ may represent an attractive

approach, especially in view that IPI-145, the oral PI3Kγ/δ dual inhibitor used in this study[14], is currently undergoing Phase III clinical trial for hematological malignancies and another more selective PI3Kγ inhibitor, IPI-549[51], is now approaching Phase I clinical evaluation.

Overall, PI3Kγ inhibition may improve prognosis of cancer patients treated with DOX by concomitantly unleashing anti-tumor immunity as well as preventing cardiotoxicity. Therefore, PI3Kγ inhibitors might eventually help to "kill two birds with one stone" in cancer patients requiring anthracycline chemotherapy.

Authors

Mingchuan Li, PhD[1], Valentina Sala, PhD[1,12], Maria Chiara De Santis, MS[1], James Cimino, BS[1], Paola Cappello, PhD[2], Nicola Pianca, PhD[3,4], Anna Di Bona, MS[3,4,5], Jean Piero Margaria, MS[1], Miriam Martini, PhD[1], Edoardo Lazzarini, PhD[6], Flora Pirozzi, MD, PhD[1,7], Luca Rossi, BS[1], Irene Franco, PhD[1§], Julia Bornbaum, PhD[8], Jacqueline Heger, PhD[8], Susanne Rohrbach, PhD[8], Alessia Perino, PhD[1#], Carlo G. Tocchetti, MD, PhD[7], Braulio H.F. Lima, PhD[9†], Mauro M. Teixeira, MD, PhD[9], Paolo E. Porporato[1], PhD, Rainer Schulz, MD, PhD[8], Annalisa Angelini, MD, PhD[5], Marco Sandri, PhD[3,4], Pietro Ameri, MD, PhD[6], Sebastiano Sciarretta, MD, PhD[10], Roberto César P. Lima-Júnior, PhD[1,11], Marco Mongillo, MD, PhD[3,4], Tania Zaglia, PhD[3,4,5], Fulvio Morello, MD, PhD[12], Francesco Novelli, PhD[2], Emilio Hirsch, PhD[1‡] and Alessandra Ghigo, PhD[1‡]

[‡]Drs Ghigo A. and Hirsch E. contributed equally to this work.

Sources of funding

This work was supported by grants from Progetto d'Ateneo - Compagnia di San Paolo (PICANCAR to A. Ghigo, PANTHER to P. Cappello and PC-METAIMMUNOTHER to F. Novelli), 2013 International Society for Heart Research (ISHR)/Servier Research Fellowship (to A. Ghigo), Italian Ministry of Health (No. GR-2013-02355449 to F. Morello and RF-2013-02354892 to F. Novelli), Associazione Italiana Ricerca sul Cancro (5 x mille no. 12182 and IG no. 15257 to F. Novelli) and Leducq Foundation (No. 09CVD01 to E. Hirsch). M. Li received a PhD studentship award from Chinese Scholarship Council (CSC). M. Martini is supported by a Fondazione Umberto Veronesi fellowship. R.C.P. Lima-Júnior is supported by a Capes Fellowship (Estágio Sênior no Exterior - Processo nº 88881.119732/2016-01) and by PRONEX/FUNCAP/CNPq (PR2-0101-00054.01.00/15).

Disclosures

E. Hirsch is co-founder of Kither Biotech S.r.l., an academic spin-off involved in the development of PI3K inhibitors. No potential conflicts of interest were disclosed by the other authors.

Affiliations

[1]Department of Molecular Biotechnology and Health Sciences, Molecular Biotechnology Center, University of Torino, Torino, ITALY.

[2]Center for Experimental Research and Medical Studies (CeRMS), Azienda Ospedaliera Universitaria Città della Salute e della Scienza di Torino, Torino, ITALY.

[3]Department of Biomedical Sciences, University of Padova, Padova, ITALY.

[4] Venetian Institute of Molecular Medicine, Padova, ITALY.

[5]Department of Cardiac, Thoracic and Vascular Sciences, University of Padova, Padova, ITALY.

[6]Cardiovascular Biology Laboratory, Department of Internal Medicine, University of Genova and IRCCS Policlinic Hospital San Martino, Genova, ITALY.

[7]Division of Internal Medicine, Department of Translational Medical Sciences, Federico II University, Napoli, ITALY.

[8]Institut für Physiologie, Justus-Liebig Universität Giessen, Giessen, GERMANY.

[9]Departamento de Bioquímica e Imunologia, Instituto de Ciências Biológicas, Universidade Federal de Minas Gerais, Belo Horizonte, Minas Gerais, BRAZIL.

[10]Department of Medical and Surgical Sciences and Biotechnologies, University of Rome "Sapienza", Latina, ITALY.

[11]Laboratory of Pharmacology of Inflammation and Cancer, Department of Physiology and Pharmacology, Universidade Federal do Ceará/UFC, Fortaleza, BRAZIL.

[12]A.O.U. Città della Salute e della Scienza di Torino, S.C. Emergency Medicine, Torino, ITALY.

[§] Current address: Dept of Biosciences and Nutrition, Center for Innovative Medicine, Karolinska Institutet, Huddinge, SWEDEN.

[†]Current address: Departamento de Farmacologia, Faculdade de Medicina de Ribeirão Preto, Universidade de São Paulo, Ribeirão Preto, São Paulo, BRAZIL.

[#]Current address: Metabolic Signaling, Institute of Bioengineering, School of Life Sciences, Ecole Polytechnique Fédérale de Lausanne, CH-1015 Lausanne, SWITZERLAND.

References

1. Zamorano JL, Lancellotti P, Muñoz DR, Aboyans V, Asteggiano R, Galderisi M, Habib G, Lenihan DJ, Lip GYH, Lyon AR, Fernandez TL, Mohty D, Piepoli MF, Tamargo J, Torbicki A, Suter TM. 2016 ESC Position Paper on cancer treatments and cardiovascular toxicity developed under the auspices of the ESC Committee for Practice Guidelines. *Eur Heart J*. 2016;37:2768–2801.
2. Cardinale D, Colombo A, Bacchiani G, Tedeschi I, Meroni CA, Veglia F, Civelli M, Lamantia G, Colombo N, Curigliano G, Fiorentini C, Cipolla CM. Early Detection of Anthracycline Cardiotoxicity and Improvement With Heart Failure Therapy. *Circulation*. 2015;131:1981–1988.
3. Lipshultz SE, Scully RE, Lipsitz SR, Sallan SE, Silverman LB, Miller TL, Barry EV, Asselin BL, Athale U, Clavell LA, Larsen E, Moghrabi A, Samson Y, Michon B, Schorin MA, Cohen HJ, Neuberg DS, Orav EJ, Colan SD. Assessment of dexrazoxane as a cardioprotectant in doxorubicin-treated children with high-risk acute lymphoblastic leukaemia: long-term follow-up of a prospective, randomised, multicentre trial. *Lancet Oncol*. 2010;11:950–961.
4. Tebbi CK, London WB, Friedman D, Villaluna D, Alarcon PAD, Constine LS, Mendenhall NP, Sposto R, Chauvenet A, Schwartz CL. Dexrazoxane-Associated Risk for Acute Myeloid Leukemia/Myelodysplastic Syndrome and Other Secondary Malignancies in Pediatric Hodgkin's Disease. *J Clin Oncol*. 2007;25:493–500.
5. Vanhaesebroeck B, Guillermet-Guibert J, Graupera M, Bilanges B. The emerging mechanisms of isoform-specific PI3K signalling. *Nat Rev Mol Cell Biol*. 2010;11:329–341.

6. Perino A, Ghigo A, Ferrero E, Morello F, Santulli G, Baillie GS, Damilano F, Dunlop AJ, Pawson C, Walser R, Levi R, Altruda F, Silengo L, Langeberg LK, Neubauer G, Heymans S, Lembo G, Wymann MP, Wetzker R, Houslay MD, Iaccarino G, Scott JD, Hirsch E. Integrating Cardiac PIP3 and cAMP Signaling through a PKA Anchoring Function of p110γ. *Mol Cell*. 2011;42:84–95.
7. Damilano F, Franco I, Perrino C, Schaefer K, Azzolino O, Carnevale D, Cifelli G, Carullo P, Ragona R, Ghigo A, Perino A, Lembo G, Hirsch E. Distinct Effects of Leukocyte and Cardiac Phosphoinositide 3-Kinase γ Activity in Pressure Overload–Induced Cardiac Failure. *Circulation*. 2011;123:391–399.
8. Kaneda MM, Messer KS, Ralainirina N, Li H, Leem C, Gorjestani S, Woo G, Nguyen AV, Figueiredo CC, Foubert P, Schmid MC, Pink M, Winkler DG, Rausch M, Palombella VJ, Kutok J, McGovern K, Frazer KA, Wu X, Karin M, Sasik R, Cohen EEW, Varner JA. PI3Kγ is a molecular switch that controls immune suppression. *Nature*. 2016;539:437–442.
9. Kaneda MM, Cappello P, Nguyen AV, Ralainirina N, Hardamon CR, Foubert P, Schmid MC, Sun P, Mose E, Bouvet M, Lowy AM, Valasek MA, Sasik R, Novelli F, Hirsch E, Varner JA. Macrophage PI3Kγ drives pancreatic ductal adenocarcinoma progression. *Cancer Discov*. 2016;6:870–85.
10. De Henau O, Rausch M, Winkler D, Campesato LF, Liu C, Cymerman DH, Budhu S, Ghosh A, Pink M, Tchaicha J, Douglas M, Tibbitts T, Sharma S, Proctor J, Kosmider N, White K, Stern H, Soglia J, Adams J, Palombella VJ, McGovern K, Kutok JL, Wolchok JD, Merghoub T. Overcoming resistance to checkpoint blockade therapy by targeting PI3Kγ in myeloid cells. *Nature*. 2016;539:443–447.

11. Patrucco E, Notte A, Barberis L, Selvetella G, Maffei A, Brancaccio M, Marengo S, Russo G, Azzolino O, Rybalkin SD, Silengo L, Altruda F, Wetzker R, Wymann MP, Lembo G, Hirsch E. PI3Kγ Modulates the Cardiac Response to Chronic Pressure Overload by Distinct Kinase-Dependent and -Independent Effects. *Cell*. 2004;118:375–387.
12. Quaglino E, Iezzi M, Mastini C, Amici A, Pericle F, Carlo ED, Pupa SM, Giovanni CD, Spadaro M, Curcio C, Lollini PL, Musiani P, Forni G, Cavallo F. Electroporated DNA Vaccine Clears Away Multifocal Mammary Carcinomas in Her-2/neu Transgenic Mice. *Cancer Res*. 2004;64:2858–2864.
13. Zhao Y, McLaughlin D, Robinson E, Harvey AP, Hookham MB, Shah AM, McDermott BJ, Grieve DJ. Nox2 NADPH Oxidase Promotes Pathologic Cardiac Remodeling Associated with Doxorubicin Chemotherapy. *Cancer Res*. 2010;70:9287–9297.
14. Winkler DG, Faia KL, DiNitto JP, Ali JA, White KF, Brophy EE, Pink MM, Proctor JL, Lussier J, Martin CM, Hoyt JG, Tillotson B, Murphy EL, Lim AR, Thomas BD, MacDougall JR, Ren P, Liu Y, Li L-S, Jessen KA, Fritz CC, Dunbar JL, Porter JR, Rommel C, Palombella VJ, Changelian PS, Kutok JL. PI3K-δ and PI3K-γ Inhibition by IPI-145 Abrogates Immune Responses and Suppresses Activity in Autoimmune and Inflammatory Disease Models. *Chem Biol*. 2013;20:1364–1374.
15. Schmid MC, Avraamides CJ, Dippold HC, Franco I, Foubert P, Ellies LG, Acevedo LM, Manglicmot JRE, Song X, Wrasidlo W, Blair SL, Ginsberg MH, Cheresh DA, Hirsch E, Field SJ, Varner JA. Receptor Tyrosine Kinases and TLR/IL1Rs Unexpectedly Activate Myeloid Cell PI3Kγ, A Single Convergent Point Promoting Tumor Inflammation and Progression. *Cancer Cell*. 2011;19:715–727.

16. Ghigo A, Perino A, Mehel H, Zahradníková A, Morello F, Leroy J, Nikolaev VO, Damilano F, Cimino J, Luca ED, Richter W, Westenbroek R, Catterall WA, Zhang J, Yan C, Conti M, Gomez AM, Vandecasteele G, Hirsch E, Fischmeister R. Phosphoinositide 3-Kinase γ Protects Against Catecholamine-Induced Ventricular Arrhythmia Through Protein Kinase A–Mediated Regulation of Distinct Phosphodiesterases. *Circulation*. 2012;126:2073–2083.
17. Oka T, Hikoso S, Yamaguchi O, Taneike M, Takeda T, Tamai T, Oyabu J, Murakawa T, Nakayama H, Nishida K, Akira S, Yamamoto A, Komuro I, Otsu K. Mitochondrial DNA that escapes from autophagy causes inflammation and heart failure. *Nature*. 2012;485:251–255.
18. Zaglia T, Milan G, Franzoso M, Bertaggia E, Pianca N, Piasentini E, Voltarelli VA, Chiavegato D, Brum PC, Glass DJ, Schiaffino S, Sandri M, Mongillo M. Cardiac sympathetic neurons provide trophic signal to the heart via β2-adrenoceptor-dependent regulation of proteolysis. *Cardiovasc Res*. 2013;97:240–250.
19. Zaglia T, Di Bona A, Chioato T, Basso C, Ausoni S, Mongillo M. Optimized protocol for immunostaining of experimental GFP-expressing and human hearts. *Histochem Cell Biol*. 2016;146:407–419.
20. Xiao DY, Luo S, O'Brian K, Liu W, Carson KR. Weight change trends and overall survival in United States veterans with follicular lymphoma treated with chemotherapy. *Leuk Lymphoma*. 2017;58:851–858.
21. Awad S, Tan BH, Cui H, Bhalla A, Fearon KCH, Parsons SL, Catton JA, Lobo DN. Marked changes in body composition following neoadjuvant chemotherapy for oesophagogastric cancer. *Clin Nutr*. 2012;31:74–77.

22. Ghigo A, Li M, Hirsch E. New signal transduction paradigms in anthracycline-induced cardiotoxicity. *Biochim Biophys Acta BBA - Mol Cell Res*. 2016;1863:1916–1925.

23. Yu X, Long YC, Shen H-M. Differential regulatory functions of three classes of phosphatidylinositol and phosphoinositide 3-kinases in autophagy. *Autophagy*. 2015;11:1711–1728.

24. Nakai A, Yamaguchi O, Takeda T, Higuchi Y, Hikoso S, Taniike M, Omiya S, Mizote I, Matsumura Y, Asahi M, Nishida K, Hori M, Mizushima N, Otsu K. The role of autophagy in cardiomyocytes in the basal state and in response to hemodynamic stress. *Nat Med*. 2007;13:619–624.

25. Zaglia T, Milan G, Ruhs A, Franzoso M, Bertaggia E, Pianca N, Carpi A, Carullo P, Pesce P, Sacerdoti D, Sarais C, Catalucci D, Krüger M, Mongillo M, Sandri M. Atrogin-1 deficiency promotes cardiomyopathy and premature death via impaired autophagy. *J Clin Invest*. 2014;124:2410–2424.

26. Li DL, Wang ZV, Ding G, Tan W, Luo X, Criollo A, Xie M, Jiang N, May H, Kyrychenko V, Schneider JW, Gillette TG, Hill JA. Doxorubicin Blocks Cardiomyocyte Autophagic Flux by Inhibiting Lysosome Acidification. *Circulation*. 2016;133:1668–87.

27. Bartlett JJ, Trivedi PC, Yeung P, Kienesberger PC, Pulinilkunnil T. Doxorubicin Impairs Cardiomyocyte Viability by Suppressing Transcription Factor EB Expression and Disrupting Autophagy. *Biochem J*. 2016;473:3769–3789.

28. Ikeda Y, Shirakabe A, Maejima Y, Zhai P, Sciarretta S, Toli J, Nomura M, Mihara K, Egashira K, Ohishi M, Abdellatif M, Sadoshima J. Endogenous Drp1 Mediates Mitochondrial Autophagy and Protects the Heart Against Energy Stress. *Circ Res*. 2015;116:264–278.

29. Hoshino A, Mita Y, Okawa Y, Ariyoshi M, Iwai-Kanai E, Ueyama T, Ikeda K, Ogata T, Matoba S. Cytosolic p53 inhibits Parkin-mediated mitophagy and promotes mitochondrial dysfunction in the mouse heart. *Nat Commun*. 2013;4:2308.

30. Luo L, Wall AA, Yeo JC, Condon ND, Norwood SJ, Schoenwaelder S, Chen KW, Jackson S, Jenkins BJ, Hartland EL, Schroder K, Collins BM, Sweet MJ, Stow JL. Rab8a interacts directly with PI3Kγ to modulate TLR4-driven PI3K and mTOR signalling. *Nat Commun*. 2014;5:4407.

31. Bohnacker T, Marone R, Collmann E, Calvez R, Hirsch E, Wymann MP. PI3Kγ Adaptor Subunits Define Coupling to Degranulation and Cell Motility by Distinct PtdIns(3,4,5)P3 Pools in Mast Cells. *Sci Signal*. 2009;2:ra27-ra27.

32. De Leo MG, Staiano L, Vicinanza M, Luciani A, Carissimo A, Mutarelli M, Di Campli A, Polishchuk E, Di Tullio G, Morra V, Levtchenko E, Oltrabella F, Starborg T, Santoro M, di Bernardo D, Devuyst O, Lowe M, Medina DL, Ballabio A, De Matteis MA. Autophagosome-lysosome fusion triggers a lysosomal response mediated by TLR9 and controlled by OCRL. *Nat Cell Biol*. 2016;18:839–850.

33. Nazio F, Strappazzon F, Antonioli M, Bielli P, Cianfanelli V, Bordi M, Gretzmeier C, Dengjel J, Piacentini M, Fimia GM, Cecconi F. mTOR inhibits autophagy by controlling ULK1 ubiquitylation, self-association and function through AMBRA1 and TRAF6. *Nat Cell Biol*. 2013;15:406–416.

34. Lamb CA, Yoshimori T, Tooze SA. The autophagosome: origins unknown, biogenesis complex. *Nat Rev Mol Cell Biol*. 2013;14:759–774.

35. Štěrba M, Popelová O, Vávrová A, Jirkovský E, Kovaříková P, Geršl V, Šimůnek T. Oxidative Stress, Redox Signaling, and Metal Chelation in Anthracycline Cardiotoxicity and Pharmacological Cardioprotection. *Antioxid Redox Signal*. 2012;18:899–929.

36. Ali K, Soond DR, Piñeiro R, Hagemann T, Pearce W, Lim EL, Bouabe H, Scudamore CL, Hancox T, Maecker H, Friedman L, Turner M, Okkenhaug K, Vanhaesebroeck B. Inactivation of PI(3)K p110δ breaks regulatory T-cell-mediated immune tolerance to cancer. *Nature*. 2014;510:407–411.

37. Mantovani A, Marchesi F, Malesci A, Laghi L, Allavena P. Tumour-associated macrophages as treatment targets in oncology. *Nat Rev Clin Oncol*. 2017;14:399–416.

38. Mantovani A, Sozzani S, Locati M, Allavena P, Sica A. Macrophage polarization: tumor-associated macrophages as a paradigm for polarized M2 mononuclear phagocytes. *Trends Immunol*. 2002;23:549–555.

39. Zhang S, Liu X, Bawa-Khalfe T, Lu L-S, Lyu YL, Liu LF, Yeh ETH. Identification of the molecular basis of doxorubicin-induced cardiotoxicity. *Nat Med*. 2012;18:1639–1642.

40. Ichikawa Y, Ghanefar M, Bayeva M, Wu R, Khechaduri A, Prasad SVN, Mutharasan RK, Naik TJ, Ardehali H. Cardiotoxicity of doxorubicin is mediated through mitochondrial iron accumulation. *J Clin Invest*. 2014;124:617–630.

41. Oudit GY, Crackower MA, Eriksson U, Sarao R, Kozieradzki I, Sasaki T, Irie-Sasaki J, Gidrewicz D, Rybin VO, Wada T, Steinberg SF, Backx PH, Penninger JM. Phosphoinositide 3-Kinase γ–Deficient Mice Are Protected From Isoproterenol-Induced Heart Failure. *Circulation*. 2003;108:2147–2152.

42. Siragusa M, Katare R, Meloni M, Damilano F, Hirsch E, Emanueli C, Madeddu P. Involvement of Phosphoinositide 3-Kinase γ in Angiogenesis and Healing of Experimental Myocardial Infarction in Mice. *Circ Res*. 2010;106:757–768.
43. Bartlett JJ, Trivedi PC, Pulinilkunnil T. Autophagic dysregulation in doxorubicin cardiomyopathy. *J Mol Cell Cardiol*. 2017;104:1–8.
44. Koleini N, Kardami E, Koleini N, Kardami E. Autophagy and mitophagy in the context of doxorubicin-induced cardiotoxicity. *Oncotarget*. 2017;doi: 10.18632/oncotarget.16944.
45. Kawaguchi T, Takemura G, Kanamori H, Takeyama T, Watanabe T, Morishita K, Ogino A, Tsujimoto A, Goto K, Maruyama R, Kawasaki M, Mikami A, Fujiwara T, Fujiwara H, Minatoguchi S. Prior starvation mitigates acute doxorubicin cardiotoxicity through restoration of autophagy in affected cardiomyocytes. *Cardiovasc Res*. 2012;96:456–465.
46. Chen Y-R, Zweier JL. Cardiac Mitochondria and Reactive Oxygen Species Generation. *Circ Res*. 2014;114:524–537.
47. Wymann MP, Zvelebil M, Laffargue M. Phosphoinositide 3-kinase signalling – which way to target? *Trends Pharmacol Sci*. 2003;24:366–376.
48. Billingham ME, Mason JW, Bristow MR, Daniels JR. Anthracycline cardiomyopathy monitored by morphologic changes. *Cancer Treat Rep*. 1978;62:865–872.
49. Krischer JP, Epstein S, Cuthbertson DD, Goorin AM, Epstein ML, Lipshultz SE. Clinical cardiotoxicity following anthracycline treatment for childhood cancer: the Pediatric Oncology Group experience. *J Clin Oncol*. 1997;15:1544–1552.
50. Rochette L, Guenancia C, Gudjoncik A, Hachet O, Zeller M, Cottin Y, Vergely C. Anthracyclines/trastuzumab: new aspects of cardiotoxicity and molecular mechanisms. *Trends Pharmacol Sci*. 2015;36:326–348.

51. Evans CA, Liu T, Lescarbeau A, Nair SJ, Grenier L, Pradeilles JA, Glenadel Q, Tibbitts T, Rowley AM, DiNitto JP, Brophy EE, O'Hearn EL, Ali JA, Winkler DG, Goldstein SI, O'Hearn P, Martin CM, Hoyt JG, Soglia JR, Cheung C, Pink MM, Proctor JL, Palombella VJ, Tremblay MR, Castro AC. Discovery of a Selective Phosphoinositide-3-Kinase (PI3K)-γ Inhibitor (IPI-549) as an Immuno-Oncology Clinical Candidate. *ACS Med Chem Lett*. 2016;7:862–867.

Figures

Figure 1. Genetic inhibition of PI3Kγ protects against DOX-induced cardiotoxicity. WT and KD mice were treated with a cumulative dose of 12 mg/kg doxorubicin (DOX) or saline via 3 weekly injections (4 mg/kg on days 0, 7 and 14). (**A**) Representative M-mode echocardiographic images (left) and fractional shortening (right) of WT (n=9) and KD (n=9) hearts before treatment and 6 weeks after the first DOX injection. White and cyan lines indicate left ventricular end-diastolic diameter (LVEDD) and left ventricular end-systolic diameter (LVESD), respectively. Scale bars, 400 ms, 4 mm. DOX 0 vs 6 weeks: ###*P*<0.001 and WT vs KD: ***P<0.001 by two-way repeated-measures ANOVA with Bonferroni's post-hoc test. (**B**) Plasma troponin T (TnT) level in WT and KD mice 3 days after the first dose of DOX or saline. (**C**) Relative quantification of *Anf* and *Bnp* mRNA levels in WT and KD whole hearts at 6 weeks after the first dose of DOX or saline. (**D**) Representative images of H&E staining and relative quantification of cardiomyocyte area in heart sections from mice treated as in (**C**). Scale bar, 20 μm. (**E**) Representative images of TUNEL staining (left) and quantification of TUNEL positive nuclei per field (right) in WT and KD in heart sections from mice treated as in (**C**). Scale bar, 30 μm. (**F**) Immunoblot (upper) and relative quantification (lower) of cleaved-caspase 9 in whole hearts from WT and KD mice treated as in (**C**). (**G**) Representative images of PicroSirius Red staining (left) and relative quantification of collagen deposition (right) in heart sections from animals treated as in (**C**). Scale bar, 50 μm. (**H**) Relative quantification of mRNA levels of pro-fibrotic genes (*Tgfb, Ctgf, Col1a1* and *Col3a1*) in whole hearts from animals treated as in (**C**). For each panel in (**B-H**), n=5-7 animals/group, DOX (+) vs saline (-): #*P*<0.05, ##*P*<0.01 and

###$P<0.001$ and WT vs KD: *$P<0.05$, **$P<0.01$ and ***$P<0.001$ by two-way ANOVA with Bonferroni's post-hoc test. Values represent mean ± SEM.

Figure 2. PI3Kγ inhibition promotes cardiac autophagy. (**A**-**B**) Representative immunoblot (left) and relative quantification (right) of the autophagic marker LC3 in WT and KD hearts 3 days (**A**) and 6 weeks (**B**) after DOX. n=5-8 animals/group. **A** through **B**, DOX (+) vs saline (-): #*P*<0.05 and ###*P*<0.001 and WT vs KD: **P*<0.05 and ***P*<0.01 by two-way ANOVA with Bonferroni's post-hoc test. (**C**) Autophagic flux analysis in WT and KD mice pre-treated with Bafilomycin A1 (BafA1, 10 mg/kg) 1 hour before a single DOX injection (4 mg/kg) for 6 hours. Representative immunoblots (left) and relative quantification (right) are shown. (**D**) Immunofluorescence staining (left) and relative quantification (right) of LC3 puncta in heart sections from animals treated as in (**C**). Scale bar, 10 μm. **C** through **D**, n=5-6 animals/group, DOX+saline (-) vs DOX+BafA1 (+): #*P*<0.05 and ###*P*<0.001 and WT vs KD: ***P*<0.01 by two-way ANOVA with Bonferroni's post-hoc test. (**E**) WT and KD NMVMs were infected with an adenovirus encoding the tandem fluorescent mRFP-GFP-LC3 probe, before treatment with DOX (1 μM, 16 hours). Representative pictures (left, magnification of Supplementary Fig. 3B) and relative quantification (right) of autophagosomes (yellow dots) and autolysosomes (red free dots) are shown. Scale bar, 2 μm. n≥4 independent experiments. DOX vs Vehicle: ##*P*<0.01 and ###*P*<0.001 and WT vs KD: ***P*<0.01 and ****P*<0.001 by two-way ANOVA with Bonferroni's post-hoc test. Values represent mean ± SEM.

Figure 3. PI3Kγ inhibition promotes autophagic clearance of damaged mitochondria. (**A**) Transmission electron micrographs of WT and KD hearts 3 days after a single injection of doxorubicin (DOX; 4 mg/kg). Scale bar, 1 μm. Black arrows and magnification insets show autophagic vacuoles containing damaged mitochondria. (**B**) Double staining of mitochondrial DNA (mtDNA) with PicoGreen (green) and autophagosomes with an anti-LC3 antibody (red), in heart sections from WT and KD mice treated as in (**A**). In merged images and magnification insets, arrows indicate double positive deposits (yellow dots). Scale bar, 10 μm. In (**A**) and (**B**), representative pictures from n = 3 experiments are shown.

Figure 4. mtDNA, PI3Kγ and TLR-9 colocalize in autolysosomes. (**A**) Double staining of mitochondrial DNA (mtDNA) and either TLR9 (red, upper panel) or PI3Kγ (red, bottom panel) in neonatal mouse ventricular myocytes (NMVMs) treated with doxorubicin (DOX, 1 μM) for 1 hour. Arrows indicate colocalization of mtDNA with either TLR9 or PI3Kγ. DOX has an intrinsic red fluorescence on nuclei. (**B**) Double staining of TLR9 (green) and PI3Kγ (red) in NMVMs treated with vehicle or a CpG-rich oligonucleotide similar to mtDNA, ODN1826 (0.2 μM; 1 hour). (**C**) Representative immunoblot (left) and relative quantification (right) of PI3Kγ bound to TLR9 in HEK-293 cells transfected with TLR9-YFP and/or PI3Kγ and treated with the TLR9 agonist ODN1826. Values represent mean ± SEM, n ⩾ 4 independent experiments, **P<0.01 by one-way ANOVA with Bonferroni's post-hoc test. (**D**) Double staining of either TRL9 (green) or PI3Kγ (green) with the autolysosomal marker LAMP2 (red) in NMVMs treated with ODN1826 (0.2 μM; 1 hour). **A**， **B** and **D**: Right panels show enlargements of the outlined areas and fluorescence intensity profiles in the green and red channels of the regions underneath the white lines. Scale bar, 5 μm. Representative pictures from n = 3 experiments are shown.

Figure 5. DOX activates a TLR9/PI3Kγ/Akt/Ulk1 pathway promoting feedback inhibition of autophagy. (**A**) WT and KD neonatal mouse ventricular myocytes (NMVMs) were treated with DOX (1 μM) for 1 hour, alone or in combination with the PI3Kγ inhibitor AS605240 (AS; 0.5 μM, 1-hour pretreatment) or with the TLR9 antagonist ODN2088 (0.2 μM, 5-hour pretreatment). Alternatively, NMVMs were stimulated with TLR9 agonist ODN1826 (0.2 μM) for 1 hour. Representative immunoblot (left) and relative quantification (right) of Akt phosphorylation on Thr308 (T308) and Ser473 (S473) residues are shown. DOX/ODN1826 vs Vehicle: ##P<0.01 and ###P<0.001 and DOX+ODN2088/AS vs DOX: **P<0.01 and ***P<0.001 by one-way ANOVA with Bonferroni's post-hoc test. n≥4 independent experiments. Values represent mean ± SEM. (**B**) Immunohistochemical analysis of the phosphorylation status of Akt (S473), mTOR (S2448) and Ulk1 (S757) in WT and KD hearts 3 days after a single injection of saline or doxorubicin (DOX; 4 mg/kg), alone or in combination with the TLR9 antagonist ODN2088 (100 μg/mouse). Scale bar, 100 μm. Representative pictures from n = 3 experiments are shown.

Figure 6. Genetic and pharmacological inhibition of autophagy abolishes cardioprotection in PI3Kγ KD mice. (**A**-**C**) PI3Kγ KD mice were transduced with an adeno-associated viral vector (AAV9) encoding GFP and either a small hairpin RNA (sh) against the *Atg7* gene (ATG7sh) or a control sh (CTRLsh), and treated with vehicle or doxorubicin (DOX, 4 mg/kg on days 0, 7 and 14). (**A**) Fractional shortening before and 4 weeks after the first DOX injection is shown. 0 vs 4 weeks: ###*P*<0.001; ATG7sh DOX vs either CTRLsh DOX or ATG7sh saline: **P<0.01 and ***P<0.001 by two-way repeated-measures ANOVA with Bonferroni's post-hoc test. ATG7sh n=9; CTRLsh DOX n=9 and ATG7sh DOX n=9. (**B**) Representative images of dystrophin and GFP staining in heart sections from KD mice treated as described in (**A**). Scale bar, 10 μm. (**C**) Quantification of the area of GFP-positive (GFP+ CMs) and -negative cardiomyocytes (GFP- CMs) in sections as shown in (**B**). GFP+ CMs vs GFP- CMs: ###*P*<0.001; ATG7sh DOX vs either ATG7sh or CTRLsh DOX: ***P<0.001 by two-way ANOVA with Bonferroni's post-hoc test. (**D**-**G**) KD mice were treated with doxorubicin (DOX, 4 mg/kg on days 0, 7 and 14; n=7), hydroxychloroquine (HCQ, 60 mg/kg daily from day 0 to 28; n=7) or a combination of DOX and HCQ (n=9). (**D**) Fractional shortening before and 4 weeks after the first DOX injection is shown. Before vs after the treatment: ##*P*<0.01 and DOX+HCQ vs single treatments (DOX or HCQ): *P<0.05 by two-way repeated-measures ANOVA with Bonferroni's post-hoc test. (**E**) Representative images of H&E staining (left) and quantification of cardiomyocyte area (right) in KD hearts 4 weeks after the first dose of DOX or saline. Scale bar, 20 μm. (**F**) Representative images of TUNEL staining (left) and quantification of TUNEL positive nuclei per field (right) in KD whole hearts treated as in (**D**). Scale bar, 30 μm. (**G**) Representative images of PicroSirius Red staining (left) and relative quantification of collagen deposition (right) in heart sections from KD animals treated as in (**D**). Scale bar, 50 μm. **E**

through **G**, DOX+HCQ vs single treatments (DOX or HCQ): **P*<0.05, **P<0.01 and ****P*<0.001, and DOX vs Saline: #*P*<0.05 by two-way ANOVA with Bonferroni's post-hoc test. Values represent mean ± SEM.

Figure 7. PI3Kγ inhibition potentiates the anti-cancer activity of DOX by restoring anti-tumor immune responses. (**A**) Tumor growth in WT and KD mice injected with 1×10^5 4T1 breast cancer cells, and treated with a cumulative dose of doxorubicin (DOX, 12 mg/kg) or saline via 3 weekly injections (4 mg/kg on days 0, 7 and 14). n=12-20 animals/group. Saline vs DOX: ###*P*<0.001 and WT vs KD: ***P<0.001 by two-way repeated-measures ANOVA with Bonferroni's post-hoc test. (**B**) Representative immunofluorescence staining from n=3 experiments of the myeloid marker CD11b in 4T1 tumors from WT and KD mice treated as in (**A**). Scale bar, 30 μm. (**C**) Representative FACS plots (left) and relative quantification (right) of $Gr1^{low}F4/80^{hi}$ (anti-tumor) and $Gr1^{int}F4/80^{low}$ (pro-tumor) macrophages in 4T1 tumors from mice treated as in (**A**). (**D-E**) Representative FACS plots (left) and relative quantification (right) of $CD206^+$ pro-tumor macrophages (**D**), characterized by low MHC-II expression ($CD206^+MHC^{low}$) (**E**) in 4T1 tumors from mice treated as in (**A**). (**F**) Relative mRNA expression of anti-tumor and pro-tumor cytokines in 4T1 tumors from mice treated as in (**A**). (**G**) Representative immunofluorescence images (left) and relative quantification (right) of $CD8^+$ T cells in 4T1 tumors from mice treated as in (**A**). Scale bar, 30 μm. **C** through **G**, n=5-8 animals/group. **C** and **E**, *P<0.05 by two-way ANOVA with Bonferroni's post-hoc test. **D, F** and **G** *P<0.05 and **P<0.01 by Student's t-test. Values represent mean ± SEM.

Figure 8. Pharmacological inhibition of PI3Kγ simultaneously prevents cardiomyopathy and tumor growth under DOX treatment. (**A**) PI3Kγ staining in human heart sections from a healthy donor (left) and a patient who developed cardiomyopathy after doxorubicin (DOX) treatment (right) (details in Online Supplementary Methods). Right panels show enlargements of the outlined areas. Scale bar, 50 μm. (**B-C**) WT and KD mice were injected with 1×10^5 4T1 breast cancer cells, and treated with doxorubicin (DOX) or saline via 3 weekly injections (4 mg/kg on days 0, 7 and 14). The PI3Kγ inhibitor IPI145 or vehicle was administered daily for 3 weeks since the first DOX injection. (**B**) Tumor growth is shown. Animals/group: Vehicle n=6, IPI145 n=6, DOX n=12, IPI145+DOX n=12. DOX vs Vehicle: ###*P*<0.001; IPI145 vs Vehicle: ***P<0.001; DOX+IPI145 vs DOX: †††P<0.001; DOX+IPI145 vs IPI145: §§§P<0.001 by two-way repeated-measures ANOVA with Bonferroni's post-hoc test. (**C**) Fractional shortening of animals treated with Vehicle+DOX (n=12) and IPI145+DOX (n=12). 0 vs 4 weeks after DOX: #P<0.05 and Vehicle vs IPI145: **P<0.01 by two-way repeated-measures ANOVA with Bonferroni's post-hoc test. Values represent mean ± SEM. (**D-F**) Her2/NeuT transgenic mice bearing spontaneous tumors (2 mm in mean diameter) were administered with saline or DOX as above, together with daily treatment with vehicle or the PI3Kγ inhibitor AS605240 (AS) for 3 weeks since the first DOX injection. (**D**) Growth curve of Her2/NeuT tumors in all mammary glands. Mean tumor volume per mammary gland is shown. Animals/group: Vehicle n=6, AS605240 n=6, DOX n=16, AS605240+DOX n=15. DOX vs Vehicle: ###*P*<0.001; AS605240 vs Vehicle: ***P<0.001; DOX+AS605240 vs DOX: †††P<0.001; DOX+ AS605240 vs AS605240: §§§P<0.001 by two-way repeated-measures ANOVA with Bonferroni's post-hoc test. (**E**) Fractional shortening of Her2/NeuT mice treated with Vehicle+DOX (n=8) or AS605240+DOX (n=8). 0 vs 4 weeks after DOX: ##*P*<0.01 and Vehicle vs AS605240: *P<0.01

by two-way repeated-measures ANOVA with Bonferroni's post-hoc test. Values represent mean ± SEM. (**F**) Kaplan-Meier survival curves of Her2/NeuT mice treated with Vehicle+DOX (n=16) and AS605240+DOX (n=15). Arrows indicate DOX injections. Log-rank test was used for statistical analysis. (**G**) Schematic representation of the diverse function of PI3Kγ in cardiomyocytes and in tumor-associated macrophages during anthracycline therapy. (Left) In the heart, DOX-damaged mitochondrial DNA activates autolysosomal TLR9/PI3Kγ pathway and engages feedback inhibition of autophagy, resulting in accumulation of damaged mitochondria and cardiotoxicity. (Right) In tumor microenvironment, macrophage PI3Kγ mediates pro-tumoral inflammation and promotes tumor growth.

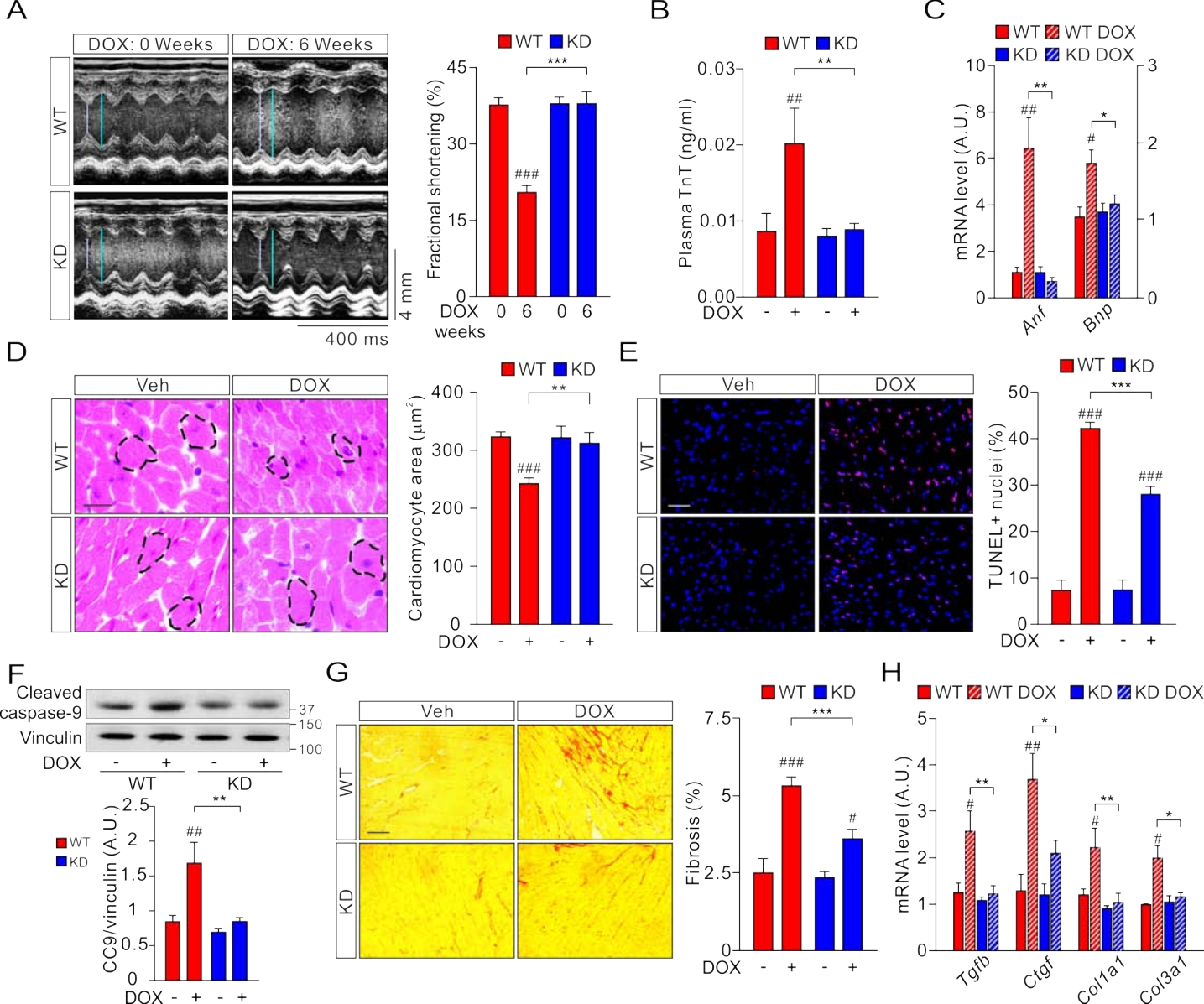
A
DOX: 0 Weeks
DOX: 6 Weeks
WT
KD
4 mm
400 ms
WT KD
Fractional shortening (%)
45
30
15
0
***
###
DOX 0 6 0 6
weeks
B
WT KD
Plasma TnT (ng/ml)
0.03
0.02
0.01
0.00
**
##
DOX - + - +
C
WT WT DOX
KD KD DOX
mRNA level (A.U.)
10
8
6
4
2
0
3
2
1
0
**
##
*
#
Anf
Bnp
D
Veh
DOX
WT
KD
WT KD
Cardiomyocyte area (μm²)
400
300
200
100
0
**
###
DOX - + - +
E
Veh
DOX
WT
KD
WT KD
TUNEL+ nuclei (%)
50
40
30
20
10
0
***
###
###
DOX - + - +
F
Cleaved caspase-9
Vinculin
37
150
100
DOX - + - +
WT
KD
WT KD
CC9/vinculin (A.U.)
2.5
2
1.5
1
0.5
0
**
##
DOX - + - +
G
Veh
DOX
WT
KD
WT KD
Fibrosis (%)
7.5
5
2.5
0
***
###
#
DOX - + - +
H
WT WT DOX
KD KD DOX
mRNA level (A.U.)
5
4
3
2
1
0
**
#
*
##
**
#
*
#
Tgfb
Ctgf
Col1a1
Col3a1

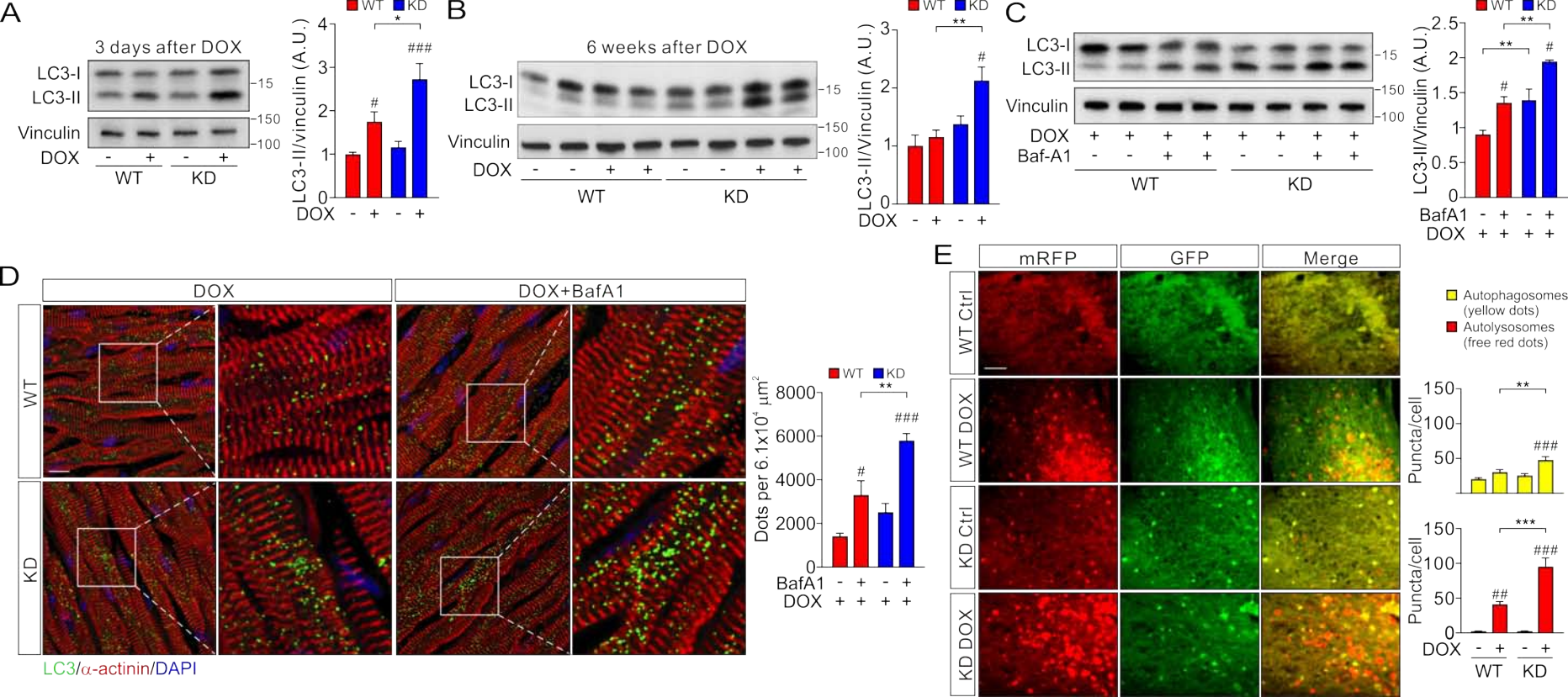
A
3 days after DOX
LC3-I
LC3-II
Vinculin
DOX
WT
KD
LC3-II/vinculin (A.U.)
B
6 weeks after DOX
C
Baf-A1
BafA1
D
DOX
DOX+BafA1
LC3/α-actinin/DAPI
Dots per 6.1x10⁴ μm²
E
mRFP
GFP
Merge
WT Ctrl
WT DOX
KD Ctrl
KD DOX
Autophagosomes (yellow dots)
Autolysosomes (free red dots)
Puncta/cell

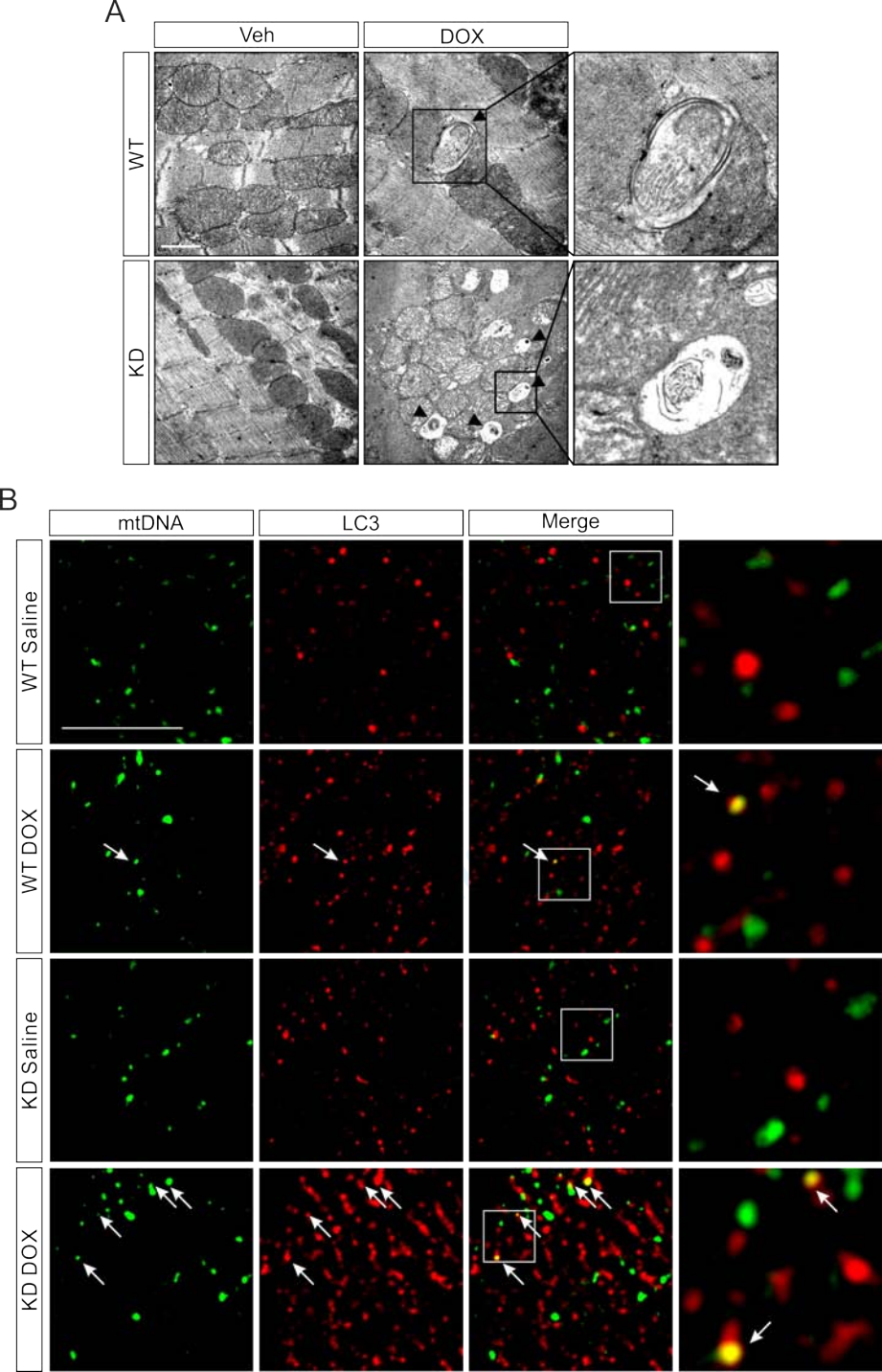
A
Veh
DOX
WT
KD
B
mtDNA
LC3
Merge
WT Saline
WT DOX
KD Saline
KD DOX

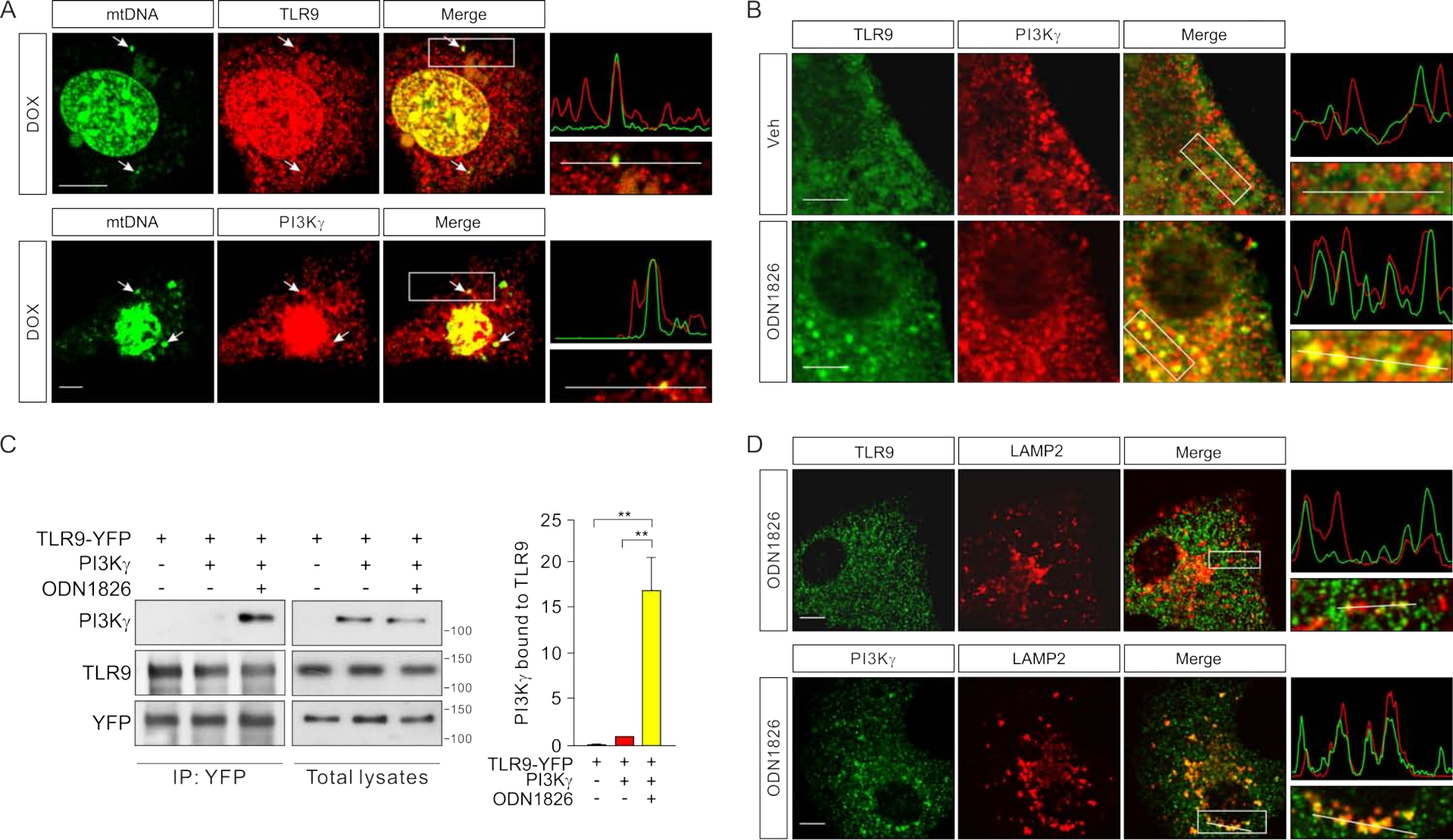
A
mtDNA
TLR9
Merge
DOX
mtDNA
PI3Kγ
Merge
DOX
B
TLR9
PI3Kγ
Merge
Veh
ODN1826
C
TLR9-YFP + + + + + +
PI3Kγ - + + - + +
ODN1826 - - + - - +
PI3Kγ
TLR9
YFP
100
150
100
150
100
IP: YFP
Total lysates
PI3Kγ bound to TLR9
25
20
15
10
5
0
**
**
TLR9-YFP + + +
PI3Kγ - + +
ODN1826 - - +
D
TLR9
LAMP2
Merge
ODN1826
PI3Kγ
LAMP2
Merge
ODN1826

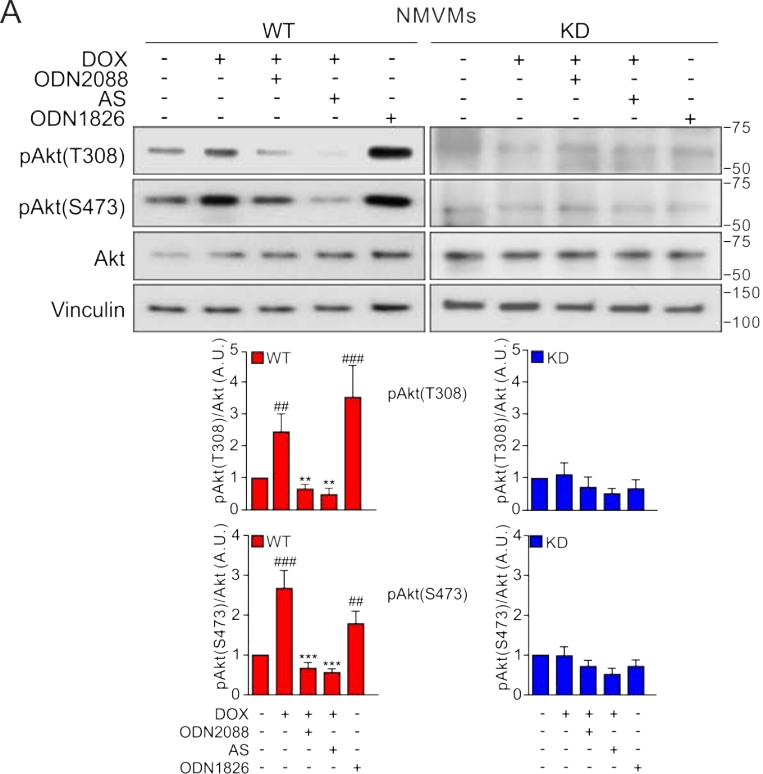
A
NMVMs
WT
KD
DOX
ODN2088
AS
ODN1826
pAkt(T308)
pAkt(S473)
Akt
Vinculin
75
50
75
50
75
50
150
100
WT
KD
pAkt(T308)/Akt (A.U.)
pAkt(S473)/Akt (A.U.)
pAkt(T308)
pAkt(S473)
##
###
**
***

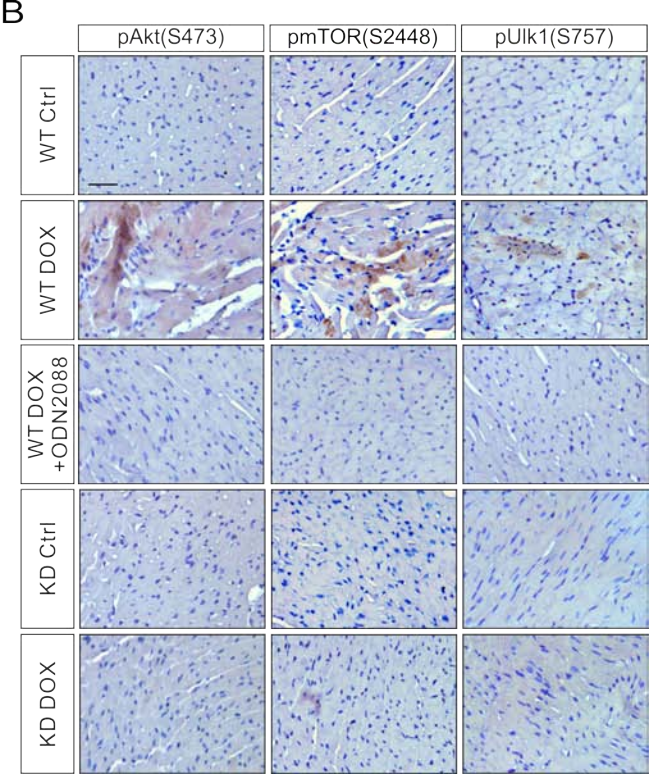
B
pAkt(S473)
pmTOR(S2448)
pUlk1(S757)
WT Ctrl
WT DOX
WT DOX +ODN2088
KD Ctrl
KD DOX

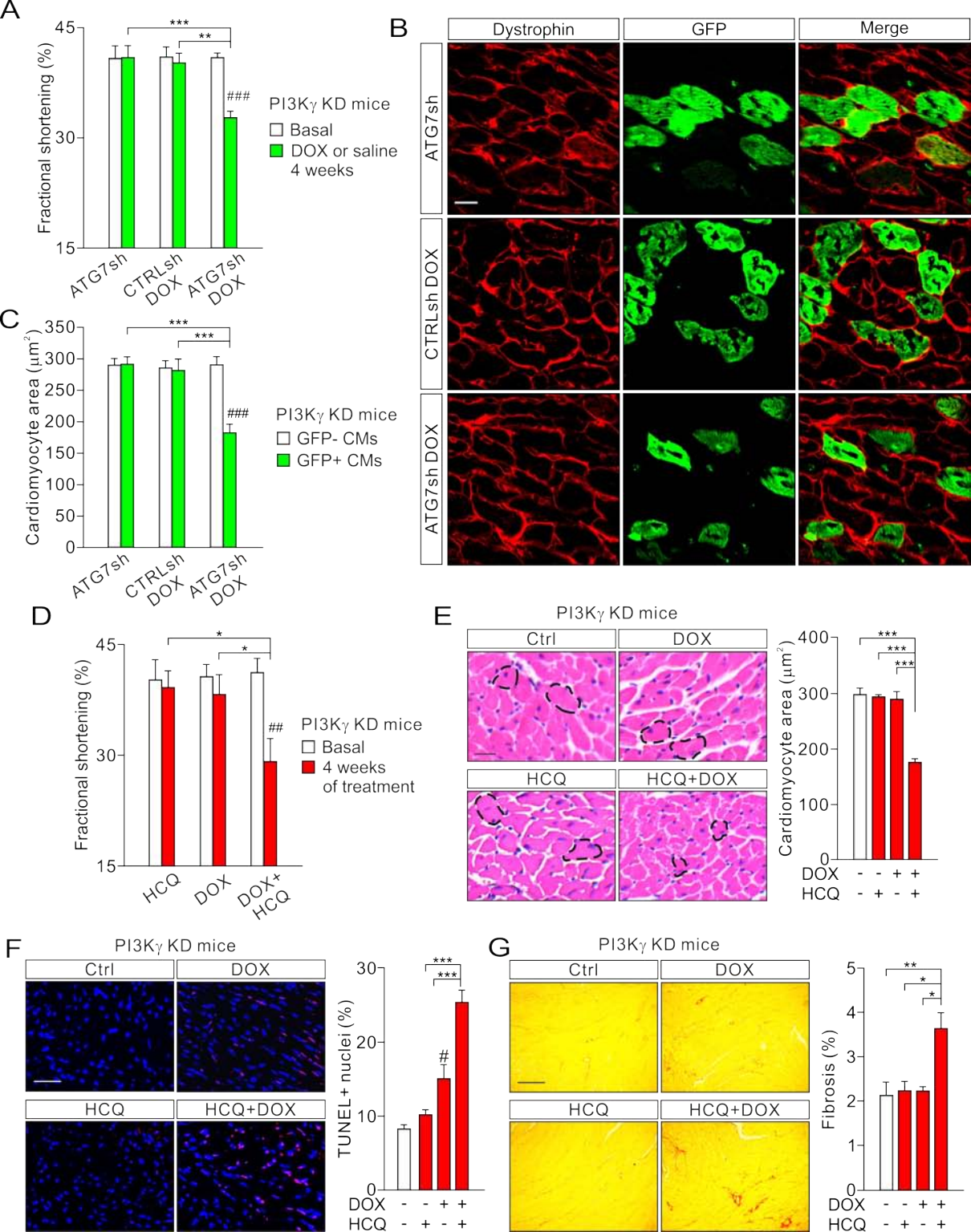
A
Fractional shortening (%)
45
30
15
***
**
###
PI3Kγ KD mice
Basal
DOX or saline
4 weeks
ATG7sh
CTRLsh DOX
ATG7sh DOX
B
Dystrophin
GFP
Merge
ATG7sh
CTRLsh DOX
ATG7sh DOX
C
Cardiomyocyte area (μm²)
350
300
250
200
150
100
50
0
***
***
###
PI3Kγ KD mice
GFP- CMs
GFP+ CMs
ATG7sh
CTRLsh DOX
ATG7sh DOX
D
Fractional shortening (%)
45
30
15
*
*
##
PI3Kγ KD mice
Basal
4 weeks
of treatment
HCQ
DOX
DOX+ HCQ
E
PI3Kγ KD mice
Ctrl
DOX
HCQ
HCQ+DOX
Cardiomyocyte area (μm²)
400
300
200
100
0
***
***
***
DOX - - + +
HCQ - + - +
F
PI3Kγ KD mice
Ctrl
DOX
HCQ
HCQ+DOX
TUNEL+ nuclei (%)
30
20
10
0
***
***
#
DOX - - + +
HCQ - + - +
G
PI3Kγ KD mice
Ctrl
DOX
HCQ
HCQ+DOX
Fibrosis (%)
5
4
3
2
1
0
**
*
*
DOX - - + +
HCQ - + - +

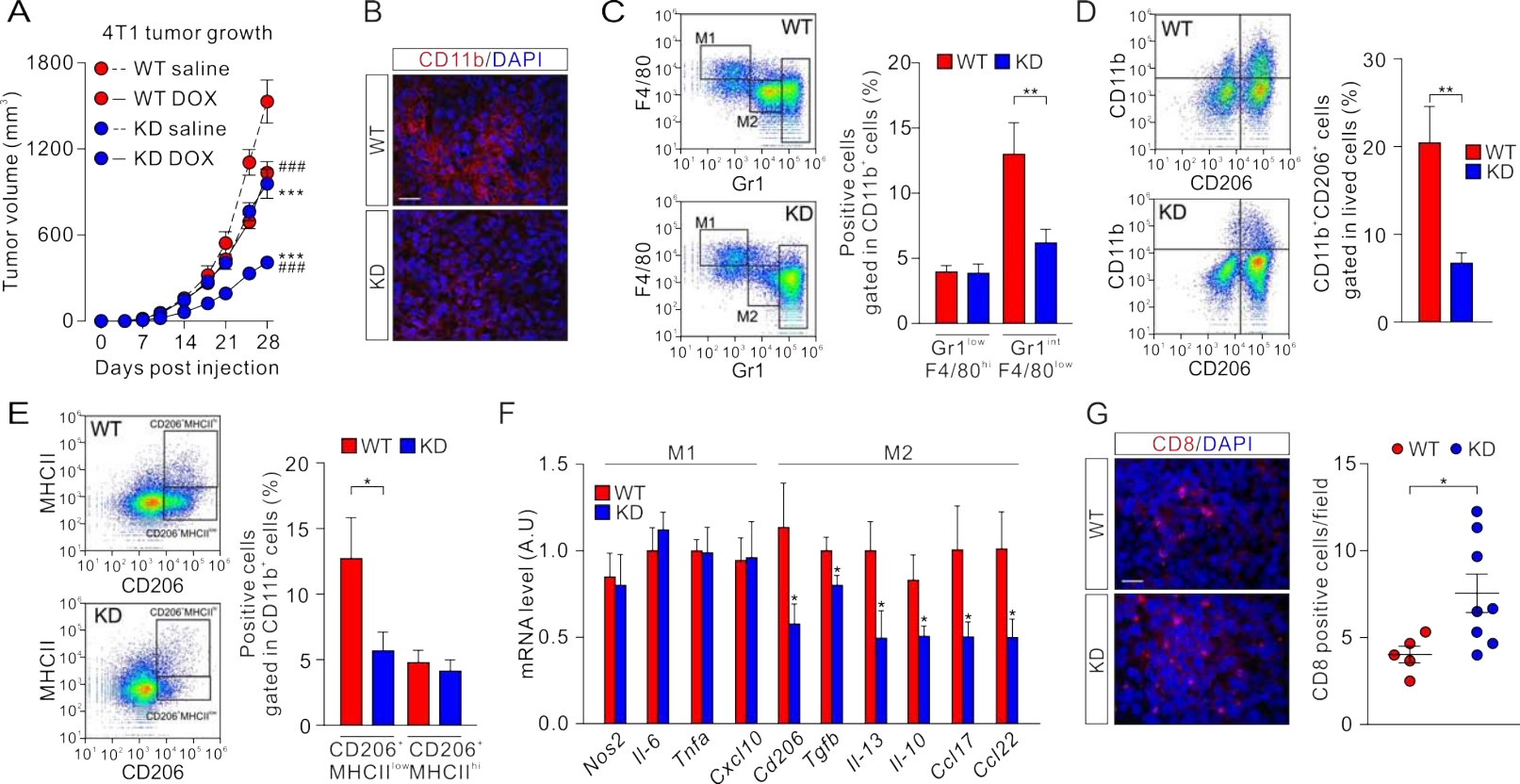
A
4T1 tumor growth
WT saline
WT DOX
KD saline
KD DOX
Tumor volume (mm3)
Days post injection
B
CD11b/DAPI
WT
KD
C
WT
KD
F4/80
Gr1
M1
M2
Positive cells gated in CD11b+ cells (%)
Gr1low F4/80hi
Gr1int F4/80low
D
CD11b
CD206
CD11b+CD206+ cells gated in lived cells (%)
E
MHCII
CD206
CD206+MHCIIhi
CD206+MHCIIlow
F
M1
M2
mRNA level (A.U)
Nos2
Il-6
Tnfa
Cxcl10
Cd206
Tgfb
Il-13
Il-10
Ccl17
Ccl22
G
CD8/DAPI
CD8 positive cells/field

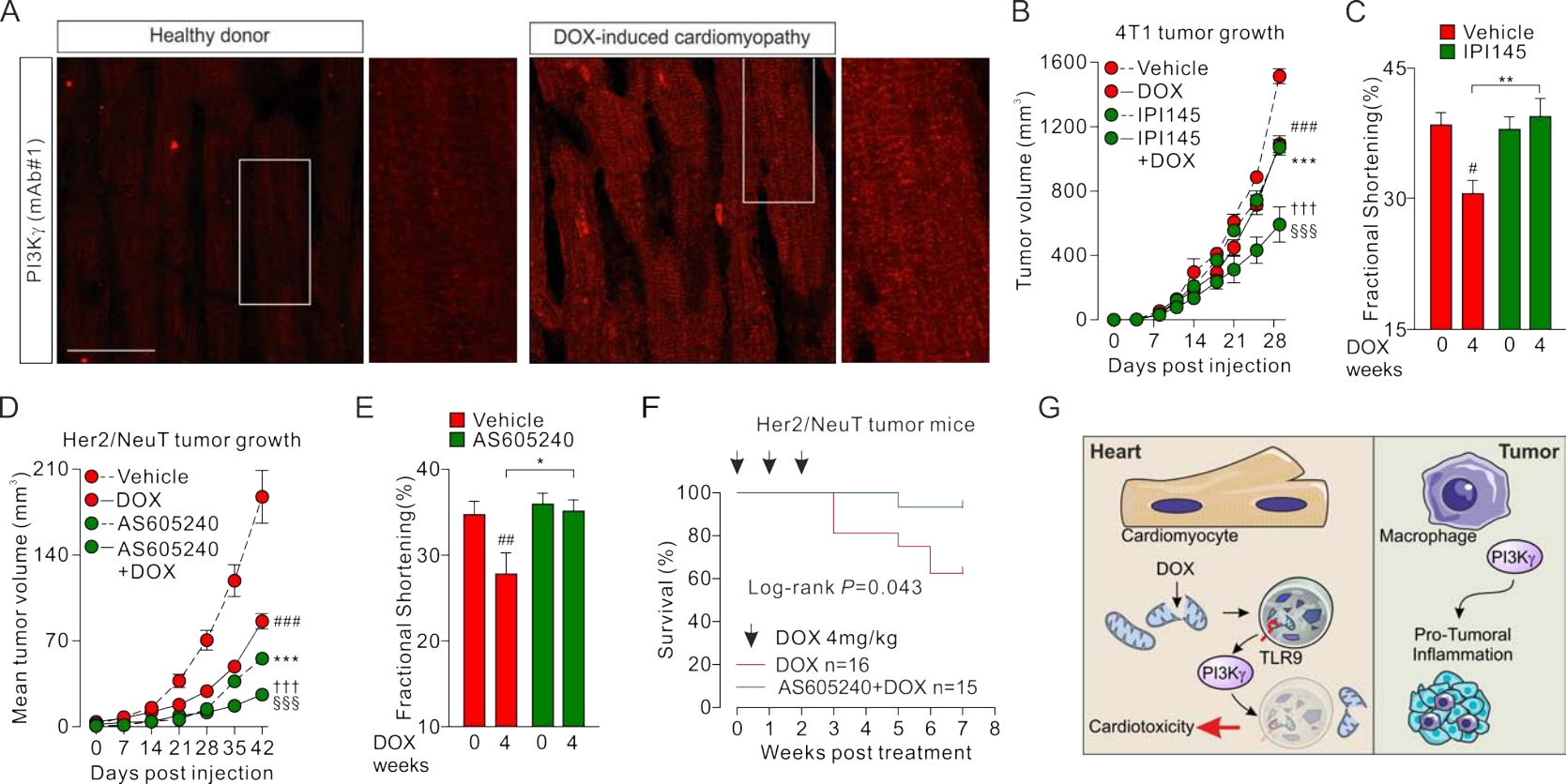
A
Healthy donor
DOX-induced cardiomyopathy
PI3Kγ (mAb#1)
B
4T1 tumor growth
Vehicle
DOX
IPI145
IPI145 +DOX
Tumor volume (mm3)
Days post injection
C
Vehicle
IPI145
Fractional Shortening(%)
DOX
weeks
D
Her2/NeuT tumor growth
Vehicle
DOX
AS605240
AS605240 +DOX
Mean tumor volume (mm3)
Days post injection
E
Vehicle
AS605240
Fractional Shortening(%)
DOX
weeks
F
Her2/NeuT tumor mice
Survival (%)
Log-rank P=0.043
DOX 4mg/kg
DOX n=16
AS605240+DOX n=15
Weeks post treatment
G
Heart
Tumor
Cardiomyocyte
Macrophage
PI3Kγ
DOX
TLR9
Pro-Tumoral Inflammation
Cardiotoxicity

SUPPLEMENTARY MATERIALS FOR

Phosphoinositide 3-kinase gamma inhibition protects from anthracycline cardiotoxicity and reduces tumor growth

Li et al.

Running title: PI3Kγ inhibition in Cardio-Oncology

Correspondences:

Alessandra Ghigo, PhD

Department of Molecular Biotechnology and Health Sciences

Molecular Biotechnology Center, University of Torino

Via Nizza 52, 10126, Torino, ITALY

Phone: +39 011 670 6335

Fax: +39 011 670 6432

Email: alessandra.ghigo@unito.it

and

Emilio Hirsch, PhD

Department of Molecular Biotechnology and Health Sciences

Molecular Biotechnology Center, University of Torino

Via Nizza 52, 10126, Torino, ITALY

Phone: +39 011 670 6425

Fax: +39 011 670 6432

Email: emilio.hirsch@unito.it

This PDF file includes:

Supplementary Methods

Supplementary Tables:

Supplementary Table 1. Primary antibodies used in this study.

Supplementary Table 2. Primers and probes used in quantitative RT-PCR.

Supplementary Table 3. LV functional parameters in DOX-treated WT and KD mice.

Supplementary Table 4. Heart, lung and liver weight of saline and DOX-treated WT and KD mice.

Supplementary Table 5. LV functional parameters in DOX-treated, 4T1 tumor-bearing WT and KD mice.

Supplementary Table 6. LV functional parameters in WT mice treated with DOX alone or together with the PI3Kγ inhibitor AS605240.

Supplementary Figures Legends:

Supplementary Figure 1. Low-dose intraperitoneal DOX does not cause systemic toxicity.

Supplementary Figure 2. Leukocyte infiltration in DOX-treated hearts.

Supplementary Figure 3. PI3Kγ inhibition promotes autophagosome formation in primary neonatal mouse ventricular myocytes (NMVMs).

Supplementary Figure 4. PI3Kγ inhibition promotes autophagic clearance of damaged mitochondria.

Supplementary Figure 5. PI3Kγ inhibition prevents DOX-induced Akt activation in H9c2 cells and neonatal mouse ventricular myocytes (NMVMs).

Supplementary Figure 6. DOX activates a TLR9/PI3Kγ/Akt/Ulk1 pathway that inhibits autophagy.

Supplementary Figure 7. Autophagy inhibition dampens the cardioprotection of KD mice.

Supplementary Figure 8. PI3Kγ inhibition prevents DOX-induced mitochondrial dysfunction, calcium mishandling, ROS production and DNA damage by unleashing autophagy.

Supplementary Figure 9. Effects of PI3Kγ inhibition or DOX on 4T1 cell growth *in vitro*.

Supplementary Figure 10. PI3Kγ staining in human heart sections from a patient with DOX-induced cardiomyopathy and a healthy subject.

Supplementary Figure 11. Cardiac function and survival of DOX-treated, tumor-bearing WT and KD mice.

Supplementary Figure 12. Cardiac atrophy, fibrosis and apoptosis in DOX-treated, tumor-bearing mice.

Supplementary Figure 13. Pharmacological inhibition of PI3Kγ protects against DOX-induced cardiotoxicity in tumor-free mice.

Supplementary References

Supplementary Methods

Mice

Knock-in mice expressing an inactive PI3Kγ holoenzyme (kinase dead, KD) were generated by inserting a point mutation in the *Pik3cg* gene encoding the p110γ catalytic subunit, as previously described[1]. Mutant mice were backcrossed for 15 generations to BALB/c mice and eight-ten-week-old females were used for experiments. Age- and gender-match BALB/c animals were used as wild-type (WT) controls. For studies on spontaneous tumors, BALB/c mice overexpressing the activated form of the Neu oncogene (BALB/c rHER-2/NeuT) in the mammary gland were used[2]. All animal experiments were approved by the animal ethical committee of the University of Torino and by the Italian Ministry of Health (Authorization n ° 738/2016-PR).

In vivo treatments

To mimic human therapeutic regimens, a cumulative dose of 12 mg/kg of doxorubicin (DOX) was administered via 3 weekly i.p. injections (4 mg/kg on days 0, 7 and 14), as previously described[3]. Survival was monitored daily and heart function was assessed by echocardiography, before and 6 weeks after the first injection of DOX.

To investigate Akt/mTOR/Ulk1 signaling *in vivo*, WT and KD mice received a single i.p. injection of 4 mg/kg DOX alone or in combination with i.v. ODN2088 (100 μg; InvivoGen, San Diego, CA).

To investigate the autophagy flux *in vivo*, mice were treated i.p. with 10 mg/kg Bafilomycin A1 (BafA1, LC Laboratories, Woburn, MA) or Vehicle (DMSO) 1 hour before a single injection of

4 mg/kg DOX. Mice were sacrificed and hearts collected for Western blot and immunofluorescence assays 6 hours after DOX administration.

To inhibit autophagy *in vivo*, mice were treated with DOX or saline as described above, followed by daily i.p. injection of 60 mg/kg of hydroxychloroquine (HCQ, Cayman Chemical, Ann Arbor, MI) or 0.3 mg/kg of BafA1 or saline, for 4 weeks. Survival was monitored daily, and heart function was assessed by echocardiography, before and 4 weeks after the first injection of DOX. Cardiomyocyte-restricted, genetic inhibition of autophagy was performed by i.v. injection of 100 μl of either AAV9-GFP-U6-ATG7-shRNA or AAV9-GFP-U6-scrmb-shRNA (both 1×10^{13} per ml; Vector Biolabs, Malvern, PA, USA) in 8/10-week-old PI3Kγ KD females. One week upon virus injection, mice were treated with DOX or saline as describe above, and heart function was assessed by echocardiography, before and 4 weeks after the first injection of DOX. At the end of the treatment, hearts were harvested and processed for immunofluorescence and molecular analyses.

Echocardiography

For the evaluation of cardiac function, mice were anesthetized with 1% isoflurane, and analyzed with a Vevo 2100 High Resolution Imaging System (Visual Sonics Inc, Toronto, Canada) equipped with a 30-MHz probe (MS550D) (VisualSonics, Toronto, Canada). Echocardiographic parameters were measured under the long-axis M-mode when heart rate was about 450 bpm. Fractional shortening (FS) was calculated as previously described[4].

Locomotor activity (open-field test)

To evaluate the spontaneous horizontal locomotor activity of DOX-treated mice, the open-field test was used as described previously[5]. The open-field apparatus consisted of a square polyvinyl chloride arena (30 cm × 30 cm divided by lines on the floor into 9 equal squares). Mice were brought into the experimental room 1 hour before testing. Each mouse was placed in the center of the open-field arena and allowed to adapt to the apparatus for 1 minute. The locomotion frequency (number of floor units crossed by the animal with all the four paws) was counted over a period of 5 minutes.

Tumor studies

Mice were subcutaneously injected with 1×10^5 4T1 or TUBO breast tumor cells. One week after cell injection, when tumors were 2 mm in mean diameter, mice were treated with DOX or saline as described above. Tumor size was measured twice a week for up to 4 weeks, and tumor volumes were calculated with the following equation: $V=4\pi/3\times(L/2)^2\times(W/2)$, where V, L and W represent the volume, length and width of the tumor. Echocardiography was used to assess cardiac function before and 4 weeks after the first DOX administration.

PI3Kγ was inhibited pharmacologically by using two previously described compounds, IPI145 (Selleckchem, Houston, TX)[6] and AS605240 (Chemdea, Ridgewood, NJ)[7]. For the 4T1 xenograft model, mice were administrated with either Vehicle (0.5% carboxymethylcellulose and 0.25% Tween 20 in ultra-pure water) or 5 mg/kg IPI145 daily through oral gavage for 3 weeks since the first injection of DOX. In the Her2/NeuT spontaneous mammary tumor model, mice bearing tumors 2 mm in mean diameter were administered with DOX as above, followed by treatment with Vehicle (0.5% carboxymethylcellulose, 0.25% Tween 20 in ultra-pure water) or 5 mg/kg AS605240 i.p. daily for 3 weeks since the first injection of DOX. Tumors in all mammary

glands were sized weekly. Tumor volumes were calculated with the above equation and mean tumor volume per mammary gland was calculated to assess tumor growth. Cardiac function was assessed as above.

Isolation of neonatal mouse ventricular cardiomyocytes (NMVMs)

Neonatal mouse ventricular cardiomyocytes (NMVMs) were isolated as previously described[8]. Briefly, hearts of 1 to 3-day-old pups were excised and atria were removed. Ventricles were minced and pre-digested with 0.5 mg/ml trypsin (USB Corporation, Cleveland, Ohio) freshly dissolved in calcium-free HBSS solution, pH 7.4, overnight at 4 ℃. The next day, ventricles were digested 3-4 times at 37 ℃ for 5 minutes with 330 U/ml collagenase type II (Worthington Biochemical, Lakewood, NJ) freshly suspended in calcium-free HBSS solution, pH 7.4. Supernatants containing isolated cells were collected from each digestion, and an equal volume of serum-rich medium was added to stop the digestion. Isolated cells were collected and centrifuged 5 minutes at 800 rpm to separate non-myocardial cells. Resuspended cells were pre-plated twice for 30 minutes to further reduce fibroblast contamination. Cardiomyocytes were finally plated in 3 cm dishes or 24-well plates at a density of $0.3\text{-}1\times10^6$ cells/well. Culture plates with/without glasses were pre-coated with PBS containing 0.2% gelatin (Sigma-Aldrich, Saint Louis, MO) and 10 μg/ml fibronectin (Sigma-Aldrich, Saint Louis, MO) for 30 minutes. Cardiomyocytes were cultured in Dulbecco's modified Eagle's medium (DMEM)/Medium 199 (M199) (3:1) High Glucose GlutaMAX (Gibco, Carlsbad, CA) mix, containing 10% Horse Serum (HS), 5% Fetal Bovine Serum (FBS), and 5 mM penicillin/streptomycin (Gibco, Carlsbad, CA). Cardiomyocytes were incubated under 5% CO_2 at 37 ℃ overnight before treatments.

Cell cultures

The rat cardiomyoblast cell line H9c2, human embryonic kidney cells 293T (HEK-293T) and breast cancer cell line 4T1 were purchased from the American Type Culture Collection (ATCC, Manassas, VA, USA) and were cultured in DMEM High Glucose GlutaMAX (Gibco, Carlsbad, CA) supplemented with 10% FBS, 5 mM penicillin/streptomycin (Gibco, Carlsbad, CA). TUBO cells[9] were kindly provided by Prof. Federica Cavallo (Dept. of Molecular Biotechnology and Health Sciences, University of Torino, Torino, Italy) and cultured in DMEM High Glucose GlutaMAX supplemented with 20% FBS, 5 mM penicillin/streptomycin. All cells were incubated under 5% CO_2 at 37 ℃. H9c2 cells were passed regularly, cultured to subconfluence (80%) and used between passage 10 and 25 for all the experiments.

Cell infection and transfection

To study the autophagic flux, 24 hours after the isolation, NMVMs were infected with an adenovirus encoding the tandem fluorescent probe mRFP-GFP-LC3 (15 MOI; kindly provided by S. Sciarretta, University of Rome "Sapienza", Latina, Italy)[10]. 24 hours after infection, cells were treated with 1 μM DOX for 16 hours. To block the fusion of autophagosome and lysosome, 100 nM Bafilomycin A1 (BafA1) was added to cells 4 hours before the end of DOX treatment.

Transfection of NMVMs with an YFP-LC3 labeled plasmid (kindly provided by M. Sandri, University of Padova, Padova, Italy) was carried out using Lipofectamine 2000 reagent (Invitrogen, California, USA), according to the manufacturer's protocol. 24 hours after the transfection, cells were treated with 1 μM DOX for 16 hours.

To inhibit autophagy *in vitro*, freshly isolated mouse NMVMs were seeded in glass-coated 24-wells (10^5 cells/well). The following day, NMVMs were infected with an adenovirus harboring

ATG7 shRNA (Ad-shATG7; 20 MOI; kindly donated by Prof. Junichi Sadoshima, New Jersey Medical School, Newark)[10]. Twenty-four hours after infection, NMVMs were washed and stimulated for 6 hours with 1 μM DOX alone or together with 0.5 μM AS605240 (1-hour pre-treatment). Cells were then fixed in ice-cold 4% PFA, processed for immunofluorescence, and mounted on cover-glasses for observation under fluorescence microscope (Apotome, Zeiss, Oberkochen, Germany).

To investigate the interaction of PI3Kγ and TLR9, HEK-293T cells were plated at low density and transfected with pcDNA3-p110γ (kindly provided by R. Wetzker, Friedrich Schiller University, Jena, Germany) and pcDNA3-TLR9-YFP (a gift from Doug Golenblock, Addgene plasmid #13642) using calcium phosphate. 24 hours after transfection, cells were treated with 0.2 μM ODN1826 or saline for 1 hour before lysis and immunoprecipitation analysis, as described below.

In vitro treatments

Twenty-four hours before stimulation, NMVMs were cultured in serum-free Dulbecco modified Eagle medium/Medium 199 mix (DMEM/M199 3:1) and H9c2 cells in DMEM supplemented with 0.5% Fetal Bovine Serum (FBS). Cells were then treated with 1 μM DOX for the indicated times (30 minutes, 60 minutes, 2 hours, 4 hours, 8 hours and 24 hours), alone or in combination with AS605240 (0.5 μM, 1-hour pre-treatment) or with the TLR9 antagonist (ODN2088; 0.2 μM, 5-hour pre-treatment), as described previously[11]. Alternatively, NMVMs and H9c2 cells were stimulated with the TLR9 agonist (ODN1826; 0.2 μM, 1 hour), with or without AS605240 pre-treatment. TLR9 agonist and antagonist were purchased from InvivoGen (San Diego, CA). At

the end of the treatment, cells were harvested and protein extracts were prepared for Western blot analysis as described previously[4].

Immunocytochemistry

mtDNA, TLR9, PI3Kγ and LAMP2 co-localization was assessed in primary mouse NMVMs stimulated with either 0.2 μM ODN1826 (TLR9 agonist) or 1 μM DOX for 1 hour. Cells were fixed at RT with 4% PFA for 15 minutes and permeabilized with blocking solution (3% BSA and 0.1% saponin in PBS) for 20 minutes at 4 ℃. Cells were then incubated for 1 hour at RT with primary antibodies against PI3Kγ, TLR9 and LAMP2 and with 3 μl/ml PicoGreen (mtDNA staining; Thermo Fisher Scientific, USA) in blocking solution. Cells were washed with 0.1% saponin and then incubated with Alexa Fluor secondary antibodies in blocking solution (1:500, Invitrogen, Paisley, UK) for 30 minutes at RT. Nuclei were counterstained with DAPI, slides were mounted in Prolong Gold antifade reagent (Cell Signaling Technology) and images acquired with a Leica SP8 confocal laser scanning microscope and processed with ImageJ software (NIH, USA). For γ-H2AX staining, 0.1% Triton X100 was used instead of saponin.

Mitochondrial membrane potential assay

NMVMs were incubated with JC-1 dye (5 ug/ml; Thermo Fisher Scientific, Waltham, MA) for 15 minutes at 37 ℃ in a 5% CO_2 incubator. Cells were washed in PBS, then pre-treated with Vehicle (0.1% DMSO) or 0.5 μM AS605240 alone or together with 100 nM Bafilomycin A1 for 1 hour before exposure to 1 μM DOX or saline for 6 hours in complete culture medium. At the end of the treatment, cells were washed and fluorescence parameters were acquired with Tecan Infinite 200 plate reader (Tecan Trading AG, Hombrechtikon, Switzerland). JC-1 monomers

were excited at λ=485 nm and the emission was read at λ=535nm, while JC-1 aggregates were excited at λ=530 nm and the emission was read at λ=590 nm. The mitochondrial membrane potential was calculated as the ratio of the fluorescence of JC-1 aggregates and monomers (F590/F535).

Calcium (Ca^{2+}) imaging in neonatal rat ventricular myocytes (NRVMs)

Ca^{2+} handling was analyzed in neonatal rat ventricular myocytes (NRVMs) isolated from 1/2-day-old Sprague Dawley rats as previously described[12]. Cells were treated with doxorubicin (1 μM DOX for 3 hours), alone or in combination with 0.5 μM AS605240 or 100 nM Bafilomycin A1, loaded with the fluorescent Ca^{2+} dye Fluo-4 AM (3 μM), and imaged with an inverted fluorescence microscope (Olympus IX70), in resting conditions (without field stimulation). Elevated spontaneous Ca^{2+} release events, in the form of macro-sparks and travelling waves, were defined as intracellular fluorescence elevations detected in at least two consecutive frames (>160ms) and higher than 2 standard deviations of the background fluorescence intensity.

Glycolysis, lactate production and oxidative phosphorylation assays

NMVMs from WT BALB/c mice were prepared as described above and pre-treated with 0.5 μM AS605240 or Vehicle (0.1% DMSO) for 1 hour before exposure to 1 μM DOX or saline for 3 hours. The activity of hexokinase (HK), phosphofructokinase (PFK), pyruvate kinase (PK) and of lactate dehydrogenase (LDH) was evaluated by spectrophotometric analysis in NMVMs lysates. Briefly, the activity of HK, PFK and PK in fresh cell lysates was inferred from $NADP^+$ reduction or NADH oxidation, as measured in a iEMS microplate reader (MTX Lab Sytems, Bradenton, FL) with absorbance wavelength at 340 nm, after 15 minutes incubation with a

reaction mix containing 100 mM Tris pH 7.4, 2 or 2.5 mM $MgCl_2$, proper substrates, including $NADP^+$ or NADH, and complementary enzymes. To determine LDH activity, cell lysates were incubated for 15 minutes with a reaction mix containing 100 mM Tris pH 7.4, 0.2 mM NADH and 1 mM sodium pyruvate, and NADH oxidation was quantified by means of the iEMS microplate reader with 340 nm absorbance wavelength.

Concentrations of lactate were determined in cell culture medium by spectrophotometric analysis. Cell culture medium was collected on ice, centrifuged to remove cellular debris, and added to a reaction mix containing 100 mM Tris pH 9, 5 mM NAD^+ and 1 U/ml LDH. The reduction of NAD^+ to NADH by LDH was quantified by reading the absorbance at 340nm before starting the reaction and after 15 minutes in an iEMS microplate reader, and the amount of lactate was calculated based on the Lambert-Beer law.

To assess the efficiency of oxidative phosphorylation, cells were permeabilized with digitonin and stimulated with 10 mM pyruvate plus 5 mM malate, together with 0.08 mM ADP. Oxygen consumption was measured at 25 ℃ in a closed chamber by means of an amperometric electrode (Unisense Microrespiration, Unisense A/S, Denmark). ATP synthesis was measured using a luminometer (GloMax 20/20n Luminometer, Promega, Italy) by the luciferin/luciferase chemiluminescent method (luciferin/luciferase ATP bioluminescence assay kit CLSII, Roche, Basel, Switzerland). The ratio between the concentration of ATP produced and the amount of oxygen consumed in the presence of exogenous substrates and ADP (P/O ratio) was then calculated as an estimate of the efficiency of the oxidative phosphorylation.

Transmission electron microscopy analysis

Hearts were harvested from WT and KD mice, in basal conditions and 3 days after DOX treatment. 1 mm^3 heart pieces from the left ventricular wall were fixed in 1.25% glutaraldhehyde (v:v in 0.1 M sodium cacodylate, pH 7.2) overnight at 4 ℃. Heart samples were washed in 0.1 M sodium cacodylate (3 times for 30 minutes), post-fixed and thin sections were imaged on a Tecnai-20 electron microscopy (Philips-FEI, Hillsboro, Oregon), as previously described[13].

Tissue preparation and immunofluorescence analysis

For *ex-vivo* analyses, hearts harvested from WT and KD mice treated with DOX or saline were either frozen directly in liquid nitrogen for biochemistry analysis or fixed in 1% PFA (Sigma-Aldrich, Saint Louis, MO) for histological and immunofluorescence (IF) analysis, as described previously[14]. 10 μm sections were obtained with a cryostat (Leica CM1850, Leica Microsystems GmbH, Wetzlar, Germany) and processed for IF analysis.

Heart samples from a 21-year-old woman diagnosed with Ewing sarcoma and subjected to triple therapy with Adriamycin, Cyclophosphamide and Vincristine were included. The patient manifested heart failure symptoms 5 years after chemotherapy and underwent heart transplantation 10 years after the diagnosis of chemotherapy-induced cardiomyopathy (Ejection fraction: 40%). Samples were archived in the historical collection of the institute of Pathological Anatomy of the University of Padova. Samples were anonymous to the investigators and used in accordance with the directives of the national committee of Bioethics and *Raccomandazione (2006) della Commissione dei Ministri degli Stati Membri sull'utilizzo di campioni biologici di origine umana per scopi di ricerca.* Formalin-fixed, paraffin-embedded heart samples were processed for IF study as described previously[15].

For IF assay, sections were incubated with primary antibodies diluted in PBS, supplemented with 1% BSA and 1% Triton X-100 overnight at 4 ℃. The following primary antibodies were used: mouse anti-α-actinin (Sigma-Aldrich, Saint Louis, MO), mouse anti-γ-H2AX (Millipore Corporation, Billerica, Massachusetts) and rabbit anti-LC3 (Cell Signaling Technologies, Massachusetts), mouse anti-dystrophin (Sigma-Aldrich, Saint Louis, MO), rabbit anti-GFP (Polyclonal antibody produced and purified at the Molecular Biotechnology Center, University of Torino, Italy). 488- and Cy3-conjugated secondary antibodies (Jackson Immuno Research Laboratories, West Grove, Pennsylvania), were used to detect primary antibodies, by incubation at 37 ℃ for 30 minutes. Heart sections were analyzed with a confocal microscope (TCS SP5 Leica, Leica Microsystems GmbH, Wetzlar, Germany) equipped with oil immersion objectives (Leica 63x, 1.4 N.A.). To quantify γ-H2AX-positive nuclei, sections were counterstained with DAPI, images acquired with a fluorescence microscope (Apotome, Zeiss, Oberkochen, Germany) and quantification was performed with ImageJ software (https://imagej.nih.gov/ij/).

Protein extraction and immunoblotting

Whole hearts, NMVMs, H9c2 and HEK-293T cells were lysed on ice for 15 minutes in 120 mM NaCl, 50 mM Tris-HCl (pH 8.0), 1% Triton X-100, protease inhibitor Complete (Roche Applied Science, Penzberg, Germany), and phosphatase inhibitors (50 mM sodium fluoride, 1 mM sodium orthovanadate, and 10 mM sodium pyrophosphate). Lysates were cleared by centrifugation at 13000 rpm for 15 minutes at 4 ℃. Protein concentration was determined by Bradford method. Proteins from hearts or cellular lysates were separated by SDS-polyacrylamide gel electrophoresis (SDS-PAGE) and transferred to methanol-activated polyvinylidene difluoride (PVDF) membranes (Millipore Corporation, Billerica, Massachusetts). Membranes were

incubated for 1 hour with 5% bovine serum albumin (BSA)-TBST [tris-buffered saline (TBS) - 0.3% Tween 20] at room temperature and overnight incubated with different primary antibodies at 4℃. Appropriate host species horseradish peroxidase-conjugated secondary antibodies were added and signals were detected with enhanced chemiluminescence (Millipore Corporation, Billerica, Massachusetts). The primary antibodies used in this study are listed in Supplementary Table 1.

Cell viability

The viability of 4T1 breast cancer cells after treatment with DOX or AS605240 was analyzed by MTT assay (Cell Proliferation Kit I, Roche Applied Science, Penzberg, Germany). In brief, 4T1 cells were seeded on 96-well plates (2000 cells/well). After 24 hours, cells were treated with different concentrations of DOX (0.1, 1, 10 μM) or AS605240 (0.3, 1, 3, 10 μM) and cell viability was measured at the indicated time points according to the supplier's protocols.

ROS production assay

ROS production was assessed in heart lysates by using the oxidant-sensitive fluorescent dye 29,79-dichlorodihydrofluoroscein diacetate (H_2DCFDA; Molecular Probes, Inc., Eugene, OR) as previously described[16]. Briefly, heart homogenates were incubated with 5 μM H_2DCFDA in phosphate buffered saline (PBS) for 30 minutes at 37℃ under 5% CO_2 atmosphere. Fluorescence was recorded at excitation and emission wavelengths of 485 nm and 530 nm, respectively, by a fluorescence plate reader (Promega). Fluorescence intensity was expressed as arbitrary fluorescence units/mg protein.

Mitochondrial subcellular fractionation

Mitochondria-enriched fractions were isolated as described previously[17]. Briefly, half of the heart was smashed to powder and lysed in 750 μl ice-cold lysis homogenization buffer (0.25 M Sucrose, 0.1 mM EGTA, 20 mM MOPS/Tris, pH 7.4) with a homogenizer (TURAX, VWR International, Radnor, Pennsylvania), at 10000 rpm for 3 seconds followed by incubation on ice for 30 minutes. The homogenate was centrifuged at 1000 g at 4°C for 4 minutes to exclude cell debris. The supernatant was collected and further centrifuged at 8000 g at 4°C for 10 minutes. The pellet, containing mitochondria, was resuspended in 40 μl MOPS/Tris buffer (120 mM KCl, 10 mM MOPS/TRIS, pH 7.4) and the supernatant was collected as cytoplasm.

Immunoprecipitation

Immunoprecipitation assays were performed as described previously[8]. Briefly, HEK-293 cell lysates, heart lysates and mitochondria-enriched fractions were incubated with a 1:1 slurry of protein A- or protein G-Sepharose (GE Healthcare, Little Chalfont, UK) and 1 mg of antibody per milligram of protein lysate for 2 hours at 4℃, rocking. Proteins bound to protein A- or protein G-Sepharose resin were washed, and subjected to SDS-PAGE and Western Blot, as described above.

Histological and Immunohistochemical (IHC) analysis

Hearts were harvested and fixed with 4% PFA overnight. Samples were de-hydrated, paraffin embedded and sectioned into 5 μm thick slices on a sliding microtome (Leica, Nussloch, Germany) and mounted on Superfrost Plus slides for IHC.

Hematoxylin and eosin (H&E) staining was performed as described previously[18]. Slices were visualized under a light microscope (Olympus BX41, Olympus Corporation, Tokyo, Japan) and cardiomyocyte area was measured using ImageJ software (https://imagej.nih.gov/ij/) by considering 6-8 images/heart and 10 cells/image.

For immunohistochemistry, rehydrated slices were subjected to antigen retrieval by microwave heating (20 minutes) in citrate buffer (pH 6), and endogenous peroxidases were inhibited by incubation with 3% H_2O_2 for 10 minutes. Sections were saturated in PBS supplemented with 5% Goat Serum, 3% BSA and 0.1% Triton X-100, for 1 hour at RT, and incubated with primary antibodies in blocking solution at 4℃ overnight. Sections were further processed with biotinylated secondary antibodies (Vector Laboratories, Burlingame, CA, USA) in PBS + 0.3% Triton X-100, and the avidin-biotin-peroxidase complex (DakoCytomation; Milano, Italy), and developed with DAB (methanol 3,3 diaminobenzide, Roche, Mannheim, Germany). Images were acquired at 20x with an Olympus BX41 microscope equipped with an Olympus DP50 camera (Olympus, Milan, Italy).

Analysis of fibrosis

To detect cardiac collagen deposition, sections were stained with PicroSirius Red as described previously[19]. Briefly, paraffin-embedded slices were dewaxed, rehydrated and stained with PicroSirus Red solution [0.1% Sirius Red (Fluka, Buchs, Switzerland) in saturated aqueous solution of picric acid (Fluka, Buchs, Switzerland)] for 1 hour. Slices were then washed 2 seconds with acidified water [5 ml acetic acid (glacial) freshly added to 1 liter of distilled water], dehydrated and mounted. The area of red positive staining (collagen) was measured with Image-

Pro Plus software (Media Cybernetics, Silver Spring, USA). The average percentage of fibrosis to total area was calculated in 6-8 images per heart.

To analyze the expression of pro-fibrotic genes, quantitative real-time PCR of *Tgfb* (TGFβ), *Ctgf* (CTGF), *Col1a1* (Collagen I) and *Col3a1* (Collagen III) was performed on cDNA prepared from total heart RNA extracts.

Evaluation of apoptosis

Apoptotic cells in paraffin-embedded heart sections were detected with terminal deoxynucleotidyl transferase dUTP nick end labeling (TUNEL) staining, according to the manufacturer's protocol (In situ cell death detection Kit, Roche Applied Science, Penzberg, Germany). The average percentage of apoptotic cells was calculated as the ratio of TUNEL-positive nuclei/DAPI-stained nuclei in 6-8 images per heart.

Protein levels of the apoptotic marker cleaved caspase 9 were assessed by Western blot on heart protein extracts.

Leukocyte infiltration analysis

To analyze leukocyte infiltration in the heart, the pan-leukocyte marker CD18 was detected by immunohistochemistry on heart sections, as previously described[19]. Briefly, paraffin-embedded slices were dewaxed and rehydrated, followed by permeabilization with 0.3% Triton-TBS for 10 minutes. Sections were then incubated with 0.3% hydrogen peroxide for 10 minutes to block endogenous peroxidase and microwave-heated in citrate buffer (10 mM citric acid, pH 6.0) for 10 minutes for antigen retrieval. After cooling, slices were blocked with 5% goat serum for 30 minutes and incubated with CD18 primary antibody (BMA, Augst, Switzerland) (1:200 diluted

in TBS containing 1.25% goat serum) overnight at 4°C. The second day, sections were incubated with a goat anti-rat biotinylated secondary antibody (Dako Cytomation, Milano, Italy) for 30 minutes. Immunoreactivity was enhanced by avidin-biotin complex interaction (Vectastain ABC HRP Kit, Vector laboratories, California, USA) and developed with DAB (3,3'-Diaminobenzidine, Sigma Aldrich, Saint Louis, MO). Sections were analyzed with light microscopy (Olympus BX41, Olympus Corporation, Tokyo, Japan). 6-8 fields per heart were counted in each sample.

Gene expression analysis

Hearts or tumors were harvested, frozen in liquid nitrogen and smashed. Total RNA was extracted using TRIzol reagent (Invitrogen, Carlsbad, CA). cDNA was synthesized from 1000 ng of total RNA using cDNA reverse transcription kits (Applied Biosystems, Foster City, CA). Relative mRNA level was analyzed by real time PCR (ABI 7900HT FAST Real-Time PCR system, Applied Biosystems, Foster City, CA) with Taqman assays, using the Universal Probe Library system (Roche Applied Science, Penzberg, Germany). 18S gene was used as housekeeping control. The primer sequences of the detected genes are shown in Supplementary Table 2.

Isolation of single cells from murine tumors

Tumors were isolated, finely minced and digested in DMEM High Glucose GlutaMAX (Gibco, Carlsbad, CA) containing 1 mg/ml collagenase A (Roche Applied Science, Indianapolis, IN, USA), at 37 ℃ for 20 minutes. Cell suspensions were filtered through 70 and 40 μm strainers (BD) and resuspended in DMEM High Glucose GlutaMAX (Gibco, Carlsbad, CA) containing

10% FBS to obtain a single-cell suspension. Cells were washed once with PBS, containing 0.2% BSA and 0.01% NaN_3, before flow cytometry analysis.

Flow cytometry staining and analysis

Single-cell suspensions ($1x10^6$ cells) were incubated with the blocking reagent anti-CD16/CD32 (Miltenyi Biotec, Bergisch Gladbach, Germany) at 4℃ for 5 minutes, followed by incubation with fluorescently-labelled antibodies at 4℃ for 30 minutes. For staining of surface markers, the following primary antibodies were used: Gr1 Ly6G/Ly6C (RB6-8C5), F4/80 (BM8) and CD11b (M1/70), all from Biolegend (San Diego, CA), and MHC class II (AMS-32.1) from BD Biosciences (San Jose, CA). For CD206 staining, cells were fixed with 2% formalin for 20 minutes at room temperature in the dark, permeabilized with 0.5% saponin and then incubated with a fluorophore-labelled antibody against CD206 (Biolegend, San Diego, CA) at 4℃ for 30 minutes. Cells were acquired with the AccuriC6 (BD Biosciences, San Jose, CA) and analyzed with FlowJo x7.5.

Gene expression meta-analysis

Raw microarray expression data of whole blood RNA from women with, and without, chemotherapy-induced cardiotoxicity were obtained from GEO dataset GSE40447[20]. PI3Kγ (p110γ) and PI3Kα (p110α) expression was analyzed in samples from women with breast cancer (i) prior to anthracycline therapy, (ii) with a history of anthracycline therapy but no heart failure, and (iii) with anthracycline-induced heart failure.

Statistical analysis

Prism software (GraphPad software Inc., La Jolla, CA, USA) was used for statistical analysis. P values were calculated with one-way ANOVA, two-way ANOVA, two-way repeated-measures ANOVA followed by Bonferroni post-hoc test or Student's t-test as appropriate. Log-rank test was used for survival analysis. Data are presented as Mean ± SEM; $P<0.05$ was considered as statistically significant.

Supplementary Tables:

Supplementary Table 1. Primary antibodies used in this study

Antibody	**Customer**	**Product number**	**Dilution**	**Application**
α-actinin	Sigma	A7811	1:200	IF
β-actin	Santa Cruz Biotechnology	sc-1616-R	1:1000	WB
Phospho-Akt (T308)	Cell Signaling Technology	13038	1:1000	WB
Phospho-Akt (S473)	Cell Signaling Technology	4060	1:1000 1:100	WB IHC
Akt	Cell Signaling Technology	4691	1:1000	WB
CD11b	Biolegend	101208	1:200	IF
CD8	BD Biosciences	553033	1:200	IF
Cleaved-caspase 9	Cell Signaling Technology	9509	1:1000	WB
Dystrophin	Sigma	D8043	1:100	IF
GAPDH	EMD Millipore	MAB374	1:1000	WB
GFP	Produced and purified at the Molecular Biotechnology Center	Purified polyclonal antibody	1:200	IF
LAMP2	Abcam	Ab13524	1:100	IF
LC3B	OriGene Technologies	TA301542	1:1000	WB
LC3B	Cell Signaling Technology	3868	1:200	IF
Phospho-mTOR	Cell Signaling Technology	5536	1:100	IHC

(S2448)				
PI3Kγ (p110γ) mAb#1	Produced and purified by Molecular Biotechnology Center[4,8]	Purified monoclonal antibody	1:50 1:100	IP IF
PI3Kγ (p110γ) mAb#2	Produced and purified by Molecular Biotechnology Center[4,8]	Hybridoma supernatant	1:1 (pure)	WB, IF
Phospho-p70 S6K (T389)	Cell Signaling Technology	9234	1:1000	WB
Phospho-ULK1 (S757)	Cell Signaling Technology	6888	1:500 1:100	WB IHC
γ-H2AX (S139)	EMD Millipore	05-636	1:100	IF
TLR9	Santa Cruz Biotechnology	Sc-25468	1:50	IF
VDAC	Abcam	ab15895	1:1000	WB
Vinculin	Cell Signaling Technology	4650	1:1000	WB
CD18	BMA Biomedicals	T-2122	1:200	IHC

Supplementary Table 2. Primers and probes used in quantitative RT-PCR

Gene	**Left primer(5'-3')**	**Right primer(5'-3')**	**Probe**
Atg7	CCGGTGGCTTCCTACTGTTA	AAGGCAGCGTTGATGACC	#71
Ccl17	TGCTTCTGGGGACTTTTCTG	GAATGGCCCCTTTGAAGTAA	#27
Ccl22	TCTTGCTGTGGCAATTCAGA	GAGGGTGACGGATGTAGTCC	#84
Cd206	CCACAGCATTGAGGAGTTTG	ACAGCTCATCATTTGGCTCA	#7
Col1a1	CATGTTCAGCTTTGTGGACCT	GCAGCTGACTTCAGGGATGT	#15
Col3a1	TCCCCTGGAATCTGTGAATC	TGAGTCGAATTGGGGAGAAT	#49
Ctgf	TGACCTGGAGGAAAACATTAAGA	AGCCCTGTATGTCTTCACACTG	#71
Cxcl10	GCTGCCGTCATTTTCTGC	TCTCACTGGCCCGTCATC	#3
Il-1b	AGTTGACGGACCCCAAAAG	AGCTGGATGCTCTCATCAGG	#38
Il-6	GCTACCAAACTGGATATAATCAGGA	CCAGGTAGCTATGGTACTCCAGAA	#6
Il-10	CAGAGCCACATGCTCCTAGA	TGTCCAGCTGGTCCTTTGTT	#41
Il-13	CCTCTGACCCTTAAGGAGCTTAT	CGTTGCACAGGGGAGTCT	#17
Nos2	CTTTGCCACGGACGAGAC	TCATTGTACTCTGAGGGCTGAC	#13
Nppa (ANP)	CACAGATCTGATGGATTTCAAGA	CCTCATCTTCTACCGGCATC	#25
Nppb (BNP)	GTCAGTCGTTTGGGCTGTAAC	AGACCCAGGCAGAGTCAGAA	#71
Tgfb	TGGAGCAACATGTGGAACTC	GTCAGCAGCCGGTTACCA	#72

Tnfa	TCTTCTCATTCCTGCTTGTGG	GAGGCCATTTGGGAACTTCT	#49

Supplementary Table 3. LV functional parameters in DOX-treated WT and KD mice

	WT Basal	WT DOX	KD Basal	KD DOX
N	9		9	
HR (bpm)	476 ±10	468 ±15	469 ±15	476 ±11
LVEDd (mm)	3.64 ±0.05	3.63 ±0.07	3.63 ±0.09	3.59 ±0.06
LVEDs (mm)	2.31 ±0.03	2.7 ±0.11**	2.29 ±0.07	2.33 ±0.08††
IVSd (mm)	0.68 ±0.02	0.61 ±0.03	0.69 ±0.02	0.71 ±0.02†
IVSs (mm)	1.09 ±0.04	0.81 ±0.04***	1.08 ±0.04	1.16 ±0.04†††
LVPWd (mm)	0.67 ±0.02	0.61 ±0.02	0.69 ±0.03	0.7 ±0.02†
LVPWs (mm)	1.05 ±0.01	0.87 ±0.04**	1.06 ±0.04	1.05 ±0.03††
FS (%)	37.6 ±0.8	24.3 ±2.3***	37.9 ±1.1	37.2 ±1.7†††
EF (%)	68.5 ±1	48.6 ±3.7***	68.5 ±1.5	68.2 ±2.5†††

NOTE: Mean ± SEM. DOX vs Basal: $^{**}P<0.01$ and $^{***}P<0.001$ and KD vs WT: $^{†}P<0.05$, $^{††}P<0.01$ and $^{†††}P<0.001$ by two-way repeated-measures ANOVA with Bonferroni's post-hoc test.

Abbreviations: DOX, doxorubicin; HR, heart rate; LVEDd, left ventricular end-diastolic diameter; LVEDs, left ventricular end-systolic diameter; IVSd, interventricular septal thickness at end-diastole; IVSs, interventricular septal thickness at end-systole; LVPWd, left ventricular posterior wall thickness at end-diastole; LVPWs, left ventricular posterior wall thickness at end-systole; FS, fractional shortening; EF, ejection fraction.

Supplementary Table 4. Heart, lung and liver weight of saline and DOX-treated WT and KD mice

	WT Saline	WT DOX	KD Saline	KD DOX
N	6	8	6	9
HW/TL (mg/mm)	4.90 ±0.09	4.39 ±0.09**	4.89 ±0.12	4.93 ±0.10†††
Lung W/TL (mg/mm)	8.46 ±0.15	8.29 ±0.32	8.63 ±0.23	8.35 ±0.31
Liver W/TL (mg/mm)	5.32 ±0.11	5.16 ±0.16	5.45 ±0.09	5.34 ±0.22

NOTE: Mean ± SEM. WT DOX vs WT Saline: **P<0.01 and KD DOX vs WT DOX: †††P<0.001 by two-way ANOVA with Bonferroni's post-hoc test.

Abbreviations: DOX, doxorubicin; N, numbers; HW/TL: heart weight/tibial length; Lung W/TL: lung weight/tibial length; Liver W/TL: liver weight/tibial length.

Supplementary Table 5. LV functional parameters in DOX-treated, 4T1 tumor-bearing WT and KD mice

	WT Basal	WT DOX	KD Basal	KD DOX
N	5		11	
HR (bpm)	438 ± 8	425 ± 8	444 ± 6	432 ± 6
LVEDd (mm)	3.70 ± 0.09	3.77 ± 0.10	3.73 ± 0.05	3.57 ± 0.08
LVEDs (mm)	2.31 ± 0.14	2.83 ± 0.12*	2.35 ± 0.07	2.31 ± 0.05††
IVSd (mm)	0.67 ± 0.06	0.68 ± 0.06	0.66 ± 0.02	0.70 ± 0.03
IVSs (mm)	1.17 ± 0.08	0.90 ± 0.07***	1.20 ± 0.02	1.10 ± 0.04*††
LVPWd (mm)	0.63 ± 0.04	0.67 ± 0.05	0.68 ± 0.02	0.71 ± 0.04
LVPWs (mm)	0.95 ± 0.04	0.82 ± 0.06	1.01 ± 0.03	1.00 ± 0.05†
FS (%)	36.9 ± 3.0	25.6 ± 2.0***	38.3 ± 1.2	37.8 ± 2.0†††
EF (%)	67.0 ± 4.0	50.9 ± 3.4***	69.2 ± 1.5	68.7 ± 2.5†††

NOTE: Mean ± SEM. DOX vs Basal: *P<0.05 and ***P<0.001 and KD vs WT: †P<0.05, ††P<0.01 and †††P<0.001 by two-way repeated-measures ANOVA with Bonferroni's post-hoc test.

Abbreviations: DOX, doxorubicin; HR, heart rate; LVEDd, left ventricular end-diastolic diameter; LVEDs, left ventricular end-systolic diameter; IVSd, interventricular septal thickness at end-diastole; IVSs, interventricular septal thickness at end-systole; LVPWd, left ventricular posterior wall thickness at end-diastole; LVPWs, left ventricular posterior wall thickness at end-systole; FS, fractional shortening; EF, ejection fraction.

Supplementary Table 6. LV functional parameters in WT mice treated with DOX alone or together with the PI3Kγ inhibitor AS605240

	Vehicle Basal	Vehicle+DOX	AS Basal	AS+DOX
N	9		11	
HR (bpm)	447 ±6	440 ±10	444 ±12	446 ±15
LVEDd (mm)	3.69 ±0.04	3.85 ±0.06*	3.79 ±0.06	3.63 ±0.04*†
LVEDs (mm)	2.47 ±0.05	2.93 ±0.04***	2.57 ±0.06	2.51 ±0.08†††
IVSd (mm)	0.72 ±0.03	0.64 ±0.03	0.67 ±0.04	0.67 ±0.03
IVSs (mm)	1.12 ±0.03	0.92 ±0.06*	1.03 ±0.06	1.01 ±0.04
LVPWd (mm)	0.69 ±0.02	0.60 ±0.01*	0.67 ±0.03	0.61 ±0.03
LVPWs (mm)	0.96 ±0.03	0.78 ±0.02***	1.01 ±0.04	0.91 ±0.04†
FS (%)	33.7 ±1.0	23.1 ±1.3***	32.1 ±1.1	30.9 ±1.7†††
EF (%)	63.2 ±1.4	46.9 ±2.2***	61.7 ±1.9	59.1 ±2.5†††
HW/TL (mg/ml)		4.65 ±0.06		5.17 ±0.13††

NOTE: Mean ± SEM. DOX vs Basal: *P<0.05 and ***P<0.001 and AS605240 (AS) vs Vehicle: †P<0.05, ††P<0.01 and †††P<0.001 by two-way repeated-measures ANOVA with Bonferroni's post-hoc test.

Abbreviations: DOX, doxorubicin; HR, heart rate; LVEDd, left ventricular end-diastolic diameter; LVEDs, left ventricular end-systolic diameter; IVSd, interventricular septal thickness at end-diastole; IVSs, interventricular septal thickness at end-systole; LVPWd, left ventricular posterior wall thickness at end-diastole; LVPWs, left ventricular posterior wall thickness at end-systole; FS, fractional shortening; EF, ejection fraction; HW/TL: heart weight/tibial length.

Suppl Figure 1

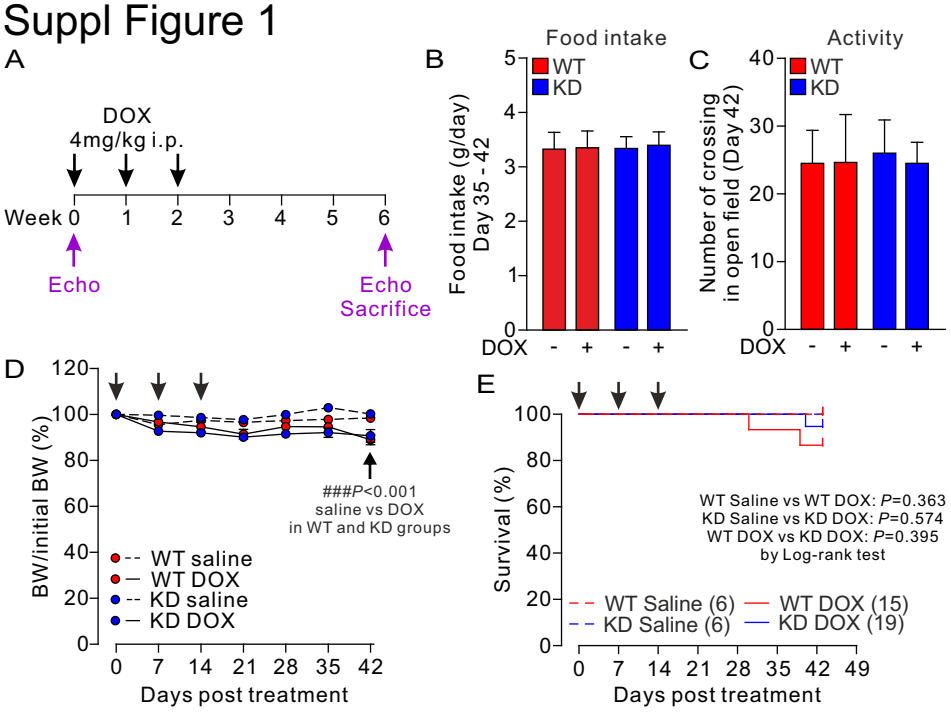

Suppl Figure 2

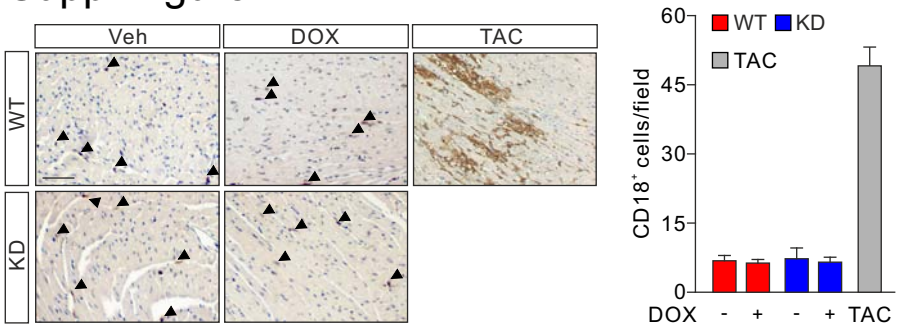

Suppl Figure 3

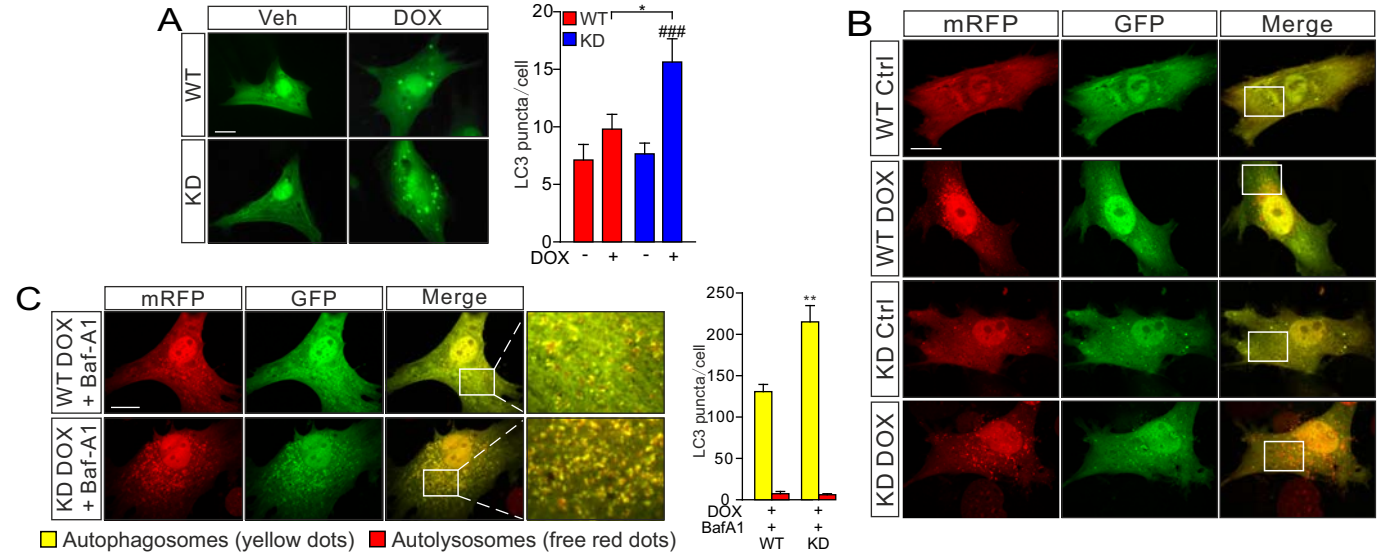

Suppl Figure 4

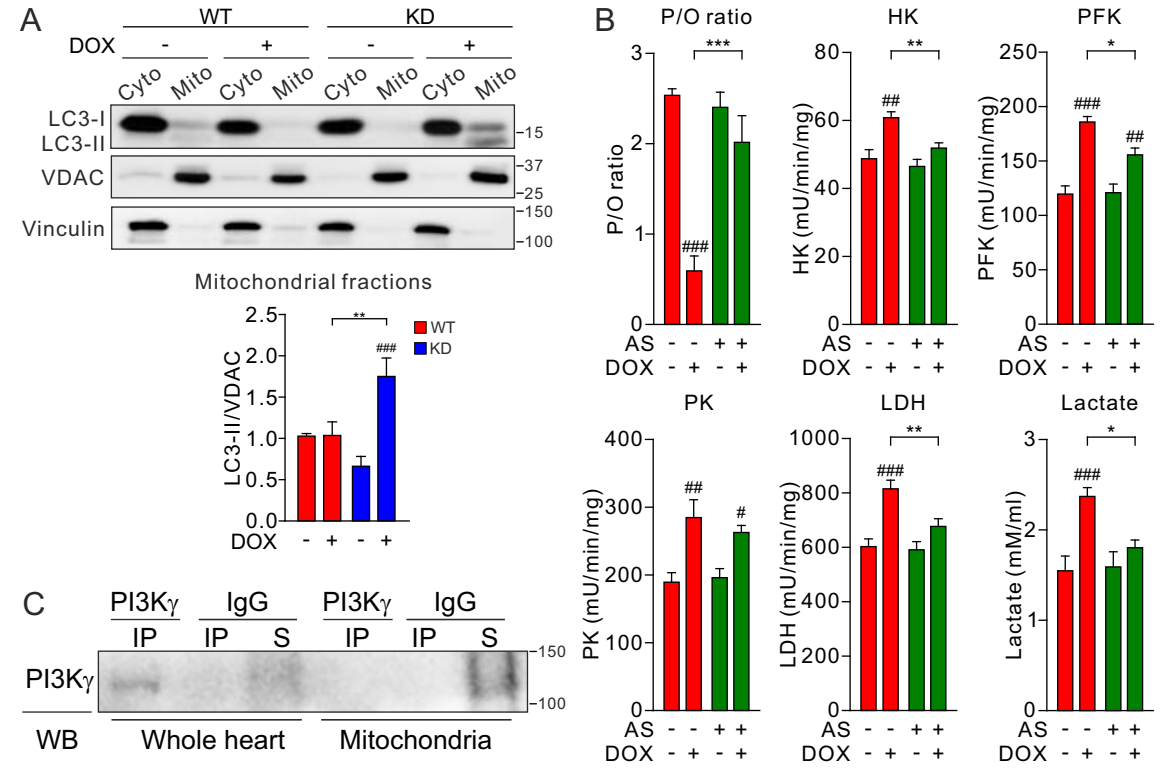

Suppl Figure 5

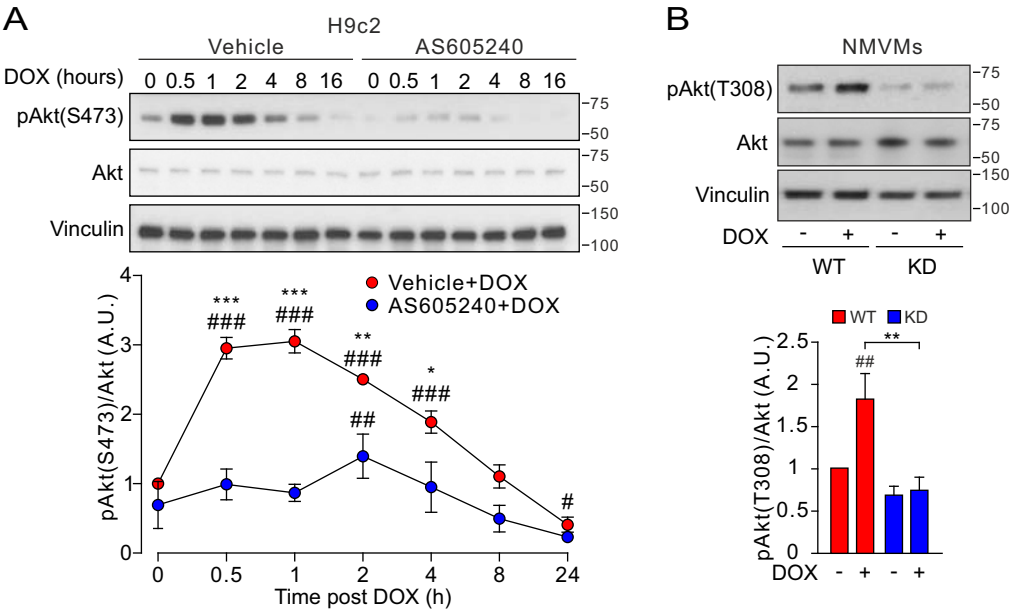

Suppl Figure 6

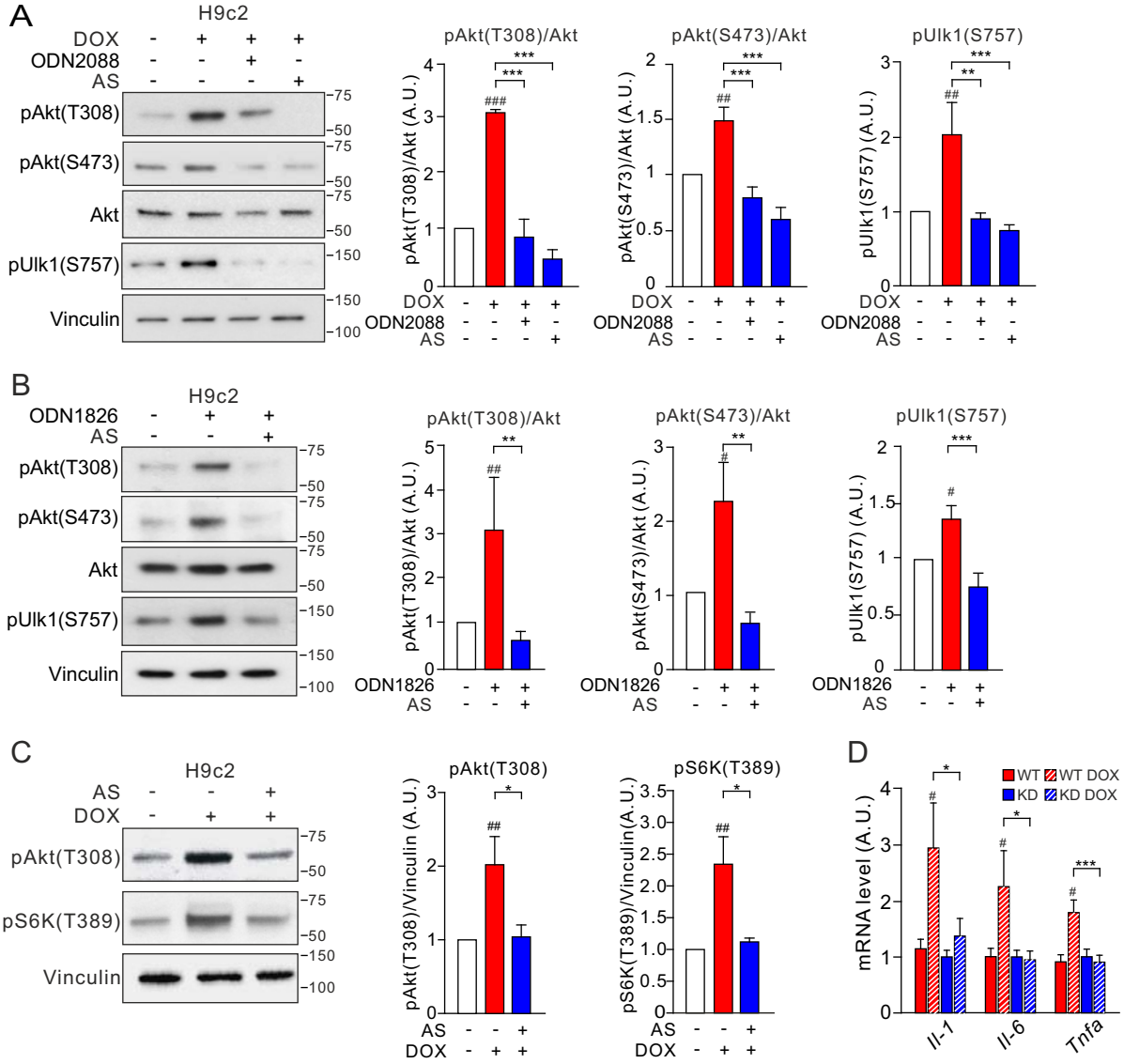

Suppl Figure 7

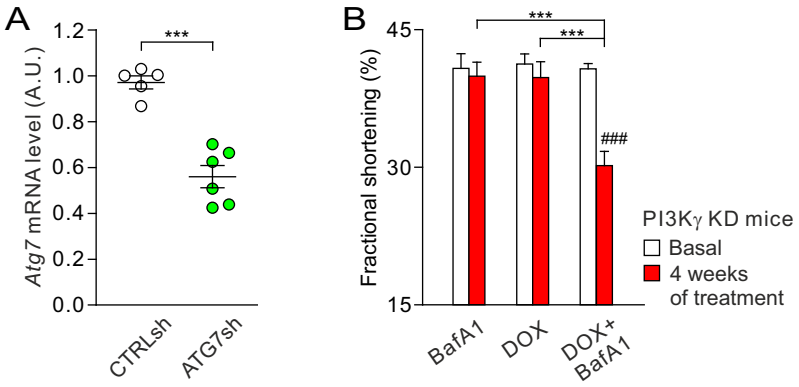

Suppl Figure 8

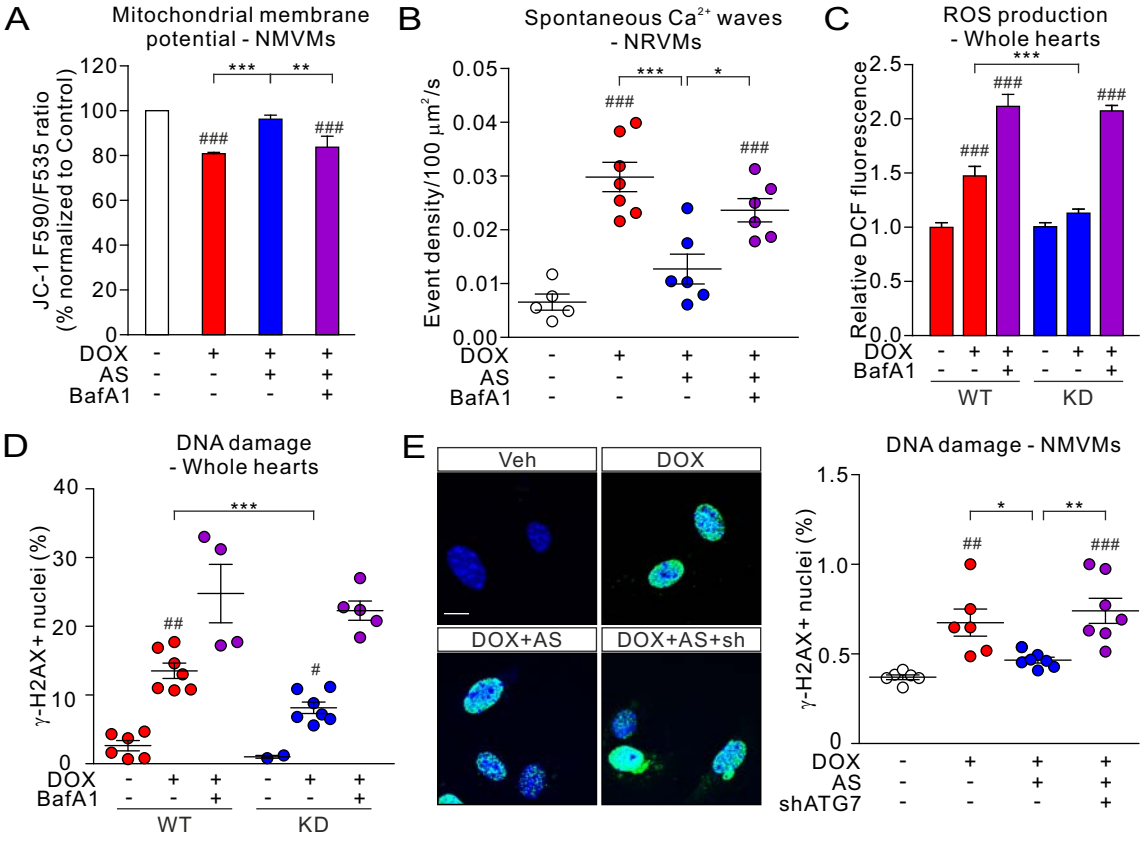

Suppl Figure 9

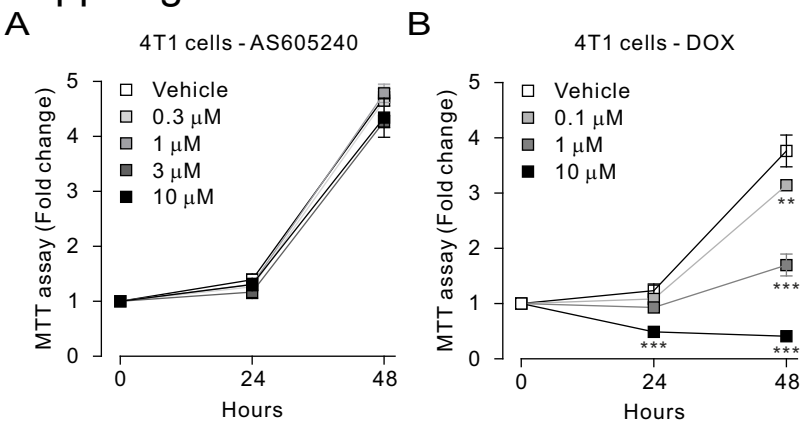

Suppl Figure 10

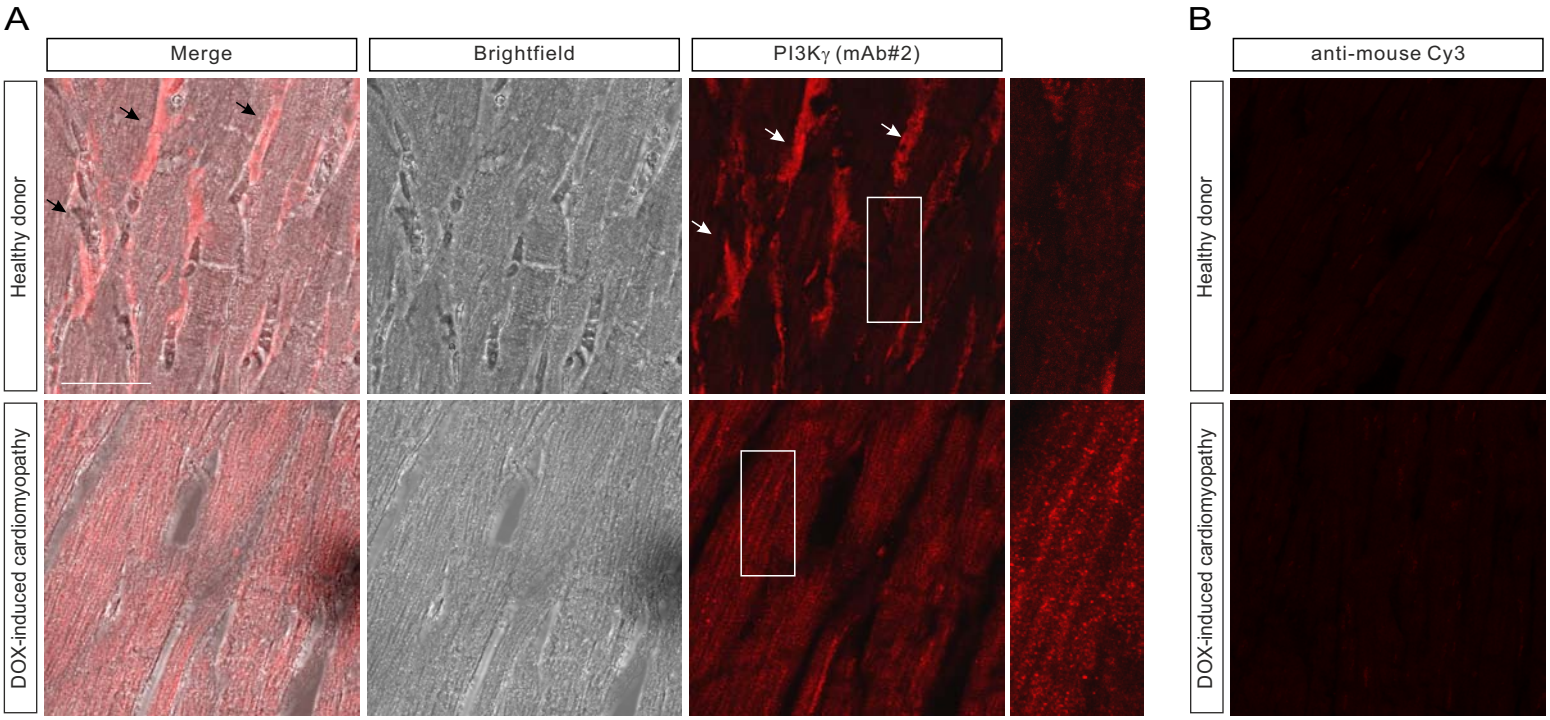

Suppl Figure 11

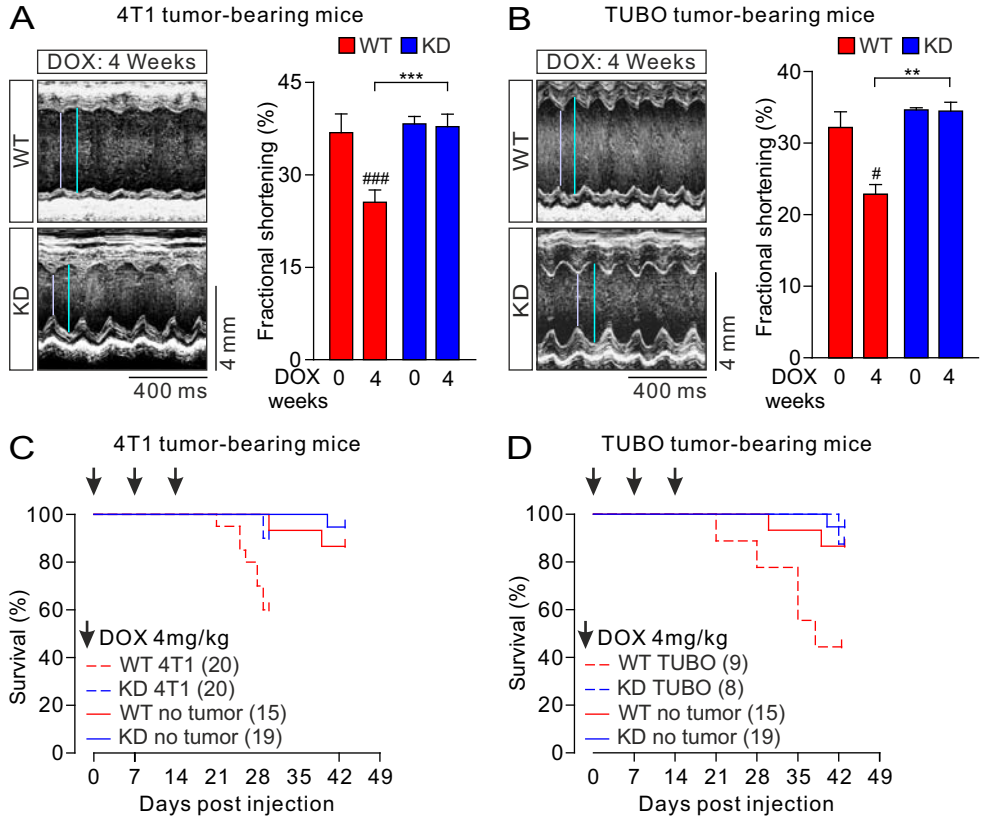

Suppl Figure 12

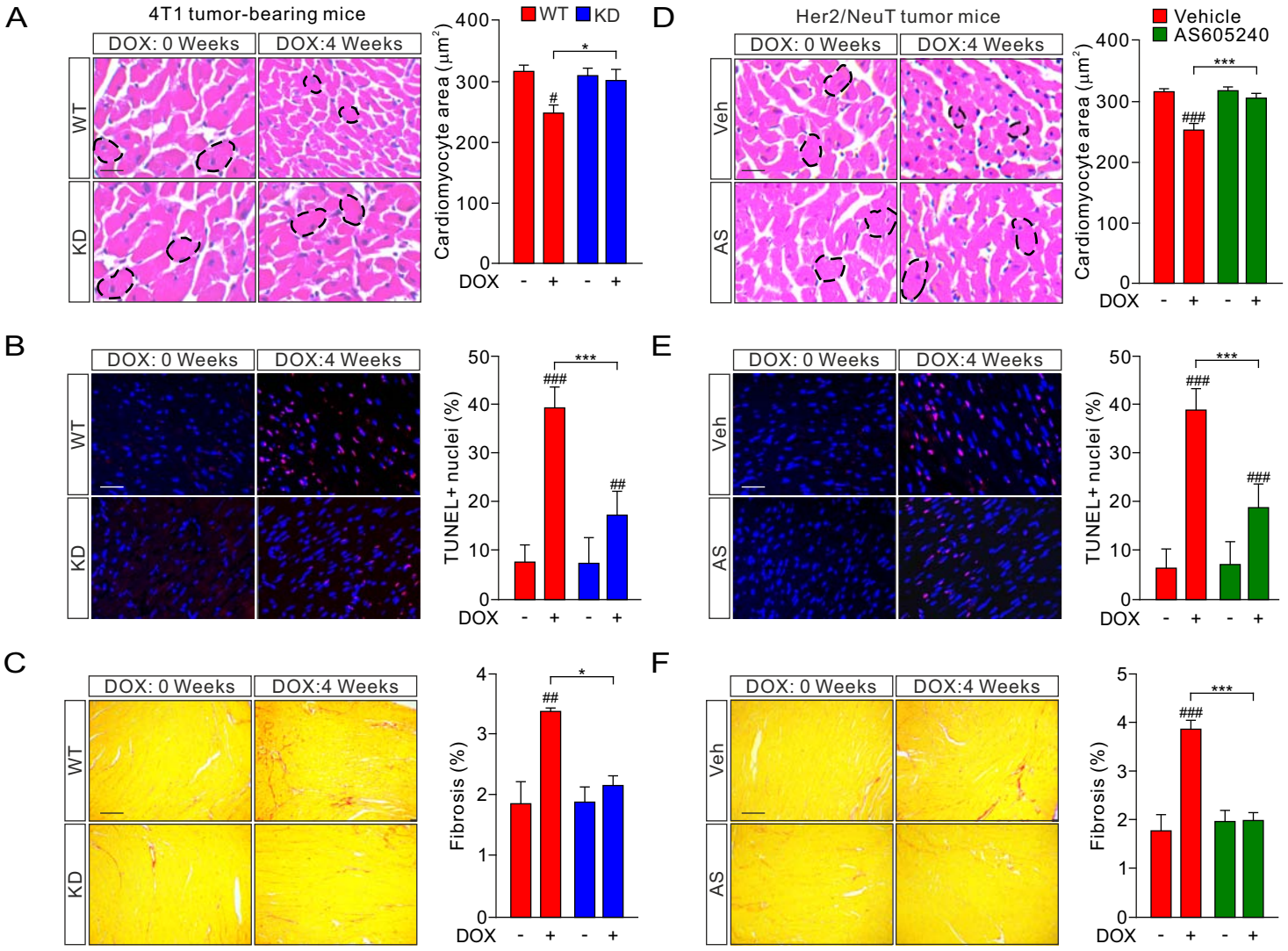

Suppl Figure 13

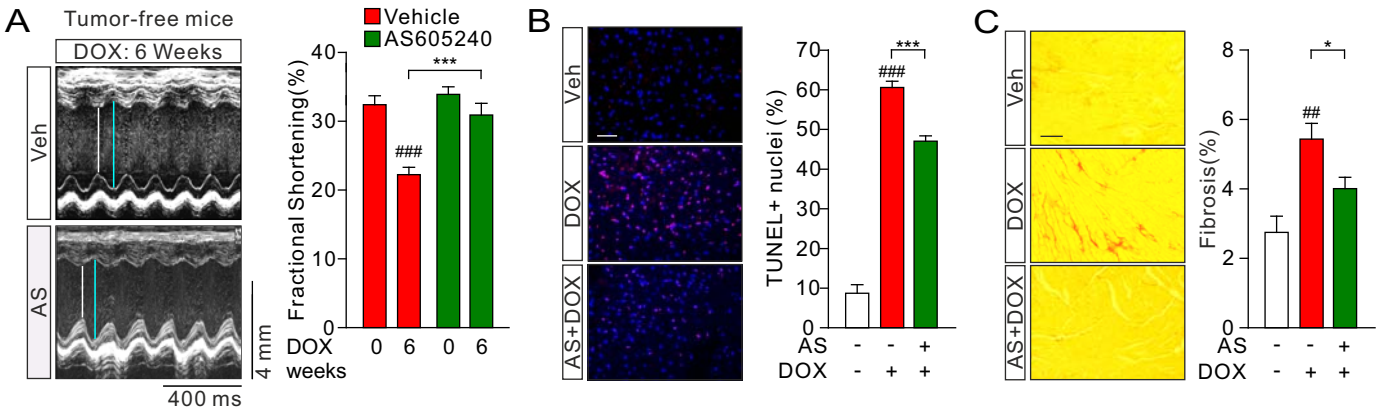

Supplementary Figure Legends

Supplementary Figure 1. Low-dose intraperitoneal DOX does not cause systemic toxicity. (**A**) Scheme of chronic doxorubicin (DOX) administration protocol. WT and KD mice were treated with a cumulative dose of 12 mg/kg DOX or saline via 3 weekly i.p. injections (4 mg/kg on days 0, 7 and 14). Echocardiography was performed before and 6 weeks after the first injection. Arrows indicate DOX injections. (**B**) Food intake of mice treated as described in (**A**). An average of food intake from day 35 to day 42 was calculated for each mouse. (**C**) Locomotor activity (number of crossings in the open-field test) of mice treated as in (**A**). Activity was measured at day 42. (**D**) Body weight change of mice treated as in (**A**). Arrows indicate DOX injections. WT saline vs WT DOX and KD saline vs KD DOX: ###$P<0.001$ at day 42 by two-way repeated-measures ANOVA with Bonferroni's post-hoc test. **B** through **D**, values represent mean ± SEM. n=6-9 animals/group. (**E**) Kaplan-Meier survival curves of WT and KD mice after treatment with saline or DOX as described in (**A**). Arrows indicate DOX injections. Log-rank test was used for statistical analysis.

Supplementary Figure 2. Leukocyte infiltration in DOX-treated hearts. Representative immunohistochemistry images (left) and relative quantification (right) of CD18 staining in hearts 3 days after the first doxorubicin (DOX) injection in WT and KD mice. Arrows indicated $CD18^{+}$ cells. Heart sections from mice subjected to 3 days of transverse aortic constriction (TAC) were used as positive control for leukocyte infiltration. Scale bar, 50 μm. Values represent mean ± SEM. n=7 animals/group. WT vs KD: not significant by one-way ANOVA with Bonferroni's post-hoc test.

Supplementary Figure 3. PI3Kγ inhibition promotes autophagosome formation in primary neonatal mouse ventricular myocytes (NMVMs). (**A**) WT and KD NMVMs were transfected with a plasmid encoding YFP-LC3, and treated with 1 μM doxorubicin (DOX) for 16 hours. Representative fluorescence images (left) and relative quantification (right) of LC3 puncta are shown. Scale bar, 10 μm. n=15-17 cells/group. Vehicle (-) vs DOX (+): ###*P*< 0.001 and WT vs KD: **P*<0.05 by two-way ANOVA with Bonferroni's post-hoc test. (**B**) WT and KD NMVMs were infected with an adenovirus encoding the tandem fluorescent probe mRFP-GFP-LC3, and treated with 1 μM DOX for 16 hours. Representative images of autophagosomes (yellow dots) and autolysosomes (red free dots) are shown. Enlargements of the outlined areas are shown in Figure 2E. Scale bar, 10 μm. (**C**) 4 hours before the end of DOX treatment (1 μM, 16 hours), BafA1 (100 nM) was added to cells as in (**B**) to block the fusion of autophagosomes and lysosomes. Representative figures and relative quantification of autophagosomes (yellow dots) and autolysosomes (red free dots) are shown. Scale bar, 10 μm. n=7-8 cells/group. Yellow puncta, WT vs KD: ***P*<0.01 by Student's t-test. Values represent mean ± SEM.

Supplementary Figure 4. PI3Kγ inhibition promotes autophagic clearance of damaged mitochondria. (**A**) Representative immunoblot of the autophagic marker LC3 in cytosolic and mitochondrial fractions of WT and KD hearts 3 days after a single injection of doxorubicin (DOX; 4 mg/kg). Relative quantification of LC3 in mitochondria-enriched fractions is shown. DOX (+) vs saline (-): ###P<0.001 and WT vs KD: **P<0.01 by two-way ANOVA with Bonferroni's post-hoc test. n=6 animals/group. (**B**) Phosphate/Oxygen ratio (P/O ratio), hexokinase (HK), phosphofructokinase (PFK), pyruvate kinase (PK) and lactate dehydrogenase (LDH) activity, and lactate production in WT neonatal mouse ventricular myocytes (NMVMs) treated with 1 μM DOX for 3 hours, with or without pre-treatment with the PI3Kγ inhibitor AS605240 (0.5 μM) for 1 hour. DOX (+) vs saline (-): #P<0.05, ##P<0.01 and ###P<0.001 and DOX vs DOX+AS: *P<0.05, **P<0.01 and ***P<0.001 by two-way ANOVA with Bonferroni's post-hoc test. n≥4 independent experiments. (**C**) PI3Kγ expression in whole hearts and in mitochondria. PI3Kγ was immunoprecipitated by incubating lysates with either an anti-PI3Kγ antibody or IgG as a control. Proteins bound to the resin (IP) or remaining in the unbound supernatant (S) were immunoblotted for PI3Kγ.

Supplementary Figure 5. PI3Kγ inhibition prevents DOX-induced Akt activation in H9c2 cells and neonatal mouse ventricular myocytes (NMVMs). (**A**) H9c2 cells were treated with 1 μM doxorubicin (DOX) for the indicated time ± 1-hour pre-treatment with the PI3Kγ inhibitor AS605240 (AS; 0.5 μM). Representative immunoblot (upper panel) and relative quantification (lower panel) of Akt phosphorylation are shown. Vehicle vs AS: **P*<0.05, ***P*<0.01 and ****P*< 0.001 and indicated time vs untreated: #*P*<0.05, ##*P*<0.01 and ###*P*< 0.001 by two-way ANOVA with Bonferroni's post-hoc test. n=3 independent experiments. (**B**) Representative immunoblot (upper panel) and relative quantification (lower panel) of Akt phosphorylation in NMVMs from WT and KD mice treated with 1 μM doxorubicin (DOX) for 1 hour. n≥4 independent experiments. DOX vs Vehicle: ##*P*<0.01 and WT DOX vs KD DOX: ***P*<0.01 by two-way ANOVA with Bonferroni's post-hoc test. n≥4 independent experiments. In each panel, values represent mean ± SEM.

Supplementary Figure 6. DOX activates a TLR9/PI3Kγ/Akt/Ulk1 pathway that inhibits autophagy. (**A**) H9c2 cells were treated with 1 μM doxorubicin (DOX) for 1 hour, alone or in combination with the PI3Kγ inhibitor AS605240 (AS; 0.5 μM, 1-hour pre-treatment) or with the TLR9 antagonist (ODN2088; 0.2 μM, 5-hour pre-treatment). Representative immunoblot (left) and relative quantification (right) of Akt (T308 and S473) and Ulk1 (S757) phosphorylation are shown. For each panel, values represent mean ± SEM, n≥4 independent experiments, DOX vs saline: ##*P*<0.01 and ###*P*<0.001 and DOX+AS/ODN2088 vs DOX: **P<0.01 and ***P<0.001 by one-way ANOVA followed by Bonferroni's post-hoc test. (**B**) H9c2 cells were stimulated with the TLR9 agonist (ODN1826; 0.2 μM) for 1 hour, alone or in combination with AS (0.5 μM, 1-hour pre-treatment). Representative immunoblot and relative quantification of Akt (T308 and S473) and Ulk1 (S757) phosphorylation are shown. n≥4 independent experiments, ODN1826 vs saline: #*P*<0.05 and ##*P*<0.01 and ODN1826+AS vs ODN1826: **P<0.01 and ***P< 0.001 by one-way ANOVA followed by Bonferroni's post-hoc test. (**C**) Representative immunoblot (left) and relative quantification (right) of phospho-Akt and phospho-p70S6K in H9c2 cells treated with 1 μM DOX for 1 hour ± 1-hour pre-treatment with the PI3Kγ inhibitor AS605240 (0.5 μM AS). DOX vs Vehicle: ##*P*<0.01 and DOX+AS vs DOX: *P<0.05 by one-way ANOVA with Bonferroni's post-hoc test. n≥4 independent experiments. (**D**) mRNA levels of TLR9 target genes (*Il-10, Il-6, Tnfa*) in WT and KD hearts 3 days after a single injection of doxorubicin (DOX; 4 mg/kg). For each panel, values represent mean ± SEM, n≥4 independent experiments, DOX vs saline: #*P*<0.05 and WT DOX vs KD DOX: *P<0.05 and ***P<0.001 by two-way ANOVA followed by Bonferroni's post-hoc test. For each panel, values represent mean ± SEM.

Supplementary Figure 7. Autophagy inhibition dampens the cardioprotection of KD mice. (**A**) mRNA levels of *Atg7* in hearts from KD mice transduced with AAV9-ATG7sh or AAV9-CTRLsh vectors as described in Figure 6A. ***P<0.001 by Student's t-test. (**B**) KD mice were treated with DOX (4 mg/kg on days 0, 7 and 14; n=7), Bafilomycin A1 (BafA1, 0.3 mg/kg daily from day 0 to 28; n=7) or a combination of DOX and BafA1 (n=8). Fractional shortening before and 4 weeks after the first DOX injection is shown. Before vs after the treatment: ###P<0.01 and DOX+BafA1 vs single treatments (DOX or BafA1): ***P<0.001 by two-way repeated-measures ANOVA with Bonferroni's post-hoc test. In each panel, values represent mean ± SEM.

Supplementary Figure 8. PI3Kγ inhibition prevents DOX-induced mitochondrial dysfunction, calcium mishandling, ROS production and DNA damage by unleashing autophagy. (**A**) Mitochondrial membrane potential measured as the ratio of JC-1 fluorescence at 590 nm and 535 nm (F590/F535) in neonatal mouse ventricular myocytes (NMVMs) pre-treated with Vehicle (0.1% DMSO), or 0.5 μM AS605240 alone or together with 100 nM Bafilomycin A1 (BafA1) for 1 hour, before exposure to 1 μM DOX or saline for 6 hours. (**B**) Spontaneous Ca^{2+} release events in neonatal rat ventricular myocytes (NRVMs) treated as in (**A**). **A** and **B**, vehicle vs treatments: ###*P*<0.001; among different treatments: **P*<0.05, ***P*<0.01 and ****P*<0.001 by one-way ANOVA with Bonferroni's post-hoc test. n>4 independent experiments. (**C**) ROS production in hearts from WT and KD mice pre-treated with Bafilomycin A1 (BafA1, 10 mg/kg) 1 hour before a single DOX injection (4 mg/kg) for 6 hours. (**D**) Quantification of DNA damage by γ-H2AX staining (% of γ-H2AX+ nuclei) in hearts from animals treated as in (**C**). **C** and **D**, vehicle vs treatments (DOX or DOX+BafA1): #*P*<0.05, ##*P*<0.01 and ###*P*<0.001; WT vs KD: ****P*<0.001 by two-way ANOVA with Bonferroni's post-hoc test. n=3-7 animals/group. (**E**) NMVMs were infected with an adenovirus carrying a ATG7 shRNA (20 M.O.I.) for 24 hours and then treated with DOX (1 μM) and the PI3Kγ inhibitor AS605240 (AS, 0.5 μM, 1-hour pre-treatment) for 6 hours. Representative images (left) and quantification (right) of γ-H2AX-positive nuclei (DAPI in blue) are shown. Vehicle vs treatments: ##*P*<0.01 and ###*P*<0.001; among different treatments: **P*<0.05 and ***P*<0.01 by one-way ANOVA with Bonferroni's post-hoc test. n>4 independent experiments. Scale bar, 8 μm. In each panel, values represent mean ± SEM.

Supplementary Figure 9. Effects of PI3Kγ inhibition or DOX on 4T1 cell growth *in vitro*. (**A**-**B**) 4T1 cells were treated with different doses of (**A**) the PI3Kγ inhibitor AS605240 (0, 0.3, 1, 3 and 10 μM) or (**B**) doxorubicin (DOX) (0, 0.1, 1 and 10 μM) for 24 to 48 hours. Cell viability was measured by MTT assay. For each panel, values represent mean ± SEM, n=3 independent experiments, treatment vs Vehicle: ***P*<0.01 and ****P*<0.001 by two-way ANOVA followed by Bonferroni's post-hoc test.

Supplementary Figure 10. PI3Kγ staining in human heart sections from a patient with DOX-induced cardiomyopathy and a healthy subject. (**A**) PI3Kγ staining with an anti-PI3Kγ monoclonal antibody (mAb#2) in heart sections from a healthy donor and a patient who developed cardiomyopathy after doxorubicin (DOX) treatment (bottom) (details in Online Supplementary Methods). Right panels show enlargements of the outlined areas. Middle and left panels show bright-field and merge images, respectively. Arrows indicate unspecific staining in inter-cardiomyocyte spaces. Scale bar, 50 μm. (**B**) Staining with a secondary anti-Cy3 antibody of sections as described in (**A)**.

Supplementary Figure 11. Cardiac function and survival of DOX-treated, tumor-bearing WT and KD mice. (**A**-**B**) Representative M-mode echocardiographic images and fractional shortening of hearts from WT and KD mice injected s.c. with (**A**) 1×10^5 4T1 breast cancer cells and (**B**) 1×10^5 TUBO breast cancer cells, and treated with doxorubicin (DOX) via 3 weekly injections (4 mg/kg on days 0, 7 and 14). **A** and **B**, scale bars, 400 ms, 4 mm. Animals/group: (**A**) WT n=5, KD n=11; (**B**) WT n=9, KD n=8. 0 vs 4 weeks: #*P*<0.05 and ###*P*<0.001; WT vs KD: **P<0.01 and ***P<0.001 by two-way repeated-measures ANOVA with Bonferroni's post-hoc test. Values represent mean ± SEM. (**C**) Kaplan-Meier survival curves of 4T1 tumor-bearing mice treated as in (**A**). Survival curves of tumor-free animals under DOX treatment from Supplementary Figure 1 are shown for comparison. Arrows indicate DOX injections. Log-rank test was used for statistical analysis. Tumor-bearing, WT vs KD: P=0.021; WT, tumor-bearing vs tumor-free: P=0.024; KD, tumor-bearing vs tumor-free: P=0.162. (**D**) Kaplan-Meier survival curves of TUBO tumor-bearing mice treated as in (**B**). Survival curves of tumor-free animals under DOX treatment from Supplementary Figure 1 are shown for comparison. Arrows indicate DOX injections. Log-rank test was used for statistical analysis. Tumor-bearing, WT vs KD: P=0.042; WT, tumor-bearing vs tumor-free: P=0.021; KD, tumor-bearing vs tumor-free: P=0.542.

Supplementary Figure 12. Cardiac atrophy, fibrosis and apoptosis in DOX-treated, tumor-bearing mice. (**A-C**) WT and KD mice were injected s.c. with 1×10^5 4T1 breast cancer cells, and treated with doxorubicin (DOX) via 3 weekly injections (4 mg/kg on days 0, 7 and 14). (**A**) Representative images of H&E staining (left) and quantification of cardiomyocyte area (right) in WT and KD hearts 4 weeks after the first dose of DOX or saline. Scale bar, 20 μm. (**B**) Representative images of TUNEL staining (left) and quantification of TUNEL positive nuclei per field (right) in WT and KD hearts treated as in (**A**). Scale bar, 30 μm. (**C**) Representative images of PicroSirius Red staining (left) and relative quantification of collagen deposition (right) in heart sections from WT and KD hearts treated as in (**A**). Scale bar, 50 μm. DOX 0 vs 4 weeks: #P<0.05, ##P<0.01 and ###P<0.001; WT vs KD: *P<0.05 and ***P<0.001 by two-way ANOVA with Bonferroni's post-hoc test. (**D-F**) Her2/NeuT transgenic mice bearing spontaneous tumors (2 mm in mean diameter) were administered with saline or DOX as above, and treated daily with vehicle or the PI3Kγ inhibitor AS605240 (AS) for 3 weeks since the first DOX injection. (**D**) Representative images of H&E staining (left) and quantification of cardiomyocyte area (right) in hearts from Her2/NeuT mice 4 weeks after the first dose of DOX or saline. Scale bar, 20 μm. (**E**) Representative images of TUNEL staining (left) and quantification of TUNEL positive nuclei per field (right) in hearts from Her2/NeuT mice treated as in (**D**). Scale bar, 30 μm. (**F**) Representative images of PicroSirius Red staining (left) and relative quantification of collagen deposition (right) in hearts from Her2/NeuT mice treated as in (**D**). Scale bar, 50 μm. DOX 0 vs 4 weeks: ###P<0.001; DOX vs DOX+AS605240: ***P<0.001 by two-way ANOVA with Bonferroni's post-hoc test. In each panel, values represent mean ± SEM.

Supplementary Figure 13. Pharmacological inhibition of PI3Kγ protects against DOX-induced cardiotoxicity in tumor-free mice. WT mice were treated with a cumulative dose of 12 mg/kg doxorubicin (DOX) via 3 weekly injections (4 mg/kg on days 0, 7 and 14). Vehicle or the PI3Kγ inhibitor AS605240 (AS, 10 mg/kg) were administered 1 hour before each injection of DOX. (**A**) Representative M-mode echocardiographic images (left) and fractional shortening (right) of mice treated with Vehicle+DOX (n=9) and AS605240+DOX (n=11), before and 6 weeks after the first DOX injection. Scale bars, 400 ms, 4 mm. 0 vs 6 weeks after DOX: ###P<0.001 and AS vs Vehicle: ***P<0.001 by two-way repeated-measures ANOVA with Bonferroni's post-hoc test. (**B**) Representative images of TUNEL staining (left) and relative quantification of TUNEL positive nuclei per field (right) of hearts treated as in (**A**). Scale bar, 50 μm. (**C**) Representative images of PicroSirius Red staining (left) and relative quantification of collagen deposition (right) of hearts treated as in **A**. Scale bar, 25 μm. **B** and **C**, n=6-8 animals/group, saline vs treatments: ##P<0.01 and ###P<0.001 and DOX+AS vs DOX: *P<0.05 and ***P<0.001 by one-way ANOVA with Bonferroni's post-hoc test. In each panel, values represent mean ± SEM.

Supplementary References

1. Patrucco E, Notte A, Barberis L, Selvetella G, Maffei A, Brancaccio M, Marengo S, Russo G, Azzolino O, Rybalkin SD, Silengo L, Altruda F, Wetzker R, Wymann MP, Lembo G, Hirsch E. PI3Kγ Modulates the Cardiac Response to Chronic Pressure Overload by Distinct Kinase-Dependent and -Independent Effects. *Cell*. 2004;118:375–387.

2. Quaglino E, Iezzi M, Mastini C, Amici A, Pericle F, Carlo ED, Pupa SM, Giovanni CD, Spadaro M, Curcio C, Lollini PL, Musiani P, Forni G, Cavallo F. Electroporated DNA Vaccine Clears Away Multifocal Mammary Carcinomas in Her-2/neu Transgenic Mice. *Cancer Res*. 2004;64:2858–2864.

3. Zhao Y, McLaughlin D, Robinson E, Harvey AP, Hookham MB, Shah AM, McDermott BJ, Grieve DJ. Nox2 NADPH Oxidase Promotes Pathologic Cardiac Remodeling Associated with Doxorubicin Chemotherapy. *Cancer Res*. 2010;70:9287–9297.

4. Perino A, Ghigo A, Ferrero E, Morello F, Santulli G, Baillie GS, Damilano F, Dunlop AJ, Pawson C, Walser R, Levi R, Altruda F, Silengo L, Langeberg LK, Neubauer G, Heymans S, Lembo G, Wymann MP, Wetzker R, Houslay MD, Iaccarino G, Scott JD, Hirsch E. Integrating Cardiac PIP3 and cAMP Signaling through a PKA Anchoring Function of p110γ. *Mol Cell*. 2011;42:84–95.

5. Wang Y, Xu R, Sasaoka T, Tonegawa S, Kung M-P, Sankoorikal E-B. Dopamine D2 Long Receptor-Deficient Mice Display Alterations in Striatum-Dependent Functions. *J Neurosci*. 2000;20:8305–8314.

6. Winkler DG, Faia KL, DiNitto JP, Ali JA, White KF, Brophy EE, Pink MM, Proctor JL, Lussier J, Martin CM, Hoyt JG, Tillotson B, Murphy EL, Lim AR, Thomas BD, MacDougall JR, Ren P, Liu Y, Li L-S, Jessen KA, Fritz CC, Dunbar JL, Porter JR, Rommel C, Palombella VJ, Changelian PS, Kutok JL. PI3K-δ and PI3K-γ Inhibition by IPI-145 Abrogates Immune Responses and Suppresses Activity in Autoimmune and Inflammatory Disease Models. *Chem Biol*. 2013;20:1364–1374.

7. Schmid MC, Avraamides CJ, Dippold HC, Franco I, Foubert P, Ellies LG, Acevedo LM, Manglicmot JRE, Song X, Wrasidlo W, Blair SL, Ginsberg MH, Cheresh DA, Hirsch E, Field SJ, Varner JA. Receptor Tyrosine Kinases and TLR/IL1Rs Unexpectedly Activate Myeloid Cell PI3Kγ, A Single Convergent Point Promoting Tumor Inflammation and Progression. *Cancer Cell*. 2011;19:715–727.

8. Ghigo A, Perino A, Mehel H, Zahradn ́kov á A, Morello F, Leroy J, Nikolaev VO, Damilano F, Cimino J, Luca ED, Richter W, Westenbroek R, Catterall WA, Zhang J, Yan C, Conti M, Gomez AM, Vandecasteele G, Hirsch E, Fischmeister R. Phosphoinositide 3-Kinase γ Protects Against Catecholamine-Induced Ventricular Arrhythmia Through Protein Kinase A–Mediated Regulation of Distinct Phosphodiesterases. *Circulation*. 2012;126:2073–2083.

9. Rovero S, Amici A, Carlo ED, Bei R, Nanni P, Quaglino E, Porcedda P, Boggio K, Smorlesi A, Lollini P-L, Landuzzi L, Colombo MP, Giovarelli M, Musiani P, Forni G. DNA Vaccination Against Rat Her-2/Neu p185 More Effectively Inhibits Carcinogenesis Than Transplantable Carcinomas in Transgenic BALB/c Mice. *J Immunol*. 2000;165:5133–5142.

10. Ikeda Y, Shirakabe A, Maejima Y, Zhai P, Sciarretta S, Toli J, Nomura M, Mihara K, Egashira K, Ohishi M, Abdellatif M, Sadoshima J. Endogenous Drp1 Mediates Mitochondrial Autophagy and Protects the Heart Against Energy Stress. *Circ Res*. 2015;116:264–278.

11. Oka T, Hikoso S, Yamaguchi O, Taneike M, Takeda T, Tamai T, Oyabu J, Murakawa T, Nakayama H, Nishida K, Akira S, Yamamoto A, Komuro I, Otsu K. Mitochondrial DNA that escapes from autophagy causes inflammation and heart failure. *Nature*. 2012;485:251–255.

12. Castaldi A, Zaglia T, Mauro VD, Carullo P, Viggiani G, Borile G, Stefano BD, Schiattarella GG, Gualazzi MG, Elia L, Stirparo GG, Colorito ML, Pironti G, Kunderfranco P, Esposito G, Bang M-L, Mongillo M, Condorelli G, Catalucci D. MicroRNA-133 Modulates the β1-Adrenergic Receptor Transduction CascadeNovelty and Significance. *Circ Res*. 2014;115:273–283.

13. Varanita T, Soriano ME, Romanello V, Zaglia T, Quintana-Cabrera R, Semenzato M, Menabò R, Costa V, Civiletto G, Pesce P, Viscomi C, Zeviani M, Di Lisa F, Mongillo M, Sandri M, Scorrano L. The Opa1-Dependent Mitochondrial Cristae Remodeling Pathway Controls Atrophic, Apoptotic, and Ischemic Tissue Damage. *Cell Metab*. 2015;21:834–844.

14. Zaglia T, Milan G, Franzoso M, Bertaggia E, Pianca N, Piasentini E, Voltarelli VA, Chiavegato D, Brum PC, Glass DJ, Schiaffino S, Sandri M, Mongillo M. Cardiac sympathetic neurons provide trophic signal to the heart via β2-adrenoceptor-dependent regulation of proteolysis. *Cardiovasc Res*. 2013;97:240–250.

15. Zaglia T, Di Bona A, Chioato T, Basso C, Ausoni S, Mongillo M. Optimized protocol for immunostaining of experimental GFP-expressing and human hearts. *Histochem Cell Biol*. 2016;146:407–419.

16. Ingoglia G, Sag CM, Rex N, De Franceschi L, Vinchi F, Cimino J, Petrillo S, Wagner S, Kreitmeier K, Silengo L, Altruda F, Maier LS, Hirsch E, Ghigo A, Tolosano E. Hemopexin counteracts systolic dysfunction induced by heme-driven oxidative stress. *Free Radic Biol Med*. 2017;108:452–464.

17. Chiabrando D, Marro S, Mercurio S, Giorgi C, Petrillo S, Vinchi F, Fiorito V, Fagoonee S, Camporeale A, Turco E, Merlo GR, Silengo L, Altruda F, Pinton P, Tolosano E. The mitochondrial heme exporter FLVCR1b mediates erythroid differentiation. *J Clin Invest*. 2012;122:4569–4579.

18. Fischer AH, Jacobson KA, Rose J, Zeller R. Hematoxylin and Eosin Staining of Tissue and Cell Sections. *Cold Spring Harb Protoc*. 2008;2008:pdb.prot4986.

19. Damilano F, Franco I, Perrino C, Schaefer K, Azzolino O, Carnevale D, Cifelli G, Carullo P, Ragona R, Ghigo A, Perino A, Lembo G, Hirsch E. Distinct Effects of Leukocyte and Cardiac Phosphoinositide 3-Kinase γ Activity in Pressure Overload–Induced Cardiac Failure. *Circulation*. 2011;123:391–399.

20. McCaffrey TA, Tziros C, Lewis J, Katz R, Siegel R, Weglicki W, Kramer J, Mak IT, Toma I, Chen L, Benas E, Lowitt A, Rao S, Witkin L, Lian Y, Lai Y, Yang Z, Fu SW. Genomic Profiling Reveals the Potential Role of TCL1A and MDR1 Deficiency in Chemotherapy-Induced Cardiotoxicity. *Int J Biol Sci*. 2013;9:350–360.